SIMULATION OF THE DYNAMIC ENVIRONMENT FOR MISSILE COMPONENT TESTING: THEORY

FINAL REPORT

FINAL TECHNICAL REPORT

ROBERT J. GLASER

SEPTEMBER 26, 1988

U. S. ARMY RESEARCH OFFICE

21113-EG

JET PROPULSION LABORATORY
CALIFORNIA INSTITUTE OF TECHNOLOGY
4800 OAK GROVE DRIVE
PASADENA, CALIFORNIA 91109

SIMULATION OF THE DYNAMIC ENVIRONMENT FOR MISSILE COMPONENT TESTING: THEORY

FINAL REPORT

FINAL TECHNICAL REPORT

ROBERT J. GLASER

SEPTEMBER 26, 1988

U. S. ARMY RESEARCH OFFICE

21113-EG

JET PROPULSION LABORATORY
CALIFORNIA INSTITUTE OF TECHNOLOGY
4800 OAK GROVE DRIVE
PASADENA, CALIFORNIA 91109

UNCLASSIFIED
SECURITY CLASSIFICATION OF THIS PAGE

REPORT DOCUMENTATION PAGE

1a. REPORT SECURITY CLASSIFICATION: Unclassified	1b. RESTRICTIVE MARKINGS
2a. SECURITY CLASSIFICATION AUTHORITY	3. DISTRIBUTION / AVAILABILITY OF REPORT: Approved for public release; distribution unlimited.
2b. DECLASSIFICATION / DOWNGRADING SCHEDULE	
4. PERFORMING ORGANIZATION REPORT NUMBER(S)	5. MONITORING ORGANIZATION REPORT NUMBER(S): ARO 21113.1-EG
6a. NAME OF PERFORMING ORGANIZATION: Jet Propulsion Laboratory; 6b. OFFICE SYMBOL (If applicable)	7a. NAME OF MONITORING ORGANIZATION: U. S. Army Research Office
6c. ADDRESS (City, State, and ZIP Code): California Institute of Technology, 4800 Oak Grove Drive, Pasadena, CA 91109	7b. ADDRESS (City, State, and ZIP Code): P. O. Box 12211, Research Triangle Park, NC 27709-2211
8a. NAME OF FUNDING / SPONSORING ORGANIZATION: U. S. Army Research Office; 8b. OFFICE SYMBOL (If applicable)	9. PROCUREMENT INSTRUMENT IDENTIFICATION NUMBER: ARO MIPR'S 118-86, 141-87, 125-85
8c. ADDRESS (City, State, and ZIP Code): P. O. Box 12211, Research Triangle Park, NC 27709-2211	10. SOURCE OF FUNDING NUMBERS: PROGRAM ELEMENT NO. / PROJECT NO. / TASK NO. / WORK UNIT ACCESSION NO.

11. TITLE (Include Security Classification)

Simulation of the Dynamic Environment for Missile Component Testing: Theory Final Report

12. PERSONAL AUTHOR(S)
Robert J. Glaser

13a. TYPE OF REPORT	13b. TIME COVERED	14. DATE OF REPORT (Year, Month, Day)	15. PAGE COUNT
Final Report	FROM 12/17/84 TO 5/31/89	88-9-26	116

16. SUPPLEMENTARY NOTATION
The view, opinions and/or findings contained in this report are those of the author(s) and should not be construed as an official Department of the Army position, policy, or decision, unless so designated by other documentation.

17. COSATI CODES		
FIELD	GROUP	SUB-GROUP

18. SUBJECT TERMS (Continue on reverse if necessary and identify by block number)
Random Testing; Spectral Matrix; Three Dimensional; Sine Testing; Structural Testing; Vibration Testing

19. ABSTRACT (Continue on reverse if necessary and identify by block number)

The objective of this phase of work was to develop generic sine and random tests for the 3-D vibration test machines. While 3-D testing is a dramatic improvement over conventional 1-D testing, to be able to use the new technology, it is necessary to use conventional test specifications to test in 3-D. In this phase we were to identify what tests should be run for sine and for random testing. In the process it was necessary to reevaluate the theoretical basis of the sine and random tests. We were also to look for any flaws in the 3-D test systems as currently implemented.

The sine test has produced two candidate sine tests. By far the simplest and least controversial is a 2-D test where the shaker head is moved in a circle. By using a sine wave in one axis and a cosine wave in the other axis, traditional swept sine tests can be run in two orthogonal axes at one time. Just as current 1-D tests require three test axes, the 2-D sine test would be run in three orthogonal planes. Of course with the 3-D machine this would require no change of axes. The machine could simply go from one axis to

20. DISTRIBUTION / AVAILABILITY OF ABSTRACT	21. ABSTRACT SECURITY CLASSIFICATION	
☐ UNCLASSIFIED/UNLIMITED ☐ SAME AS RPT. ☐ DTIC USERS	Unclassified	
22a. NAME OF RESPONSIBLE INDIVIDUAL	22b. TELEPHONE (Include Area Code)	22c. OFFICE SYMBOL

DD FORM 1473, 84 MAR — 83 APR edition may be used until exhausted. All other editions are obsolete.

SECURITY CLASSIFICATION OF THIS PAGE
UNCLASSIFIED

another with a short pause between axes. Since the test would excite response from two directions of testing, it would be necessary to double the sweep rate, or halve the duration in some other manner. Three existing 1-D test levels would completely define the specification for such a test.

To improve on the 2-D sine test, it is necessary to give up on the sinusoidal test waveform. Much the same thing can be accomplished by using wavelets that are virtually all at a single frequency. Through a complicated procedure of rotating the circle from the 2-D test about an axis, and then tumbling the axis, a 3-D sine test can be achieved whose trajectory resembles a ball of string. The extent to which this test produces similar gains and fatigue cycle counts compared to the conventional 1-D test has been demonstrated. The 3-D test is better at exciting fatigue cycles spatially than three 1-D tests; however, since it does not have a sinusoidal waveform the gain is substantially reduced. Thus there are advantages and disadvantages to the 3-D sine test, while the 2-D sine test has no disadvantages. The 3-D test is also implementable without any extra data given three 1-D test levels.

The 3-D random test is specified in terms of the spectral matrix defining the state of vibration at the table. The appropriate 3-D test is achieved when the three 1-D test specifications are used as specification values for the diagonal with zero off diagonal terms. In order for the specification amplitudes to be the largest and smallest amplitudes experienced spatial from the test, it is necessary for the real part of the off diagonal terms to be zero. This insures that the specification values are the principal values for the Hermitian spectral matrix. The imaginary part of the spectral matrix can be any value, thus zero is a good choice. The imaginary part does not affect the PSD values at all, but determines the relative phase angles spatially. Since single structural modes do not respond to the relative phase angle, the imaginary part is less important than the real part.

In developing these results two potentially significant problems have been uncovered with the 3-D system. Traditionally signals for random testing are clipped at three sigma (i.e. three times the wideband RMS). Thus this same practice was followed for the 3-D system; each shaker output was individually clipped at three sigma. This produces a box shaped region where the test resides. Unfortunately the corners of the box are over five sigma away, thus raising the possibility of having repeated tests with unequal peak amplitudes. Worse, the peak amplitude is a function of spatial orientation. It is different in the shaker directions than at an angle to the shaker. This problem has now been widely understood and there are plans to correct it later in the program. The resultant vector will be clipped at a level consistent with the chi-squared distribution, e.g., 3.76 sigma.

The other problem that may have been uncovered is much newer and consequently hasn't reached the same level of maturity. The random control system reportedly operates on a preference order of 1) PSD values, 2) coherence magnitudes, and 3) phase angles. As was argued earlier, the real part of the spectral matrix is what matters. It would be better if the preference order was 1) PSD values, 2) real off diagonal values, 3) imaginary off diagonal values. This would control the structural response more adequately.

The work to date has been very successful in achieving the objectives sought. The project is in excellent position to move on to the "innovative" as opposed to "generic" part of the program.

Table of Contents

LIST OF FIGURES iv

LIST OF TABLES v

NOTATION v

GENERIC 3-D SINE TESTING 1-1

Introduction 1-1
Equations For the Generic 1-D Sine Test 1-1
Extension to Generic 2-D Sine Testing 1-3
The Rotated Circle Sine Test 1-5
The Tumbled Circle Test 1-7
Frequency Decomposition 1-10
Gain Spikes in 3-D 1-12
Steady State Shock Spectra in 3-D 1-17
Transient Response Shock Spectra 1-19
3-D Fatigue Cycle Counting 1-25
Conclusions 1-29

DISTRIBUTION THEORY IN 3-D RANDOM TESTING 2-1

Introduction 2-1
The Gaussian or Normal Distribution 2-1
The Standard Normal Distribution 2-3
The Spherical Normal Distribution 2-4
The Chi-Squared Distribution 2-7
Clipping the Resultant Vector 2-8
Implementation of Clipping on the Resultant Vector 2-11
Clipping the Component Amplitudes 2-12
The 2-D Clipped Distribution Function 2-12
The 3-D Clipped Distribution Function 2-18
Random Vibration Test Specification for Clipping 2-20
More Advanced Distribution Functions 2-20

COVARIANCE THEORY IN 3-D 3-1

Introduction 3-1
Basic Data 3-1
The Vector Method of Demonstrating the RMS Surface 3-2
Definition of the Covariance Matrix 3-3
RMS Values and the Correlation Matrix 3-4
Three Dimensional RMS 3-5
Principal Components of the Covariance Matrix 3-6
Physically Realizable Correlation Coefficients 3-9
Principal Directions of the Covariance Matrix 3-9
Euler angle transformation and the Principal RMS Values . . 3-11
Conclusions 3-11

Table of Contents

GENERIC 3-D RANDOM TESTING 4-1

Introduction 4-1
The Fourier Transform 4-1
Summation Versus Integration 4-3
The Spectral Matrix 4-4
Power Spectral Densities and the RMS Amplitude 4-7
The Coherence Function 4-7
The Transfer Function 4-10
Significance of Averaging 4-10
3-D Response of a Mode to Random Excitation 4-11
Meaning of Real/Imaginary Parts of the Spectral Matrix . . 4-12
Constraints on Specification Writers 4-13
Constraining the Real Part of the Spectral Matrix 4-17

EMPIRICAL 3-D RANDOM TEST RESULTS 5-1

Random Phase, Constant Amplitude Coherence 5-1
Constant Angle, Random Amplitude Coherence 5-5
90° Phase, Constant Amplitude Coherence 5-7
90° Phase, Random Amplitude Coherence 5-9
Conclusions 5-10

3-D COLOR GRAPHICS 6-1

Introduction 6-1
Operations Prior to Data Displays 6-3
Displays Autocorrelation and Cross Correlation 6-5
Displays Distribution Function 6-5
Displays Finite Fourier Transform 6-6
Displays Harmonic Analysis 6-6
Displays Oscillographs 6-7
Displays Principal Components 6-8
Displays Spectral Matrix 6-9
Displays Transfer Functions 6-10
Displays Wideband RMS and Tracking Filter 6-11
Displays Zoom Fourier Transform 6-12
Displays 3-D Oscilloscope 6-12
Conclusions 6-13

List of Figures

GENERIC 3-D SINE TESTING 1-1

Figure 1 Conventional 1-D Sine Test Modal Input by Direction 1-3
Figure 2 2-D Sine Test Modal Input by Direction 1-5
Figure 3 Rotated Circle Shaker Trajectory 1-6
Figure 4 Rotated Circle Time Histories 1-6
Figure 5 Tumbled Circle Test Shaker Trajectory 1-8
Figure 6 Tumbled Circle Test Time History 1-8
Figure 7 Steady State Z-Axis Input/Response For Tumbled Circle Test . 1-14
Figure 8 Rotated Circle Gain Spikes 1-15
Figure 9 Tumbled Circle Test Gain Spikes 1-16
Figure 10 Rotated Circle Gain as a Function of Latitude 1-17
Figure 11 Tumbled Circle Gain as a Function of Latitude 1-17
Figure 12 Rotated Circle Spatial Gain 1-18
Figure 13 Tumbled Circle Spatial Gain 1-19
Figure 14 Conventional Swept Sine Shock Spectra Input/Response . . . 1-20
Figure 15 Z Axis of Tumbled Circle Test Swept Input/Response. 1-21
Figure 16 Rotated Circle Gain Versus Sweep Rate 1-22
Figure 17 Tumbled Circle Test Gain Versus Sweep Rate 1-23
Figure 18 Rotated Circle Transient Spatial Gain 1-23
Figure 19 Tumbled Circle Test Transient Spatial Gain 1-24
Figure 20 1-D Sine Test Fatigue Cycle Surface 1-26
Figure 21 2-D Sine Test Fatigue Cycle Surface 1-26
Figure 22 Rotated Circle Fatigue Cycle Surface 1-27
Figure 23 Tumbled Circle Fatigue Cycle Surface 1-28

DISTRIBUTION THEORY IN 3-D RANDOM TESTING 2-1

Figure 1 Integrand of the Normal Distribution 2-2
Figure 2 Regions of the Clipped 2-D Distribution 2-12

COVARIANCE THEORY IN 3-D 3-1

Figure 1 General Ellipsoidal RMS Surface 3-7

EMPIRICAL 3-D RANDOM TEST RESULTS 5-1

Figure 1 Random Phase, Constant Amplitude Coherence 5-2
Figure 2 Constant Phase, Random Amplitude Coherence 5-4
Figure 3 90° Phase, Constant Amplitude Coherence 5-6
Figure 4 90° Phase, Random Amplitude Coherence 5-8

List of Tables

GENERIC 3-D SINE TESTING 1-1

Table 1 Rotated Circle Frequency Decomposition 1-10
Table 2 Tumbled Circle Test Frequency Decomposition 1-11

DISTRIBUTION THEORY IN 3-D RANDOM TESTING 2-1

Table 1 The Standard Normal Distribution 2-5
Table 2 Chi-Squared Probabilities 2-8
Table 3 The Chi-squared Distribution 2-9
Table 4 Extrema of the Chi-Squared Distribution 2-10
Table 5 2-D Box Clipping 2-15
Table 6 3-D Clipping Rate Vrs Frequency of Hitting Corner 2-19

Notation

A_j^x = the j-th amplitude in the finite Fourier expansion for X(t).

$A(X)$ = the probability of the standard normal distributed random variable x being in the region $-X \leq x \leq X$.

$A(x_1, x_2 | \mu, \sigma)$ = the probability of the normally distributed random variable X being in the region $x_1 \leq X \leq x_2$ given that the mean of X is μ and the standard deviation of X is σ.

A_i = i axis sine test amplitude, may vary with frequency.

C = any constant; in sine test gain calculations, the cosine term unknown coefficient being solved for.

C_0^x = the constant in the finite Fourier expansion, 0 because the mean of the data is zero.

C_j^x = the j-th cosine coefficient in the finite Fourier expansion for X(t).

$\cos_i$ = the direction cosine in the i axis direction.

$\vec{d}^{out}$ = a displacement value as opposed to acceleration or velocity.

$\{\vec{F}^i\}_{\ell \times 1}$ = the external forces applied at physical location ℓ and component i.

$\vec{F}_i(f)$ = the theoretical continuous Fourier transform of component i.

F_c = the force term associated with the cosine.

F_s = the force term associated with the sine.

$G_{ii}(f)$ = the real, ii-th term from the spectral matrix diagonal.

$\vec{G}_{ij}(f)$ = the complex, ij-th term from the spectral matrix.

[G] = the spectral matrix at a point in space.
3×3

$\vec{H}(\omega)$ = the transfer function for the modal gain spike.

$\vec{H}_{ij}(f)$ = the transfer function from the i-th component to the j-th component.

$\Im$ = the imaginary part of a complex number.

L = the number of terms in the finite Fourier series = (n-1)/2.

ℓ = the number of locations for the structural modes.

$L(X,Y|\rho)$ = the probability of the standard normal distributed random variables x and y being in the region $-\infty \le x \le X$ and $-\infty \le y \le Y$ given that the correlation coefficient between x and y is ρ, i.e., the bivariate normal distribution.

N = the number of frames used in averaging frequency domain data.

n = the number of data points in the time history being considered.

n = the sweep rate in octaves per minute for sine testing.

$N(X \ge 3\sigma)$ = a normal distribution where the region of interest is specified in the argument.

P = a probability.

P(X) = the probability of the standard normal distributed random variable x being in the region $-\infty \le x \le X$.

$P(\chi^2|v)$ = the probability of the chi-squared distributed random variable X^2 being in the region $0 \le X^2 \le \chi^2$ given there are v degrees of freedom.

$P(x|\mu,\sigma)$ = the probability of the normally distributed random variable X being in the region $-\infty \le X \le x$ given that the mean of X is μ and the standard deviation of X is σ.

$P(\langle X \rangle | [V])$ = the probability of the normally distributed random variables $\langle x \rangle$ all being in the region $-\infty \leq x_i \leq X_i$ given the values for the covariance matrix, V, i.e., the multivariate normal distribution.

$Q(X)$ = the probability of the standard normal distributed random variable x being in the region $X \leq x \leq \infty$.

$Q(x|\mu,\sigma)$ = the probability of the normally distributed random variable X being in the region $x \leq X \leq \infty$ given that the mean of X is μ and the standard deviation of X is σ.

q = intermediate variable calculating the roots of a 3×3 matrix.

q_j = the modal response of the j-th mode.

$\Re$ = the real part of a complex number.

r = intermediate variable calculating the roots of a 3×3 matrix.

R = the resultant vector or the radius vector depending on context.

$R(X)$ = the probability of the standard normal distributed random variable x being in either of the two regions $X \leq x \leq \infty$ and $-\infty \leq x \leq X$.

$R(x|\mu,\sigma)$ = the probability of the normally distributed random variable X being in either of the two regions $x \leq X \leq \infty$ and $-\infty \leq X \leq x$ given that the mean of X is μ and the standard deviation of X is σ.

$R_i(\theta)$ = the Euler angle rotation through θ angle about the i axis. 3×3

RMS = root mean square value.

RMS_i = the root mean square response of the i-th component.

S = the sine term unknown coefficient being solved for.

s_1 = intermediate variable calculating the roots of a 3×3 matrix.

s_2 = intermediate variable calculating the roots of a 3×3 matrix.

S_j^x = the j-th sine coefficient in the finite Fourier expansion for X(t).

$S(X,Y,Z)$ = the spherical normal distribution.

T = the time between samples = 1/sampling rate.

U_i = a column vector with one in component i and zero everywhere else. 3×1

V = the covariance matrix.

V_i = principal roots of the covariance matrix.

[V] = the covariance matrix.
3×3

V_{ii} = the variance or mean square value of the i-th component.

V_{ij} = the covariance between the i and j components.

X = a standard normal or normally distributed random deviate.

x = a normally distributed or standard normal random deviate.

X(t) = the time history for the X axis.

<X> = a row vector of normally distributed random deviates.

{X} = a column vector of normally distributed random deviates.

[X] = the observations matrix: number of data points by 3 coordinates.
n×3

[X'] = the transpose of [X]. In general, prime means transpose.
3×n

x_i = the x component of the i-th 3-D data point.

$\bar{x}$ = the average value of the x components of the data <u>assumed zero</u>.

X_{new} = rescaled values of the x_i data found by dividing by RMS_x.

Y = a standard normal distributed random deviate usually associated with the Y axis shaker.

Y(t) = the time history for the Y axis.

y_i = the y component of the i-th 3-D data point.

$\bar{y}$ = the average value of the y components of the data <u>assumed zero</u>.

Y_{new} = rescaled values of the y_i data found by dividing by RMS_y.

Z = A standard normal distributed random deviate usually associated with the Z axis shaker.

Z(t) = the time history for the Z axis.

$Z(x|\mu,\sigma)$ = the integrand of the normal distribution with mean μ and standard deviation σ.

z_i = the z component of the i-th 3-D data point.

$\bar{z}$ = the average value of the z components of the data assumed zero.

Z_{new} = rescaled values of the z_i data found by dividing by RMS_z.

α = any angle.

β = any angle.

$\bar{\gamma}_{ij}(f)$ = the coherence function between the i-th and j-th components.

ζ_j = the critical damping ratio of the j-th mode.

θ = Euler angle rotation about z.

θ_j^x = the j-th phase angle in the finite Fourier expansion for X(t).

$\theta_i(f)$ = the phase angle of the i-th component at a frequency.

λ = the perturbation variable in the characteristic equation.

μ = the mean of a random variable.

ρ_{ij} = the correlation coefficient between the i and j components.

σ = the standard deviation of a random variable.

τ_i = the tumble frequency about the i direction.

ϕ = Euler angle rotation about y.

ϕ_i = modal response in direction i at the shaker head.

$\{\phi\}_{3\times1}$ = a general rotation vector, i.e., $\phi_x^2+\phi_y^2+\phi_z^2=1$.

$[\phi]_{3\times3}$ = the eigen values of the variance matrix.

$\langle\phi_j^i\rangle_{1\times\ell}$ = the mode shape for the j-th mode over all i locations.

χ^2 = A chi-squared distributed random deviate.

ψ = Euler angle rotation about x.

ψ = the input sinusoid initial phase angle with respect to t=0.

ω = forcing frequency in radians/second.

$\omega(t)$ = the swept sinusoidal time history.

ω_j = the modal frequency (in radians/sec) of the j-th mode.

ω_n = the undamped natural frequency of the mode.

ω_o = the initial frequency for the swept sine test.

* = the complex conjugate, i.e., $\vec{z}_{ij}{}^*\vec{z}_{ji} = \Re\vec{z}_{ij}\Re\vec{z}_{ji} + \Im\vec{z}_{ij}\Im\vec{z}_{ji}$.

$\bar{}$ = the average value.

$\vec{}$ = a complex quantity with an amplitude and a phase.

$\hat{}$ = a rotated value in some other orientation than the original X, Y, Z orientation.

$\angle$ = the phase angle of a complex quantity.

$|\vec{x}|$ = the magnitude of a complex quantity or determinant of a matrix.

$\simeq$ = the point in the equations where continuous theoretical variables are equated to physical quantities.

CHAPTER 1 GENERIC 3-D SINE TESTING

INTRODUCTION

Work has been underway for several years on a three axis test machine at Harry Diamond Laboratories (HDL).[1] At this time a 3-D test machine is a one of a kind item built to the specifications of the customer. Other 3-D test facilities exist and some information is available about 3-D random testing, however, there doesn't appear to be information about 3-D sine testing. HDL has requirements to test hardware with sine tests and would like a test procedure that can be implemented based on the existing 1-D test specification. Such a test has been termed a "generic" sine test as opposed to an "innovative" test technique.

Since the 3-D system has three shakers and is capable of operating in three dimensions at once, it seems reasonable that a 3-D system could perform a single test in 3-D that would be equivalent to testing in three independent directions with conventional equipment. The test time should be reduced to 1/3 the time for three conventional one axis tests. Also, the added capability of controlling in 3-D should allow better spatial coverage. Instead of being satisfied with shaking the test article to the test level in three orthogonal directions, it should be possible to shake the test article to the prescribed levels in *all* possible directions.

Unfortunately, the sinusoidal waveform is, at most, fundamentally 2-D. As will be demonstrated, it is not possible to shake in three dimensions at once with sinusoidal forcing, e.g., to have three orthogonal components being excited at a single frequency at the same time. By testing in a circle in 2-D it is possible to excite two dimensions at once with sinusoidal forcing. Performing three orthogonal tests in circles is the *simplest and probably the best* solution to sine testing in 3-D. However, true 3-D testing can be achieved by rotating the circle. Using this approach the time history is sinusoidal in one direction and a modulated sinusoid in the other two directions. There is a preferred orientation. By slowly rotating in multiple directions at different frequencies thus tumbling the circle, all directions become reasonably equal. The spatial trajectory for this test looks fairly random, and the time histories in all three directions are roughly equivalent, modulated sinusoids.

EQUATIONS FOR THE GENERIC 1-D SINE TEST

In 1-D, the shaker motion of the conventional sine test can be represented by the following very simple equation:

$$X(t) = A_X \sin(\omega t) \qquad 1)$$

Where the frequency, ω, is typically swept at a sweep rate of n octaves/min as shown below (t is assumed to be in seconds):

$$\omega(t) = \omega_o \, e^{(\ln 2/60)nt} \qquad 2)$$

Exponential sweep rates result in a constant change in frequency per cycle of the resulting test. Differentiating Equation 2 ($\partial\omega/\partial t$) gives Equation 3:

$$\Delta\omega/\text{cycle} = (\partial\omega/\partial t)\ (1/\omega) = (\ln 2/60)\ n = .011552\ n \qquad 3)$$

Equation 3 says that for each cycle of the sine test, the frequency advances a constant amount. At n=1 oct/min sweep rate, the frequency increases by .011552 Hz on every cycle no matter what frequency the cycle occurs at.

The frequency delta between half power points on a mode is about $2\zeta\omega$. Thus the number of cycles between half power points on a mode is as shown in Equation 4:

$$\text{cycles} = 2\zeta\omega\ /\ (\ln 2/60)n \qquad 4)$$

Evaluating this expression at normal test values, e.g., $Q = 1/2\zeta = 20$ so $\zeta = .025$, n= 2 oct/min, ω = 10 Hz = 62.8 radians/sec gives 136 cycles between the half power points. The value of 136 cycles is a low value for typical operation. At very low frequencies, low damping, or high sweep rates the number of cycles between half power points can be even lower. In order for a 3-D test to use conventional swept sine sweep rates, it is necessary for the 3-D surface to be spatially covered many times in 136 cycles.

The conventional sine test is extended into 3-D by performing three 1-D sine tests in three orthogonal directions. By doing this, a structural mode oriented in any arbitrary direction is excited by the component of each sine test in the modes' direction. Suppose the local mode shape at the shaker interface is $\langle\phi_x,\phi_y,\phi_z\rangle$. Normalizing this vector, gives the direction cosines for the mode's local direction:

$$\text{dir cos} = \left\langle \frac{\phi_x}{\sqrt{\phi_x^2+\phi_y^2+\phi_z^2}}, \frac{\phi_y}{\sqrt{\phi_x^2+\phi_y^2+\phi_z^2}}, \frac{\phi_z}{\sqrt{\phi_x^2+\phi_y^2+\phi_z^2}} \right\rangle = \langle \cos_x, \cos_y, \cos_z \rangle \qquad 5)$$

The component of each sine test in the mode's local direction is simply the dot product of the direction cosines times the amplitude of the test oriented along each axis:

$$\begin{aligned} &\text{component from X test} = \langle A_x,0,0\rangle \cdot \langle \cos_x,\cos_y,\cos_z\rangle = A_x\cos_x \\ &\text{component from Y test} = \langle 0,A_y,0\rangle \cdot \langle \cos_x,\cos_y,\cos_z\rangle = A_y\cos_y \qquad 6) \\ &\text{component from Z test} = \langle 0,0,A_z\rangle \cdot \langle \cos_x,\cos_y,\cos_z\rangle = A_z\cos_z \end{aligned}$$

The mode will respond along it's local direction to each of these three inputs in turn. By plotting the locus of the points over all direction cosines from a single 1-D sine test, one obtains two circles in 2-D or two spheres in 3-D. A three view drawing of the surface for a single Z axis test is shown in Figure 1. Figure 1 illustrates the amplitude of the input to a mode as a function of direction. A ray from the origin intercepts the surface in Figure 1 at a value indicating the amplitude a mode in that direction would experience as its input. The largest input is equal to one and occurs when the mode is directed along the Z axis in the test direction. The input is attenuated to zero when the mode lies in the X-Y plane. The sine test shaker head motion would plot as a line between -1 and 1 along the Z axis.

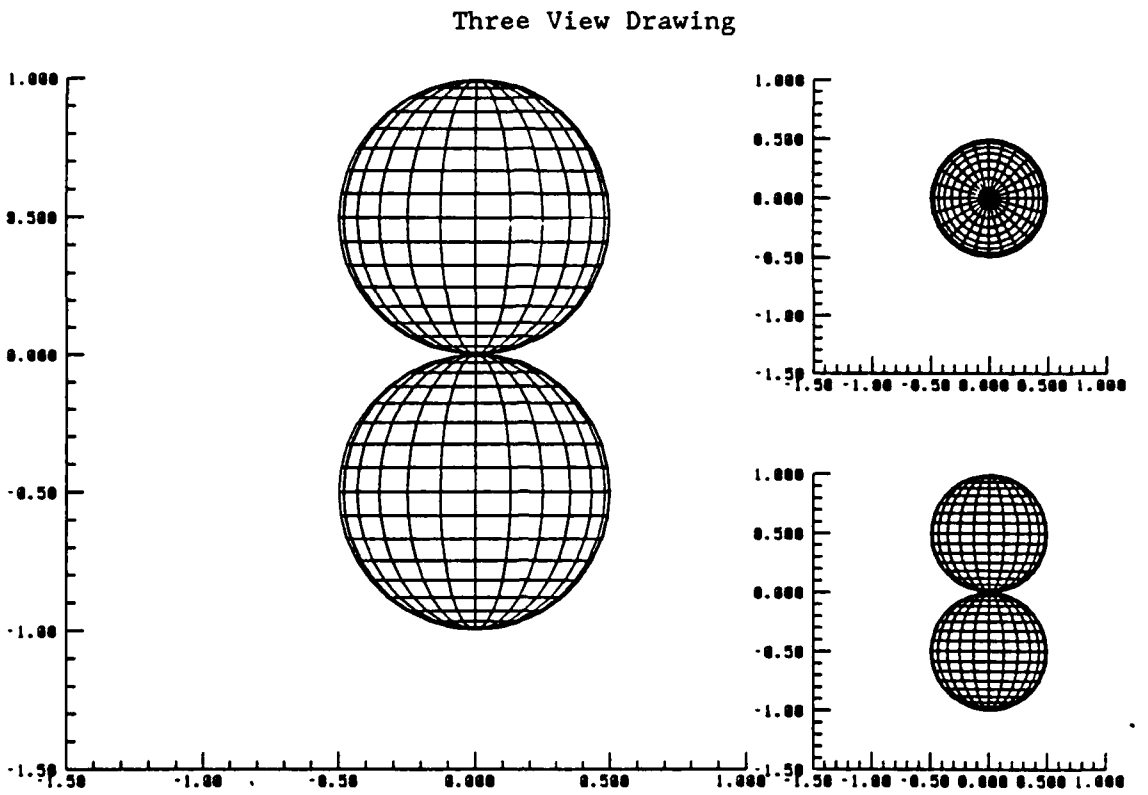

Figure 1 Conventional 1-D Sine Test Modal Input by Direction

EXTENSION TO GENERIC 2-D SINE TESTING

By shaking in a circle it is possible to shake in two directions at once using sinusoidal forcing. Two orthogonal components can be exciting at the same time by using a sine in one direction and a cosine in the other direction.

$$X(t) = A_X \sin(\omega t)$$
$$Z(t) = A_Z \cos(\omega t) \qquad \text{where: } \omega(t) = \omega_o \, e^{(\ln 2/60)nt} \qquad 7)$$

This is a very efficient method of sine testing because the shaker is moving at full amplitude at all times during the test. In the conventional 1-D test, the shaker head spends most of its time in the vicinity of the origin. Using a circle, the shaker head never goes through the origin at all. The shaker is always testing at full amplitude in some direction. Since the waveform is sinusoidal the shock spectra response, fatigue cycle count, frequency content, and sweep rate attenuation are all exactly the same in the test axis directions as for a conventional 1-D sine test. Further, in the plane of the test, all of these quantities are the same in *any* direction if the input levels are equal. If the input levels are not equal, the envelopes are ellipsoidal with the two test levels as the major and minor axes.

When one axis can be eliminated, it is sufficient to run the shaker in only one swept 2-D test. When many specimens are tested at once and they are randomly oriented in the test fixture, one 2-D test will suffice. Alternatively, a 2-D

test might be used when there is an axis of symmetry in the test specimen. Under either of these conditions, the circular test is ideal. The elapsed test time can be cut by half and only one axis of test is required.

To achieve 3-D spatial coverage with this test, it is necessary to operate one at a time in three circles at right angles to each other. Three separate tests must be run, but no axis changes need to be made, since the shaker system moves in all three directions. The X-Z test would excite both the X and Z axis fully, the X-Y test would excite both the X and Y axis fully, and finally the Y-Z test would excite both the Y and Z axis fully. Notice two tests excite each axis fully. To avoid putting twice as many cycles on the test article as in three 1-D tests, it is necessary to either double the sweep rate, or perform up sweeps on one test and down sweeps on another test, or some other procedure to halve the test time.

The circular test is by far the simplest test identified to date that takes advantage of the 3-D shaker. It achieves improved spatial coverage because the entire plane is tested to an ellipsoidal level (if $A_X \neq A_Z$) instead of simply orienting all the energy along the axes. For example, consider a mode at the direction cosines from Equation 5

$$\text{component from X-Z test} = \langle A_x,0,A_z\rangle \cdot \langle \cos_x,\cos_y,\cos_z\rangle = A_x\cos_x + A_z\cos_z$$

$$\text{component from X-Y test} = \langle A_x,A_y,0\rangle \cdot \langle \cos_x,\cos_y,\cos_z\rangle = A_x\cos_x + A_y\cos_y \qquad 8)$$

$$\text{component from Y-Z test} = \langle 0,A_y,A_z\rangle \cdot \langle \cos_x,\cos_y,\cos_z\rangle = A_y\cos_y + A_z\cos_z$$

Since the sine test amplitudes go in both the plus and minus directions, the extra term in Equation 8 always adds to the amplitude in one direction or the other. Thus the amplitude from the 2-D test is always larger than the amplitude from the 1-D test. It is equal to the 1-D test plus a positive term. The maximum deviation from the ideal spherical surface for the 2-D sine test occurs at 45° to the test axis and is exactly equal to the worst behavior for the 1-D test at the same angle. However, for three axes of 2-D tests there are only eight points where this worst case behavior occurs, while there are eight lines where the worst case occurs in three axes of 1-D tests.

Plotting the locus of the maximum of these points over all combinations of direction cosines, one obtains a circle in 2-D (i.e., at full amplitude) or a circular donut in 3-D as shown in Figure 2. Figure 2 illustrates the amplitude of the input to a mode from an X-Y, 2-D sine test as a function of direction assuming the shakers move in a circle (i.e., $A_X = A_Y$).

The 2-D test improves the spatial coverage and doubles the test time with no losses at all. There is still some attenuation in the off axis directions (i.e., ideally Figure 2 should be a sphere) but it is as good or better than the conventional three 1-D tests. To keep the fatigue cycle count the same (e.g., in the test axis directions), it is necessary to halve the test duration, since each test is operating in two directions at a time. This test is the simplest test found to date and has very few drawbacks. *This probably is the test that will ultimately be accepted by the testing community.*

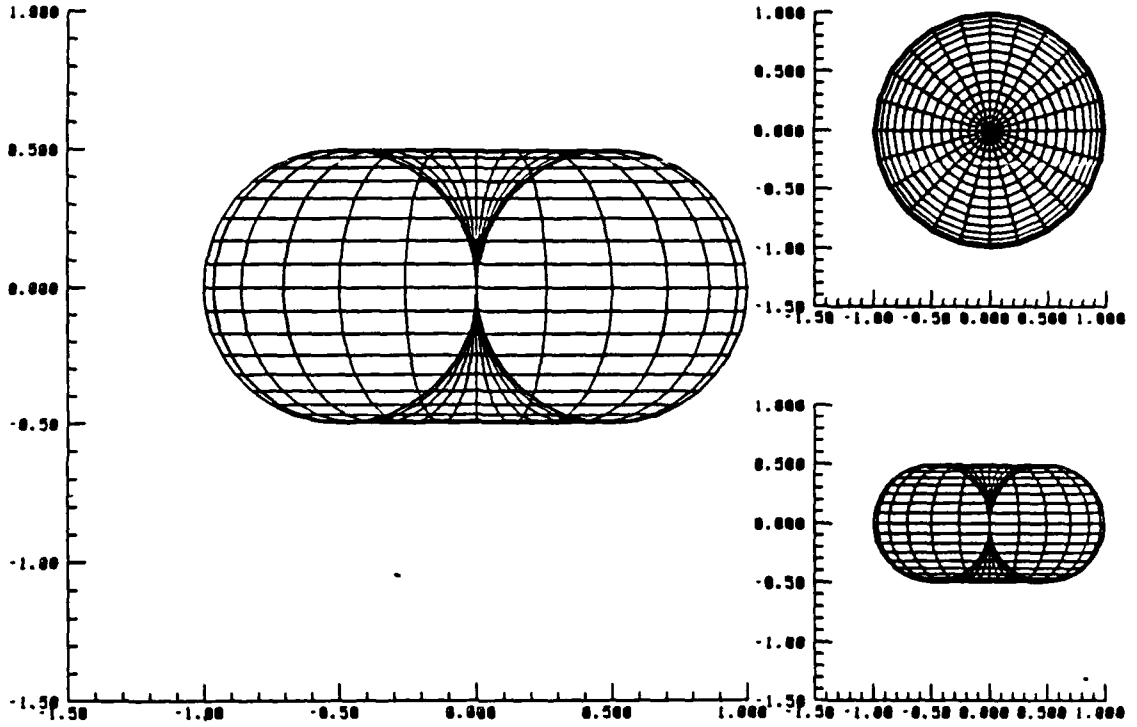

Figure 2 2-D Sine Test Modal Input by Direction

The trick used to obtain a circle in the 2-D test is to use both the sine and the cosine together. These are orthogonal functions and produce 2-D motion. If only sines or only cosines are used, the motion would be planar, along a line at an angle to the axes. To do the same thing in three dimensions, one would need a third function at the same frequency, which is orthogonal to both the sine and cosine. Since no such function can exist (a result from orthogonality), it is not possible to produce a 3-D test similar to the 2-D test. Some other approach is required.

THE ROTATED CIRCLE SINE TEST

Sine testing implies a specific 1-D waveform. Strictly speaking a sine test requires a sinusoidal waveform operating at one frequency. However, even in the conventional 1-D test this has been modified. Frequencies are swept exponentially with a slow sweep rate as illustrated in Equation 2. This introduces low amplitude harmonics of the fundamental sine frequency, but it allows continuous frequency coverage.[2] When 3-D is introduced into sine testing, it is also necessary to compromise the waveform to achieve spatial coverage. The only really good option available for doing this is to continuously move the direction of shake while the frequency is being swept.

The problem is deciding what constitutes a sine test. In its purest form, a sine test is 1-D at one frequency. Since this is impractical, it is necessary to decide how much to compromise. As a working definition, a test is a sine

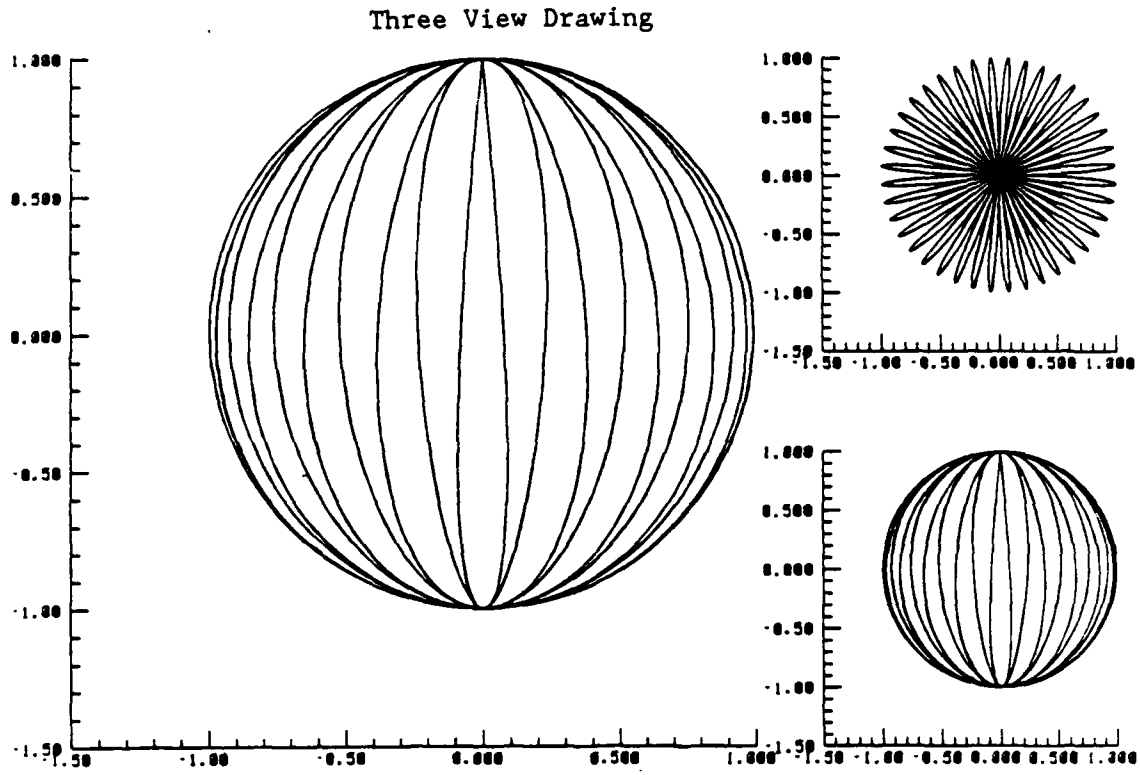

Figure 3 Rotated Circle Shaker Trajectory

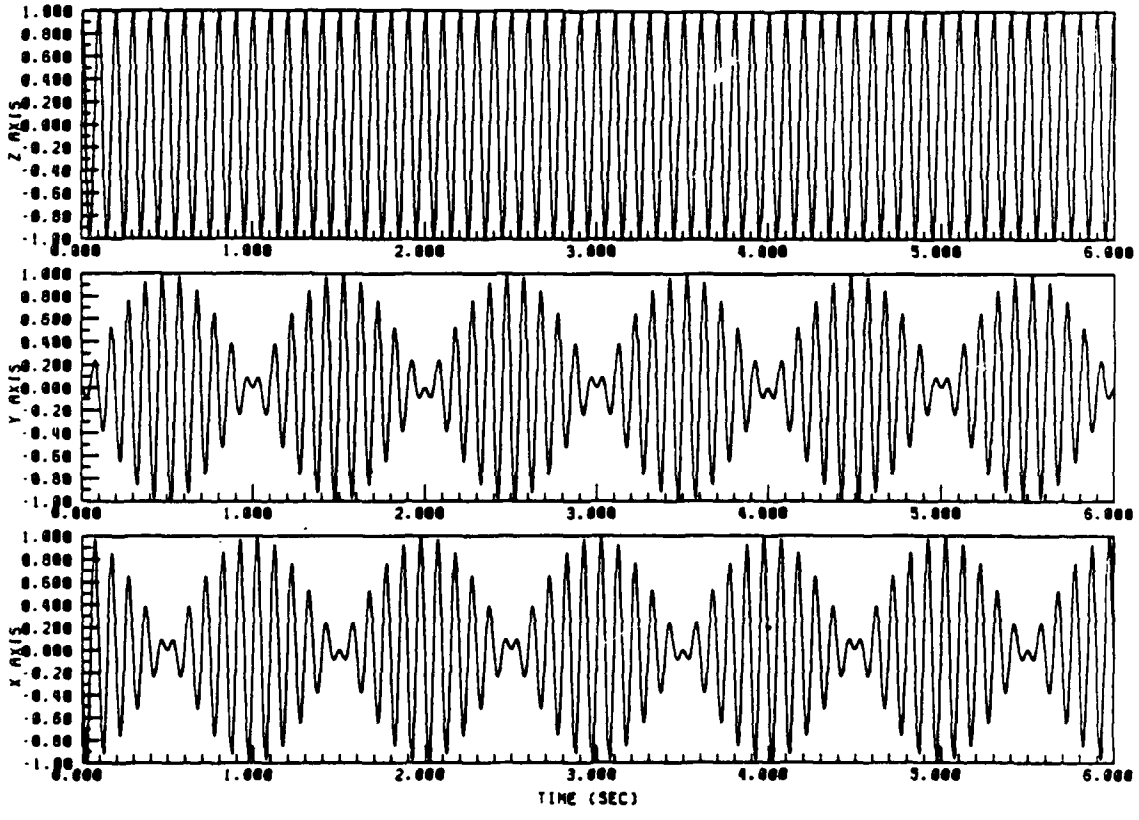

Figure 4 Rotated Circle Time Histories

test if 1) the fundamental frequency is about 20 times the fastest subharmonic and 2) the orthogonal components of the test are modulated sinusoids in waveform and mapped on the ideal ellipsoidal surface. In the form of equations, this is as shown below:

$$X = A_X \cos\theta \sin\phi \qquad \text{Where:} \quad \theta = \omega_\theta t \quad \leftarrow \text{subharmonic}$$

$$Y = A_Y \sin\theta \sin\phi \qquad \phi = \omega t \quad \leftarrow \text{fundamental} \qquad 9)$$

$$Z = A_Z \cos\phi$$

And the requirement that the fundamental is at least 20 times the subharmonics is as follows:

$$\omega \geq 20\ \omega_\theta \qquad 10)$$

Equation 9 is not nearly as complicated as it may appear. It is just the familiar transformation between spherical and cartesian coordinates. Because of the requirement that the sine test must be mapped on an ellipsoid, this is all the complexity that the assumptions can support.

Figure 3 illustrates the shaker head motion for this system of equations. The time for the test to repeat in space is given by $1/\omega_\theta$ which is related to the fundamental frequency by enforcing equality in Equation 10. As long as the ratio of the two frequencies is kept fixed, the shaker head motion will move in exactly the same trajectory while the frequency is swept.

Assuming that the fundamental is at 10.0 Hz then the subharmonic is at 0.5 Hz (i.e., 10 Hz/20 = 0.5 Hz). The time to repeat for this waveform is 2.0 seconds (i.e., period = 1/0.5 Hz = 2.0 seconds). At ten Hertz this is 20 cycles which is adequate compared to the 136 cycles between half power points for Q=20. Time histories for the motions along the three axes are shown in Figure 4. Notice that the waveforms in the X and Y directions are modulated sinusoids - an unavoidable consequence of testing in 3-D. Inspecting the shaker trajectory, the spatial coverage is dramatically better than could be obtained with either the conventional or 2-D sine test. The waveform illustrated in Figures 3 and 4 is one possible solution for the 3-D generic sine test.

Still, this test has a few drawbacks. It spends a larger amount of time testing the Z axis than the other two axes. In fact, the time history in the Z direction (Equation 9 with $\phi = \omega t$) is a pure sinusoid (i.e., $A_Z\cos(\omega t)$). The other two directions are tested equally, but receive significantly less attention than the Z axis. Also notice that this test spends too much time at the poles along the Z axis. Much more time is spent there than at the equator in the X-Y plane.

THE TUMBLED CIRCLE TEST

To overcome these problems, it is possible to move the Z axis from Figure 3 slowly in space so the preferential treatment is distributed over space. Mathematically we need to introduce unitary rotations as follows:

Three View Drawing

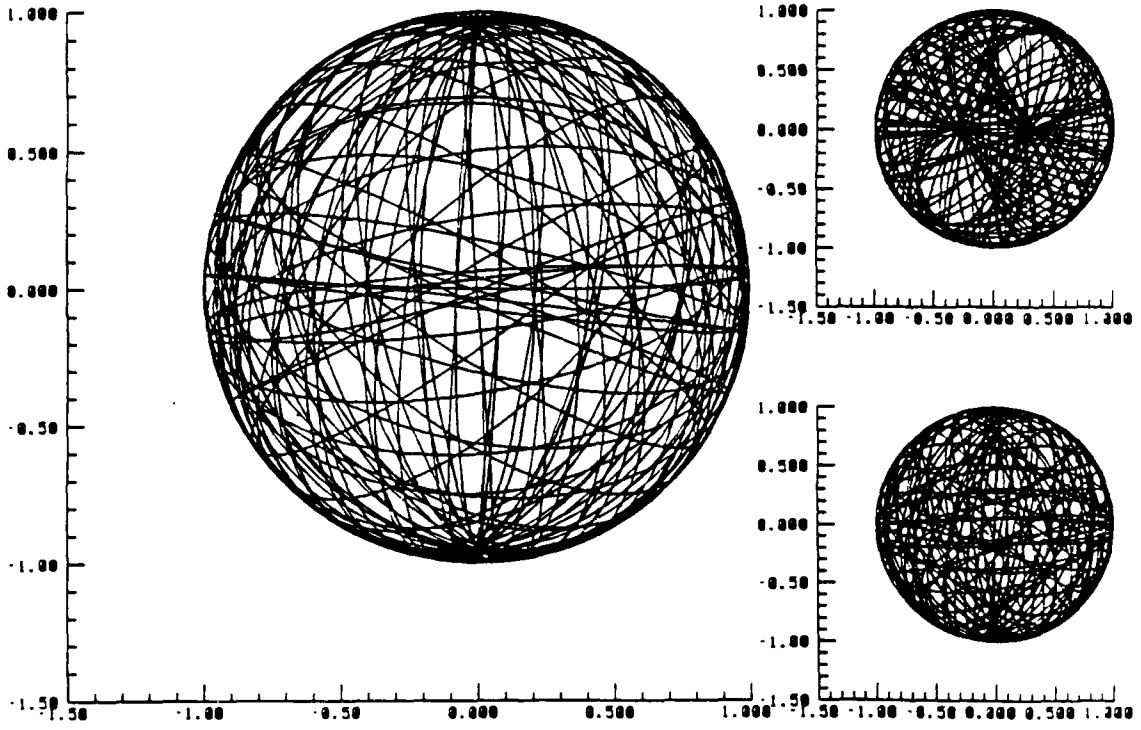

Figure 5 Tumbled Circle Test Shaker Trajectory

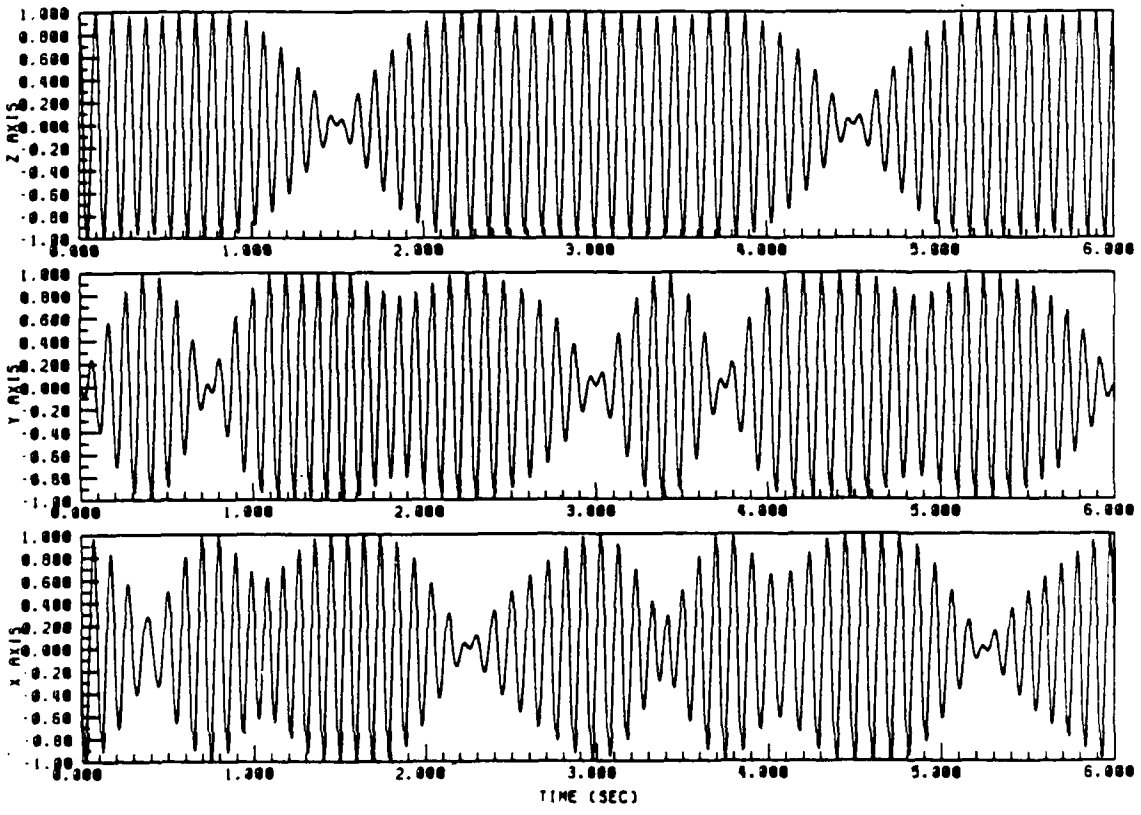

Figure 6 Tumbled Circle Test Time History

$$R_{x}(\theta)_{3\times3} = \begin{bmatrix} 1 & 0 & 0 \\ 0 & \cos\theta & -\sin\theta \\ 0 & \sin\theta & \cos\theta \end{bmatrix} \qquad U_{x_{3\times1}} = \begin{Bmatrix} 1 \\ 0 \\ 0 \end{Bmatrix}$$

$$R_{y}(\theta)_{3\times3} = \begin{bmatrix} \cos\theta & 0 & -\sin\theta \\ 0 & 1 & 0 \\ \sin\theta & 0 & \cos\theta \end{bmatrix} \qquad U_{y_{3\times1}} = \begin{Bmatrix} 0 \\ 1 \\ 0 \end{Bmatrix} \tag{11}$$

$$R_{z}(\theta)_{3\times3} = \begin{bmatrix} \cos\theta & -\sin\theta & 0 \\ \sin\theta & \cos\theta & 0 \\ 0 & 0 & 1 \end{bmatrix} \qquad U_{z_{3\times1}} = \begin{Bmatrix} 0 \\ 0 \\ 1 \end{Bmatrix}$$

To obtain a 2-D circle, we simply have to multiply one of the rotations, R, by U as follows:

$$R_{y}(\omega t)_{3\times3} U_{z_{3\times1}} = \begin{bmatrix} \cos\omega t & 0 & -\sin\omega t \\ 0 & 1 & 0 \\ \sin\omega t & 0 & \cos\omega t \end{bmatrix} \begin{Bmatrix} 0 \\ 0 \\ 1 \end{Bmatrix} = \begin{Bmatrix} -\sin\omega t \\ 0 \\ \cos\omega t \end{Bmatrix} \tag{12}$$

To upgrade to the rotated circle test, we add another rotation in front of Equation 12:

$$R_{z}(\omega_{\theta} t)_{3\times3} R_{y}(\omega t)_{3\times3} U_{z_{3\times1}} = \begin{bmatrix} \cos\omega_{\theta} t & -\sin\omega_{\theta} t & 0 \\ \sin\omega_{\theta} t & \cos\omega_{\theta} t & 0 \\ 0 & 0 & 1 \end{bmatrix} \begin{Bmatrix} -\sin\omega t \\ 0 \\ \cos\omega t \end{Bmatrix} = \begin{Bmatrix} -\sin\omega t \cos\omega_{\theta} t \\ -\sin\omega t \sin\omega_{\theta} t \\ \cos\omega t \end{Bmatrix} \tag{13}$$

There are some basic requirements on this kind of rotation. If two rotations in a row occur about the same axis they are equivalent to one rotation with the sum of the angles (e.g., $R_x(\theta)R_x(\phi) = R_x(\theta+\phi)$). Also, if a rotation is about an axis, it doesn't change that axis's time history at all (e.g., $R_x(\omega t)$ doesn't change X(t) at all because of the one in the rotation matrix). Finally, if you want a left handed rotation, simply change the sign of the frequency term (e.g., $-\omega t$ gives counter clockwise rotation). The reason there is a sign difference between Equation 13 and Equation 9 is that the fundamental rotation, ω, is going in the opposite direction.

To achieve the tumbled circle test, we must add two more rotations in the middle of Equation 13. Two rotations are required instead of just one rotation because whatever axis we rotate about must not be the same axis as the previous rotation to avoid summing the angles, and a rotation about either of the other two axes leaves the axis rotated about undisturbed. Thus the tumbled circle test is structured as shown in Equation 14 and illustrated in Figure 5:

$$R_{z}(\omega_{\theta} t)_{3\times3} R_{y}(\tau_{y} t)_{3\times3} R_{x}(\tau_{x})_{3\times3} R_{y}(\omega t)_{3\times3} U_{z_{3\times1}} =$$

$$\begin{bmatrix} \cos\omega_{\theta} t & -\sin\omega_{\theta} t & 0 \\ \sin\omega_{\theta} t & \cos\omega_{\theta} t & 0 \\ 0 & 0 & 1 \end{bmatrix} \begin{bmatrix} \cos\tau_{y} t & 0 & -\sin\tau_{y} t \\ 0 & 1 & 0 \\ \sin\tau_{y} t & 0 & \cos\tau_{y} t \end{bmatrix} \begin{bmatrix} 1 & 0 & 0 \\ 0 & \cos\tau_{x} t & -\sin\tau_{x} t \\ 0 & \sin\tau_{x} t & \cos\tau_{x} t \end{bmatrix} \begin{Bmatrix} -\sin\omega t \\ 0 \\ \cos\omega t \end{Bmatrix} \tag{14}$$

While this is messy as an expression for a time history, it produces more satisfactory time histories illustrated in Figure 6. Empirically, the time histories have more cycles together with significant amplitudes if the higher

frequencies are to the outside of the rotation (e.g. ω_θ should be higher than τ_X). Because of the order of the frequencies, the time history shown in Figure 6 has more large cycles together than the time history in Figure 4 for the rotated sine test. It doesn't seem to make very much difference what sign is chosen for the rotations, the features of the test move from axis to axis with sign changes, but the amplitudes are unaffected.

Figure 6 illustrates a test of the form of Equation 14 with ω_θ=1/2 Hz and τ_Y=1/3 Hz and τ_X=1/6 Hz, with the fundamental, ω=10 Hz. The choice of frequencies to tumble the data at comes from the need to have the waveform repeat itself after a fairly short period of time. There are two main advantages to having the waveform repeat itself: 1) the test time history can be built in frames that have the digitization rate changed and nothing else, this potentially simplifies the test control system, and 2) with a repeating waveform it is easy to analyze whether the spatial coverage is adequate. If the waveform doesn't repeat, it is necessary to study the entire frequency range to see if there are gaps in the spatial coverage.

To obtain a waveform that repeats, it is necessary for the three tumble frequencies, τ_X=1/6 Hz, τ_Y=1/3 Hz, and ω_θ=1/2 Hz, to have periods that are multiples of each other. In the case from Figure 6, all three frequencies repeat after 6 seconds, τ_X goes through 1 oscillation, τ_Y goes through 2 oscillations, and ω_θ goes through 3 oscillations. Of course during a sine sweep these frequencies would move together. At ω=20 Hz the three tumble frequencies would be: ω_θ=1 Hz and τ_Y=2/3 Hz and τ_X=1/3 Hz. The shaker path from Figure 5 remains exactly the same for the entire sweep, only the rate that it moves around the path changes. For the second set of frequencies at 20 Hz, the period to repeat is three seconds instead of six seconds.

FREQUENCY DECOMPOSITION

A good intermediate step to understanding the waveforms from these two tests is to decompose them into individual frequencies. While this is rather tedious in the case of a complicated waveform like Equation 14, it greatly simplifies subsequent calculations since the waveform can be expressed as a sum of sine waves. To illustrate the procedure consider the rotated circle test:

$$X(t) = A_X \sin \omega t \cos \omega_\theta t = A_X \left[\tfrac{1}{2}\sin(\omega_\theta+\omega)t - \tfrac{1}{2}\sin(\omega_\theta-\omega)t\right]$$

$$Y(t) = A_y \sin \omega t \sin \omega_\theta t = A_y \left[\tfrac{1}{2}\cos(\omega_\theta-\omega)t - \tfrac{1}{2}\cos(\omega_\theta+\omega)t\right] \qquad 15)$$

$$Z(t) = A_Z \cos \omega t$$

These results can be summarized in Table 1 below:

Table 1 Rotated Circle Frequency Decomposition

Frequency	Hz	X		Y		Z	
		cos	sin	cos	sin	cos	sin
$\omega+\omega_\theta$	10.5000	(0.000,	0.500)	(0.500,	0.000)	(0.000,	0.000)
$\omega-\omega_\theta$	9.5000	(0.000,	-0.500)	(-0.500,	0.000)	(0.000,	0.000)
ω	10.0000	(0.000,	0.000)	(0.000,	0.000)	(1.000,	0.000)

Any waveform that is composed of the products of sines and cosines can be decomposed into sums of sines and/or cosines at frequencies which cover all the permutations of sums and differences of the original frequencies. Thus X(t) and Y(t) are expressed in terms of the frequencies $(\omega+\omega_\theta)$ and $(\omega-\omega_\theta)$. The fundamental only appears as a positive number, while all permutations of the other frequencies are covered. Also, the frequency of the fundamental, ω, doesn't appear at all as a single frequency unless some of the sums cancel.

This process is susceptible to computer analysis. The tumbled circle test decomposition in Table 2 was produced with a computer code that recognizes all possible combinations of sine and cosine products and knows the decomposition of all four possible products:

$$\sin\alpha \sin\beta = \tfrac{1}{2}\cos(\alpha-\beta) - \tfrac{1}{2}\cos(\alpha+\beta)$$

$$\cos\alpha \cos\beta = \tfrac{1}{2}\cos(\alpha-\beta) + \tfrac{1}{2}\cos(\alpha+\beta) \qquad (16)$$

$$\sin\alpha \cos\beta = \tfrac{1}{2}\sin(\alpha+\beta) + \tfrac{1}{2}\sin(\alpha-\beta)$$

$$\cos\alpha \sin\beta = \tfrac{1}{2}\sin(\alpha+\beta) - \tfrac{1}{2}\sin(\alpha-\beta)$$

Table 2 Tumbled Circle Test Frequency Decomposition

Frequency	Hz	X		Y		Z	
		cos	sin	cos	sin	cos	sin
$\omega+\tau_y+\omega_\theta$	10.8333	(0.000,-0.250)		(0.250, 0.000)		(0.000, 0.000)	
$\omega+\tau_y-\omega_\theta$	9.8333	(0.000,-0.250)		(-0.250, 0.000)		(0.000, 0.000)	
$\omega-\tau_y+\omega_\theta$	10.1667	(0.000,-0.250)		(0.250, 0.000)		(0.000, 0.000)	
$\omega-\tau_y-\omega_\theta$	9.1667	(0.000,-0.250)		(-0.250, 0.000)		(0.000, 0.000)	
$\omega+\tau_x+\tau_y+\omega_\theta$	11.0000	(0.000,-0.125)		(0.125, 0.000)		(0.000, 0.000)	
$\omega+\tau_x+\tau_y-\omega_\theta$	10.0000	(0.000,-0.125)		(-0.125, 0.000)		(0.000, 0.000)	
$\omega+\tau_x-\tau_y+\omega_\theta$	10.3333	(0.000, 0.125)		(-0.125, 0.000)		(0.000, 0.000)	
$\omega+\tau_x-\tau_y-\omega_\theta$	9.3333	(0.000, 0.125)		(0.125, 0.000)		(0.000, 0.000)	
$\omega-\tau_x+\tau_y+\omega_\theta$	10.6667	(0.000,-0.125)		(0.125, 0.000)		(0.000, 0.000)	
$\omega-\tau_x+\tau_y-\omega_\theta$	9.6667	(0.000,-0.125)		(-0.125, 0.000)		(0.000, 0.000)	
$\omega-\tau_x-\tau_y+\omega_\theta$	10.0000	(0.000, 0.125)		(-0.125, 0.000)		(0.000, 0.000)	
$\omega-\tau_x-\tau_y-\omega_\theta$	9.0000	(0.000, 0.125)		(0.125, 0.000)		(0.000, 0.000)	
$\omega+\tau_x+\omega_\theta$	10.6667	(-0.250, 0.000)		(0.000,-0.250)		(0.000, 0.000)	
$\omega+\tau_x-\omega_\theta$	9.6667	(0.250, 0.000)		(0.000,-0.250)		(0.000, 0.000)	
$\omega-\tau_x+\omega_\theta$	10.3333	(0.250, 0.000)		(0.000, 0.250)		(0.000, 0.000)	
$\omega-\tau_x-\omega_\theta$	9.3333	(-0.250, 0.000)		(0.000, 0.250)		(0.000, 0.000)	
$\omega+\tau_y$	10.3333	(0.000, 0.000)		(0.000, 0.000)		(0.500, 0.000)	
$\omega-\tau_y$	9.6667	(0.000, 0.000)		(0.000, 0.000)		(-0.500, 0.000)	
$\omega+\tau_x+\tau_y$	10.5000	(0.000, 0.000)		(0.000, 0.000)		(0.250, 0.000)	
$\omega+\tau_x-\tau_y$	9.8333	(0.000, 0.000)		(0.000, 0.000)		(0.250, 0.000)	
$\omega-\tau_x+\tau_y$	10.1667	(0.000, 0.000)		(0.000, 0.000)		(0.250, 0.000)	
$\omega-\tau_x-\tau_y$	9.5000	(0.000, 0.000)		(0.000, 0.000)		(0.250, 0.000)	

Structures respond to the harmonic decomposition frequencies just like they were input as single frequencies. Superposition holds for linear differential equations, so the response of a structural mode is simply the sum of the responses to the individual frequencies. This will be made extensive use of later in the discussion of shock spectra.

The bandwidth associated with the test is easily identified from a frequency decomposition. Notice that the highest frequency in the table is $(\omega + |\omega_\theta| + |\tau_x| + |\tau_y|) = 10 + 1/2 + 1/6 + 1/3 = 11$ while the lowest frequency is $(\omega - |\omega_\theta| - |\tau_x| - |\tau_y|) = 10 - 1/2 - 1/6 - 1/3 = 9$. The absolute value signs are necessary because the frequencies can be negative. All the decomposition test frequencies fall between these two frequencies and these two frequencies are always present, thus the bandwidth for the rotated sine test is $\pm|\omega_\theta| = \pm.5$ Hz and the tumbled circle test is $\pm[|\omega_\theta|+|\tau_x|+|\tau_y|] = \pm1$ Hz. When the bandwidth gets large compared to $\pm\zeta\omega = \pm.025\times10 = \pm.25$ Hz (the width between half power points on the mode), the mode tends to produce separate gain spikes for each side of the test frequencies as will be illustrated next.

GAIN SPIKES IN 3-D

The differential equation governing the response of a structural mode is as follows (assuming the modes are normalized so the generalized mass is one):

$$\frac{d^2q}{dt^2} + 2\zeta\omega_n\frac{dq}{dt} + \omega_n{}^2 q = \underset{1\times\ell}{\langle\phi_j\rangle}\underset{\ell\times1}{\{F_j\}} \qquad 17)$$

Assuming the forcing $\{F_j\}$ is at only one location and is a pure sinusoid, the term on the right becomes $\phi(F_s \sin\omega t + F_c \cos\omega t)$, where ϕ is the mode shape value at the point where the force is being applied. This type of assumption is not at all limiting because Equation 17 is a linear differential equation. Superposition of solutions allows any initial condition problem to be solved based on this simple solution and a Fourier decomposition of the force time history. Superposition can extend the solution for as many forcing locations and as complicated a time history as are required in the real problem.

We proceed to obtain the steady state solution by assuming the form of solution is the same as the input. Differentiating and solving for the values of the two undetermined constants, S and C:

$$q = (S \sin\omega t + C \cos\omega t)$$

$$\frac{dq}{dt} = (\omega S \cos\omega t - \omega C \sin\omega t) \qquad 18)$$

$$\frac{d^2q}{d^2t} = (-\omega^2 S \sin\omega t - \omega^2 C \cos\omega t)$$

Substituting Equation 18 into the differential equation (Equation 17) gives Equation 19:

$$-\omega^2 S \sin\omega t - \omega^2 C \cos\omega t + 2\zeta\omega_n\omega S \cos\omega t - 2\zeta\omega_n\omega C \sin\omega t$$
$$+ \omega_n^2 S \sin\omega t + \omega_n^2 C \cos\omega t = \phi(F_s \sin\omega t + Fc \cos\omega t) \quad (19)$$

Since the sines can not <u>in general</u> be equal to cosines and vica versa:

$$(\omega_n^2-\omega^2)S - 2\zeta\omega_n\omega C = \phi F_s$$
$$2\zeta\omega_n\omega S + (\omega_n^2-\omega^2)C = \phi F_c \quad (20)$$

Solving for S and C:

$$S = \frac{\phi F_s(\omega_n^2 - \omega^2) + \phi F_c 2\zeta\omega_n\omega}{(\omega_n^2 - \omega^2) + (2\zeta\omega_n\omega)^2}$$
$$C = \frac{\phi F_c (\omega_n^2 - \omega^2) - \phi F_s 2\zeta\omega_n\omega}{(\omega_n^2 - \omega^2) + (2\zeta\omega_n\omega)^2} \quad (21)$$

This messy expression can be simplified somewhat by converting over to amplitude and phase coordinates. The displacement amplitude of the oscillation from Equation 18 is, after some algebra, as follows:

$$\sqrt{S^2 + C^2} = \frac{\phi\sqrt{F_s^2+F_c^2}}{\sqrt{(\omega_n^2 - \omega^2)^2 + (2\zeta\omega_n\omega)^2}} \quad (22)$$

Notice that the displacement amplitude of the response depends only on the amplitude of the input in the numerator of Equation 22. The phase angle of the input is irrelevant to the response amplitude. The phase angle can be calculated by forming the ratio of either of the S or C terms from Equation 21 to the overall amplitude from Equation 22. Then the total phase angle, β, is as shown in Equation 23:

$$\sin\beta = \frac{F_s (\omega_n^2 - \omega^2) + F_c 2\zeta\omega_n\omega}{\sqrt{F_s^2+F_c^2}\sqrt{(\omega_n^2 - \omega^2)^2 + (2\zeta\omega_n\omega)^2}} \quad (23)$$

However, we can recognize these terms as the original phase angle of the input forcing, ψ, and the new phase angle relative to the original input, θ. Then Equation 23 is simply: $\sin\beta = \sin\psi\cos\theta + \cos\psi\sin\theta$; and $\beta = \psi + \theta$.

$$\sin\psi = \frac{F_s}{\sqrt{F_s^2+F_c^2}} \qquad \cos\psi = \frac{F_c}{\sqrt{F_s^2+F_c^2}}$$
$$\sin\theta = \frac{2\zeta\omega_n\omega}{\sqrt{(\omega_n^2 - \omega^2)^2 + (2\zeta\omega_n\omega)^2}} \qquad \cos\theta = \frac{(\omega_n^2 - \omega^2)}{\sqrt{(\omega_n^2 - \omega^2)^2 + (2\zeta\omega_n\omega)^2}} \quad (24)$$

The modal gain is defined as the ratio of the output divided by the input. Also it is most common to convert the output to acceleration by multiplying by ω^2. Converting to acceleration also changes in the sign of θ in Equation 24 above because there is a sign change as illustrated in Equation 18.

The gain spike can be made to represent a displacement, velocity, or acceleration output by suitable multiplication by the forcing frequency, ω. Also, similar derivations can be performed to obtain the gain with respect to a displacement of the base of the mode, or the application of an acceleration time history to the base of the mode. For any of these cases, the gain spike defined in Equation 25 will be appropriate as long an there is no difference in the units of the input and the output. To correct for a difference in units some power of ω must be used along with appropriate conversions between lb_f and lb_m, etc. In any event, some modal gain constant (e.g., modal gain constant = $\phi_{in}\phi_{out}/GM$) needs to be multiplied times the gain spike to produce physical as opposed to modal outputs.

$$\text{Gain} = \frac{\sqrt{S^2 + C^2}}{\phi \sqrt{F_s^2 + F_c^2}} \omega^2 = \frac{\omega^2}{\sqrt{(\omega_n^2 - \omega^2)^2 + (2\zeta\omega_n\omega)^2}} \qquad 25)$$

The modal gain from Equation 25 is typically plotted versus forcing frequency (e.g., ω) to produce a gain spike for a single sinusoidal input. This same concept can be used for the more complicated time histories from the various sine tests already introduced. Given the frequency decomposition for the tests, it is easy to sum solutions for the individual sinusoidal components to

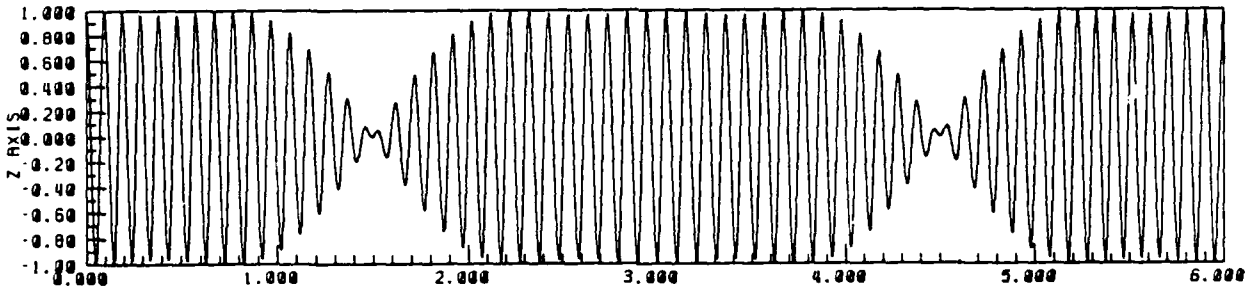

Figure 7a Steady State Z-Axis Input For The Tumbled Circle Test

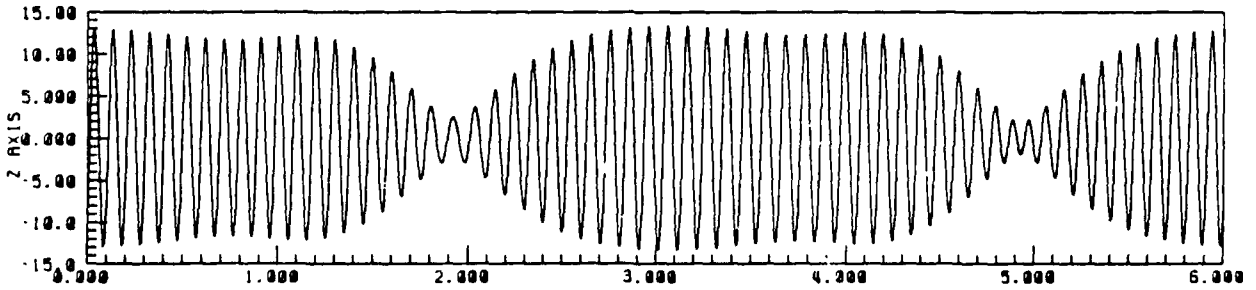

Figure 7b Steady State Z-Axis Response For The Tumbled Circle Test

get steady state modal acceleration for each of these tests at a fixed modal frequency (e.g., ω_n) as a function of the center frequency for the test (e.g., ω). Since the steady state response frequencies are the same as the forcing frequencies, the steady state acceleration time history repeats itself in the same period as the forcing time history.

Figure 7 illustrates this process for the Z axis of the tumbled circle test. The input time history shown in Figure 7a is converted to a steady state response time history as shown in Figure 7b. The input time history from Figure 7a and the output time history from Figure 7b will repeat themselves endlessly. Notice that the response is at a much higher amplitude than the input because of the modal gain, $1/2\zeta$. Of course the full modal gain of $1/2\zeta$ is not achieved for the waveform from Figure 7a since it is not a pure sinusoid. The gain for this time history is taken as the maximum absolute value for the entire time history, i.e., the entire output time history is reported as one maximum number (13.36) at the center frequency of the excitation (10 Hz in this example). Making other time history plots with different center frequencies generates the gain spike for the waveform being analyzed.

The gain spikes produced in this way appear similar to the conventional 1-D gain spike though the details of the shape are different. The 2-D sine test has exactly the same waveform and consequently has the same gain spike as the conventional 1-D test. Figure 8 compares the conventional sine test (the circles) to the rotated circle sine test along the three coordinate directions. The 1-D sinusoidal waveform concentrates all of it's energy at the fundamental frequency and consequently has the highest gain possible. The Z axis of the rotated circle sine test is sinusoidal so it has the same gain spike as the

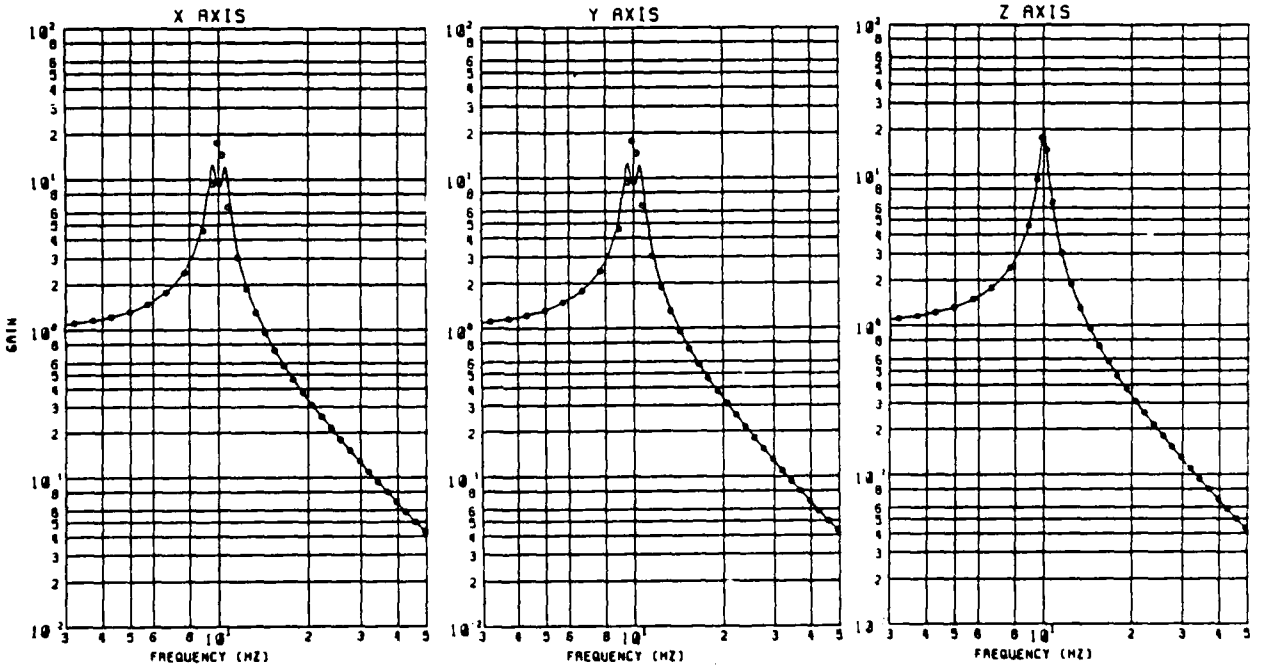

Figure 8 Rotated Circle Gain Spikes

conventional test. The X and Y axes are different from the Z axis but the X axis has the same waveform as the Y axis (just shifted in time) so they have equal, attenuated, gain spikes.

For the tumbled circle test the results are shown in Figure 9. All three axes have slightly different gain spikes with significant attenuation compared to 1-D. The Z axis is slightly higher than the other two, with all three axes tending to separate into two distinct gain spikes. Many other choices exist for test waveforms, however, to date no combinations have been found that 1) repeat in a short period of time (a maximum of 6 seconds), 2) have equal gain spikes, and 3) do not separate into two gain spikes.

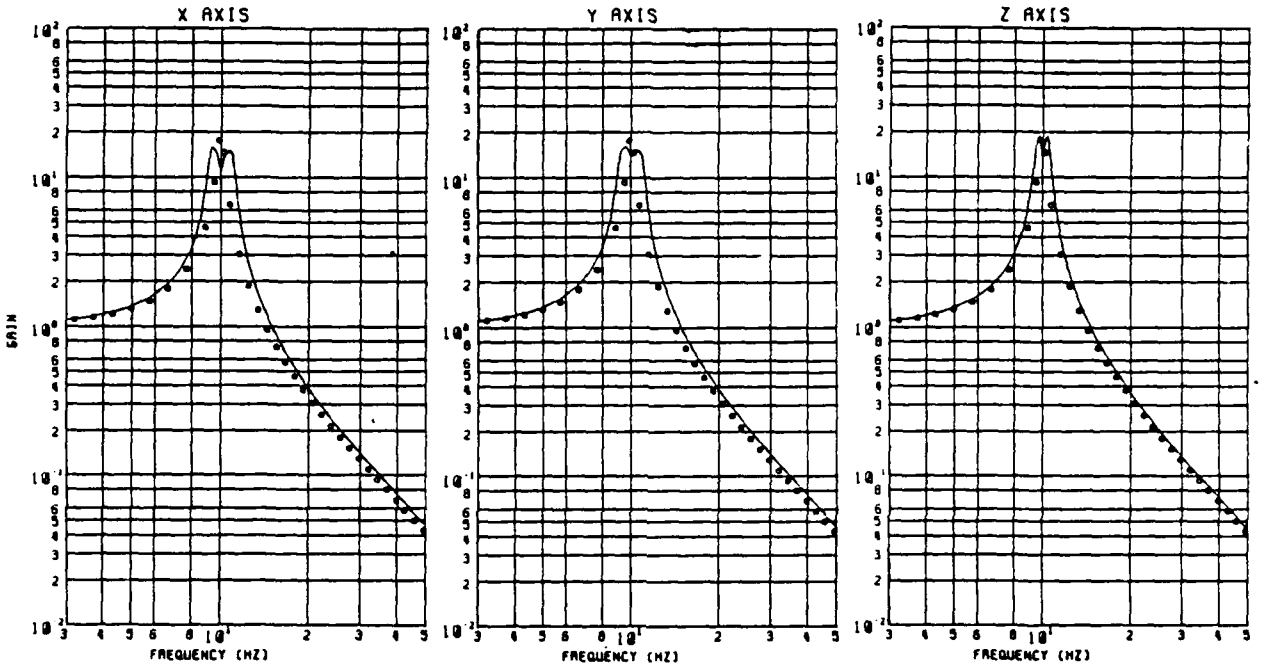

Figure 9 Tumbled Circle Test Gain Spikes

With complicated waveforms, the gain spike tends to separate into two different spikes when the damping is low. Looking at the gain equation, if $\omega \approx \omega_n$ then the gain is simply $Q=1/2\zeta$. In the curves illustrated to date, the damping ($\zeta=.025$) was 2.5% critical damping. If the damping is increased to 5% critical damping, then the gain decreases from $1/(2\times.025) = 20$ to $1/(2\times.05) = 10$. At the same time, the width of the gain spike at it's half power points, $\pm\zeta\omega$, increases from $\pm.025\times10=.25$ Hz to $\pm.05\times10=.5$ Hz. The separation between the high frequency e.g., $(\omega+\omega_\theta) = 10+1/2 = 10.5$ Hz and the low frequency e.g., $(\omega-\omega_\theta) = 10-1/2 = 9.5$ Hz, becomes smaller relative to the width of the mode so that the response is more in one peak. For any test with multiple frequencies there will always be a damping value small enough that the frequencies will separate - *this a serious objection to multiple frequency waveforms*. Still, even if the gain spike does separate, the only real consequence is that it is hard to estimate precisely the frequency associated with a mode.

one order. The direction cosine terms ($\cos_X$, $\cos_Y$, and $\cos_Z$) can multiply either the input time histories (X(t), Y(t), or Z(t)), or the response time histories in each axis given by the mode's transfer function operating on the time history ($\vec{H}(\omega)X(t)$, $\vec{H}(\omega)Y(t)$, and $\vec{H}(\omega)Z(t)$). Notice that the three steady state response time histories are responses for three different modes oriented in different directions.

$$R(t) = \cos_X \vec{H}(\omega)\ X(t) + \cos_Y \vec{H}(\omega)\ Y(t) + \cos_Z \vec{H}(\omega)\ Z(t) \qquad 26)$$

While Figures 10 and 11 are useful for the purpose of obtaining numbers, they do not create much understanding of the shape of the gain spike in space. What is required is a way to plot the same data in three dimensions. This has been done in the form already shown in Figure 1 for the 1-D sine test modal input, and in Figure 2 for the 2-D sine test modal input. The same plot routine has been used to plot the maximum gain (over frequencies) as a function of direction for all possible directions. This is shown in Figure 12 for the rotated circle test. A line drawn from the center of the coordinate system to the surface of the plot is the steady state amplitude for a mode oriented in that direction.

The irregular shape of the surface can be seen to correspond to the bumps in Figure 10. This result is somewhat disappointing because it has such a large ratio between the gain at the poles and at the equator. This is the result of the modulated waveform in the X and Y directions causing less than $1/2\zeta$ gain at the equator. Since the Z axis is sinusoidal, the gain is $1/2\zeta$ at the poles.

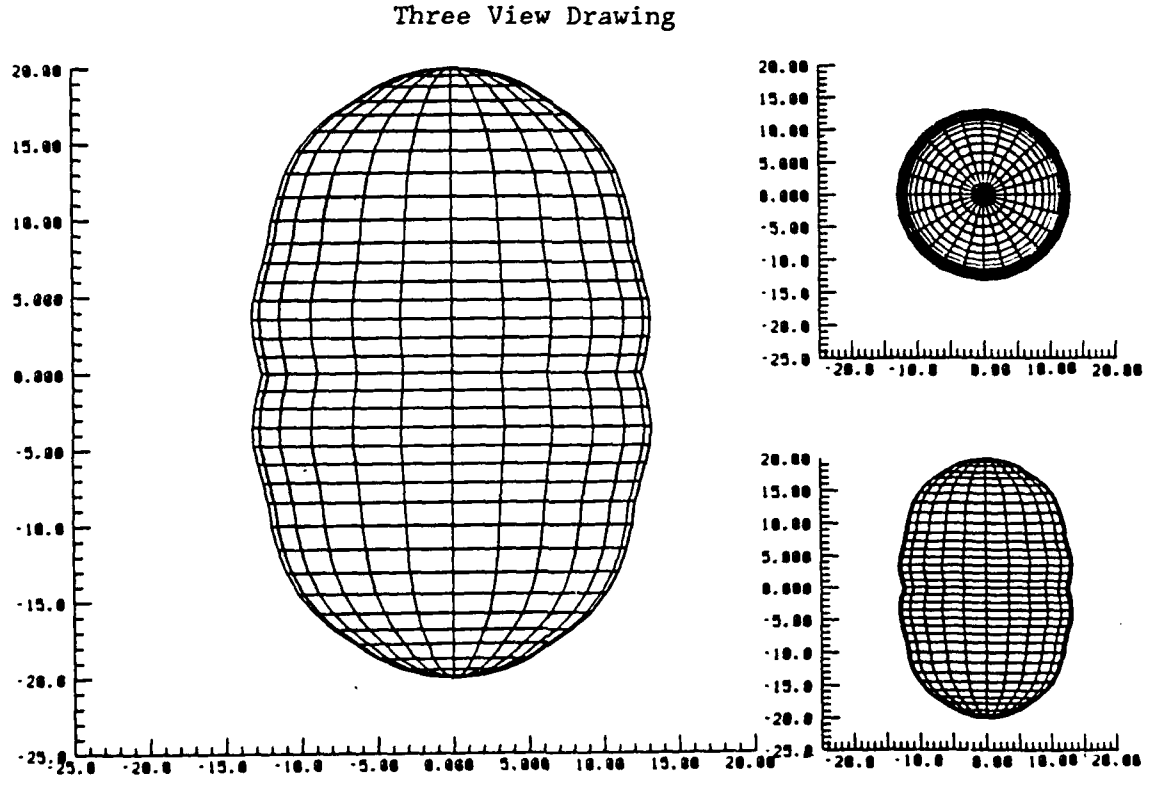

Figure 12 Rotated Circle Spatial Gain

The same plot for the tumbled circle test is shown in Figure 13 below. The more complicated geometry causes bumps and irregularities. This reveals a weakness in the plot routine in that you can see through the gain plot to the back surface. The plots are not hidden line plots and show both the front and back surface. The results for the tumbled circle test in Figure 13, while far from being a sphere, are more regular than the rotated circle test in Figure 14.

Plots for the 1-D test and the 2-D tests are not required since the waveform for these tests are pure sinusoids. The gain surface is simply $Q=1/2\zeta$ times the input surface presented earlier as Figure 1 for the 1-D test and Figure 2 for the 2-D test. In these cases, the gain spike doesn't separate into two gain spikes, and it is not necessary to obtain the maximum amplitude gain over the range of frequencies. Only one frequency is present in the excitation.

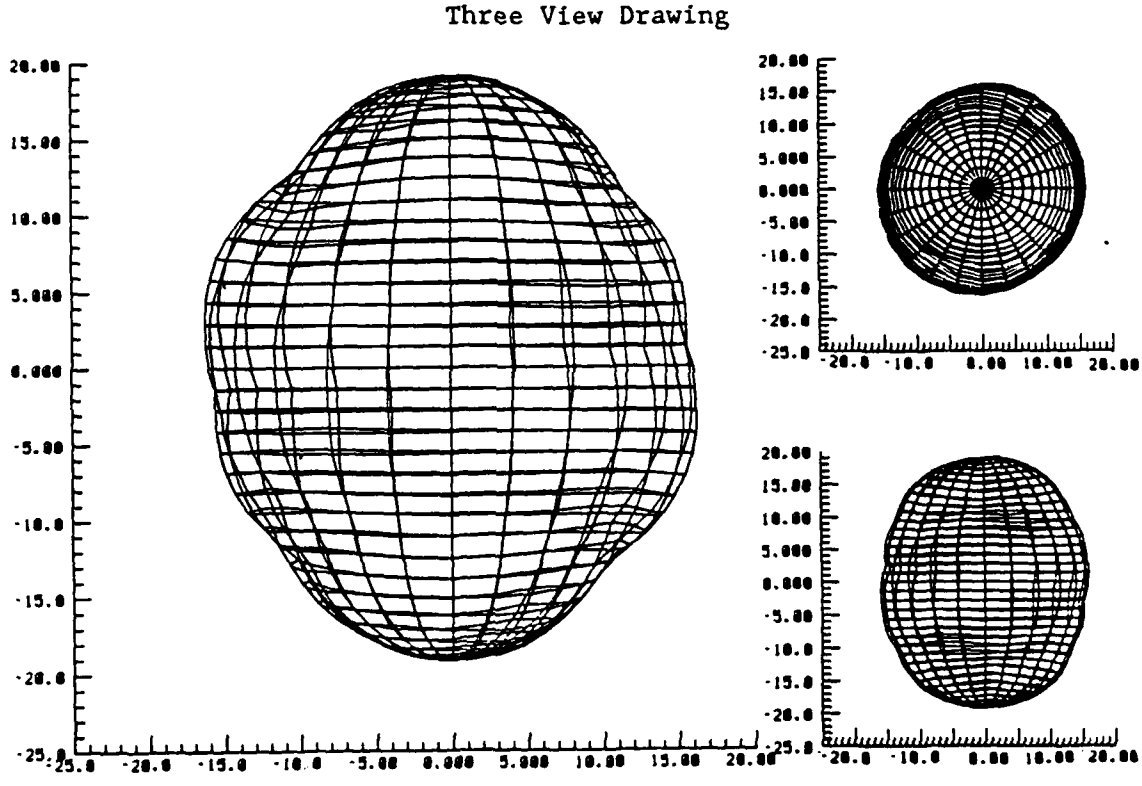

Figure 13 Tumbled Circle Spatial Gain

TRANSIENT RESPONSE SHOCK SPECTRA

Using the frequency decomposition of the various sine tests it is possible to calculate steady state response of a structural mode to an input time history. To observe this response it would be necessary to run the excitation at a constant frequency for a long time until the steady state response was achieved. This is not the way real sine tests are conducted. As was described earlier, the conventional sine test is swept at a fixed sweep rate (e.g., 2 octaves/minute), with a range of test frequencies being swept out (e.g., 5 to 2000 Hz). Thus there is an issue how much the sweep rate will attenuate the

shock spectra response at a frequency. In other words, how much the response will be transient in nature as opposed to steady state.

To answer these types of questions, a slightly different shock spectra routine is called for. The differential equation from Equation 20 can be solved numerically using the recursive filter technique[3]. Using the recursive filter technique, the response Y(nT) is estimated in terms of the input X(nT) at discrete time points as shown in Equation 27 below:

$$Y(nT)=b_0X(nT) + b_1X((n-1)T) + b_2X((n-2)T) - a_1Y((n-1)T) - a_2Y((n-2)T) \qquad 27)$$

Where:

n - counts data points

T - the time between samples = 1/(digitization rate)

ω_d - the damped natural frequency = $\omega\sqrt{1 - \zeta^2}$

$$b_0 = 1 - \frac{e^{-\zeta\omega T}\sin(\omega_d T)}{\omega_d T}$$

$$b_1 = 2\left[\frac{e^{-\zeta\omega T}\sin(\omega_d T)}{\omega_d T} - e^{-\zeta\omega T}\cos(\omega_d T)\right]$$

$$b_2 = e^{-2\zeta\omega T} - \frac{e^{-\zeta\omega T}\sin(\omega_d T)}{\omega_d T}$$

$$a_1 = -2e^{-\zeta\omega T}\cos(\omega_d T)$$

$$a_2 = e^{-2\zeta\omega T}$$

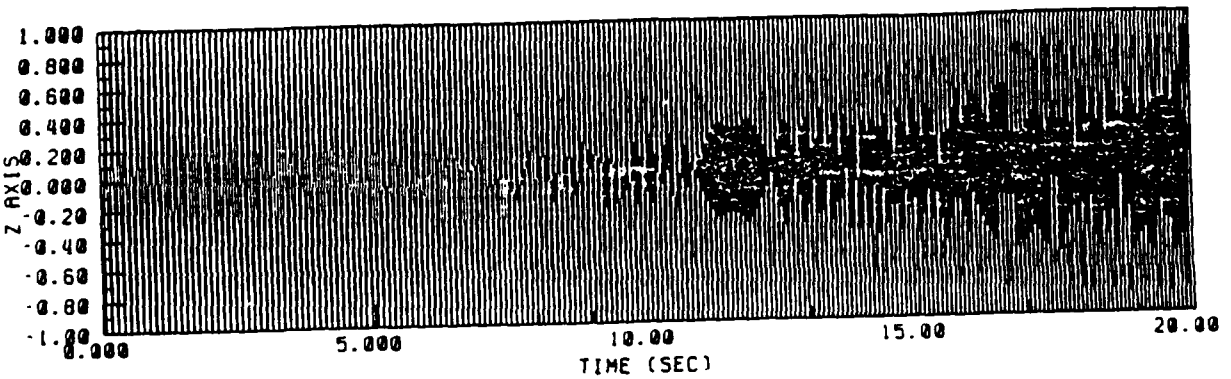

Figure 14a Conventional Swept Sine Shock Spectra Input

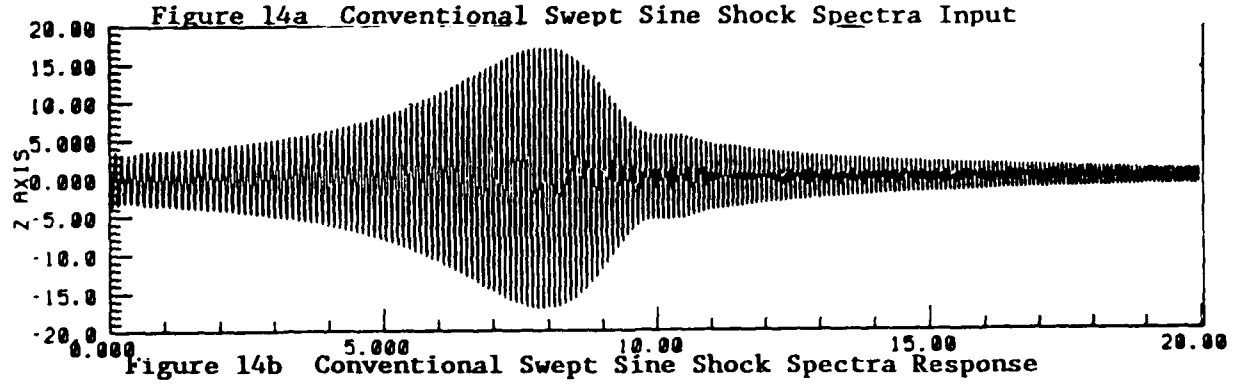

Figure 14b Conventional Swept Sine Shock Spectra Response

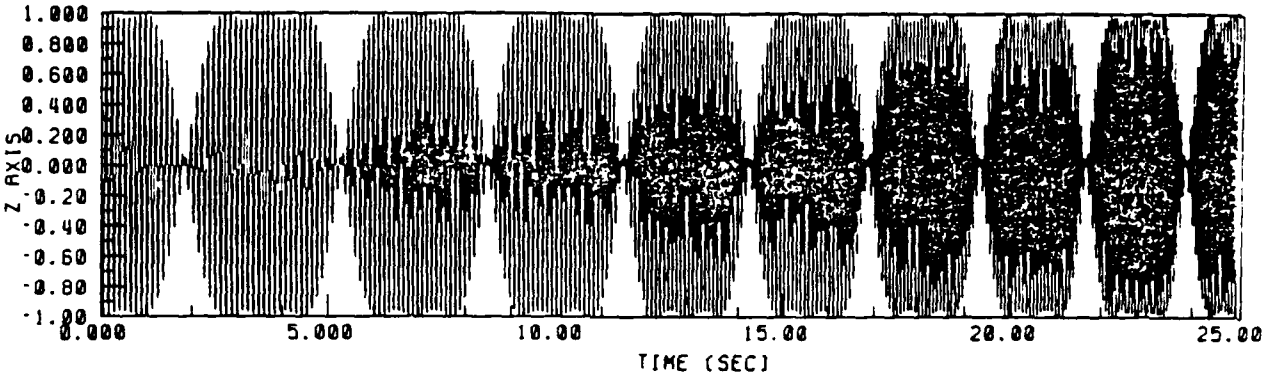

Figure 15a Z Axis of Tumbled Circle Test Swept Input

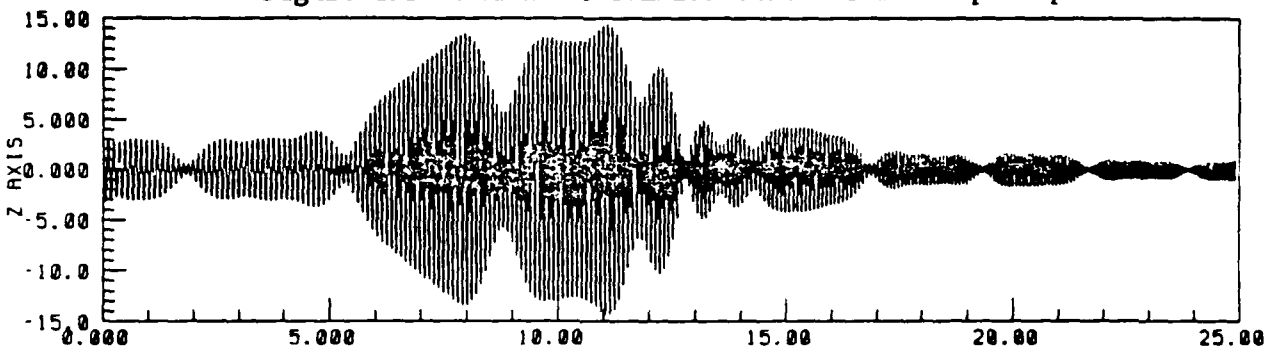

Figure 15b Z Axis of Tumbled Circle Test Swept Response

Using this type of solution, both the homogeneous and particular solution to the differential equation will be obtained. Thus it is possible to analyze data with a sweep rate; however, it is necessary to start the process in some realistic way. For this analysis, the recursion relationship was started at steady state (from the gain spike discussion) and run through a modal frequency which was held constant. Starting at steady state is reasonable because typical test techniques use a dwell to get up to level before sweeping. Figure 14a illustrates the input time history data for the Z axis of the rotated circle sine test (i.e., a conventional swept sine). Notice that the input frequency is being swept so that there is a higher frequency at later times. The response in Figure 14b shows a typical bloom that looks exactly like a modal gain spike from a conventional test. This very normal looking gain spike is the reason shock spectra is so widely used - it analyzes the phenomenon that actually happens in a real swept sine test.

Figure 14b produces a single shock spectra number equal to the maximum amplitude of the absolute value of the response over the entire time history (e.g., a gain of 18.0 for the case shown: 2 oct/min sweep rate with the mode at 10 H). This should be compared to the steady state gain of 20. The difference is the attenuation of the amplitude due to the sweep rate. Of course this is for a conventional sine test. The result varies by sweep rate, frequency of the mode, the assumed damping value, and procedure for initializing the data.

Figure 15a and 15b illustrate the same type of data for the Z axis of the tumbled circle test. Notice the swept waveform for the input in Figure 15a. The period decreases as time increases but the waveform looks exactly the same. Also notice the tendency of the response to separate into two peaks. This is a result of the gain spikes separating into two spikes as discussed in the

section on 3-D gain spikes. The shock spectra result from Figure 15b is a single number, the maximum absolute value for the entire plot (14.37 over all frequencies). This number should be compared to the steady state result from the gain spike calculation of the same waveform in Figure 8 (13.36 at 10 Hz). For slow sweep rates they are very close.

The issue is how much attenuation there will be in the steady state signal as a function of sweep rate. By repeating the calculation on the rotated circle sine test for different sweep rates, the results in Figure 16 were generated. Clearly much more attenuation with amplitude occurs in the modulated waveforms from the X and Y axes than in the conventional swept sine test in the Z direction. However, more of the attenuation is associated with the waveform than the sweep rate for reasonable sweep rates. This is because the reason sweep rate attenuates the amplitude is that it limits the number of cycles the mode experiences at the correct frequency. The modulated waveform also limits the number of consecutive cycles at the mode's natural frequency by 1) limiting the amplitude and 2) by changing the phase. Since the modulated waveform tends to be more limiting at low sweep rates, the system tends to exhibit little additional sweep rate attenuation.

While the attenuation of modal gain may seem disturbing at first, it is not all bad. The most serious objection to sine testing is that the waveform almost never occurs in the real world, and real world waveforms exhibit substantially less gain that the sine wave. The modulated sine waveform is far closer to a rocket staging transient waveform than a pure sinusoid would be. The sine environment is unique in that of all possible waveforms, it has the highest modal gain that can ever be achieved. These modulated waveform sine tests also have a high modal gain, just not as high as the conventional sine test.

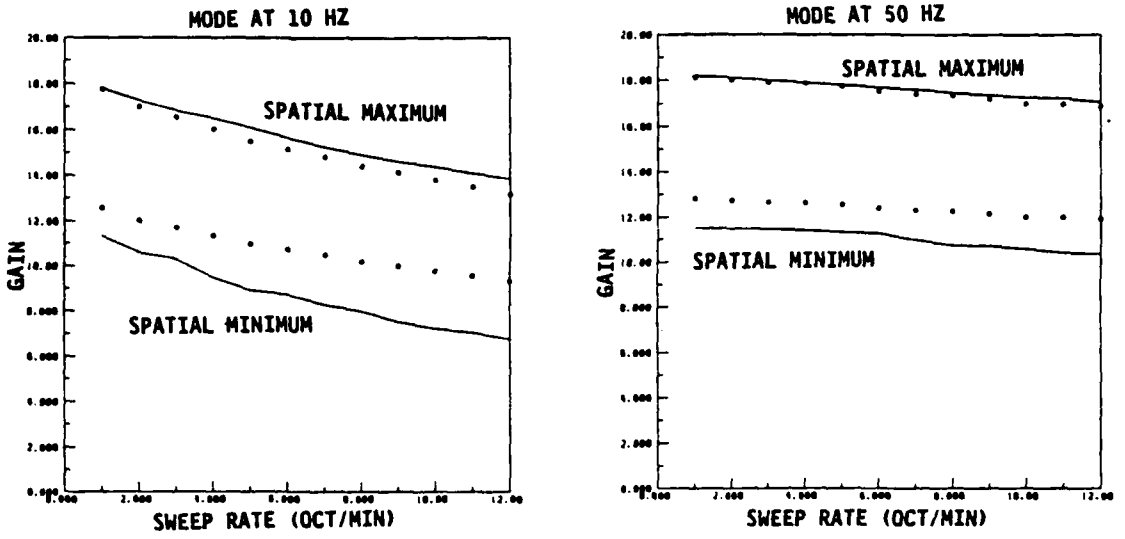

Figure 16 Rotated Circle Gain Versus Sweep Rate

The corresponding data for the tumbled circle test is shown in Figure 17. Again for low sweep rates the further attenuation with sweep rate is small. Notice that the characteristics of the three axes are much closer together with the tumbled circle test than the rotated circle sine test. This leads one to expect that the attenuation with sweep rate is fairly uniform spatially.

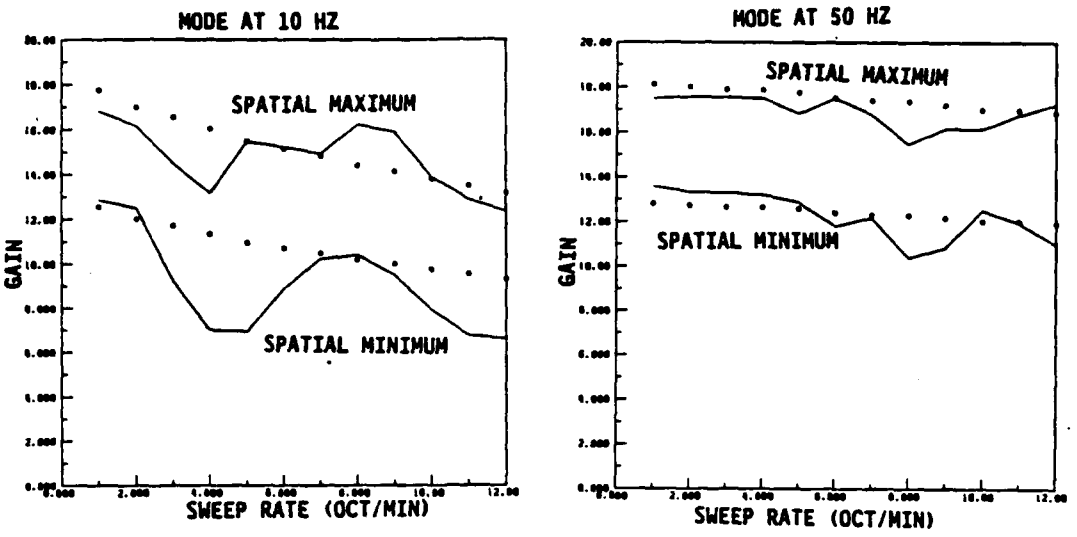

Figure 17 Tumbled Circle Test Gain Versus Sweep Rate

Of course this spatial distribution of the sweep rate effects are calculable just as the spatial distribution of the steady state gain was calculated. Superposition again is the key to calculating the shock spectra gain spatially. Three response time histories in the X, Y, and Z directions are calculated independently. Then direction cosines are applied to the time histories to calculate a new response time history in the direction of the direction cosines. Doing this over all directions results in a plot of the form shown in Figure 18 for the rotated circle test.

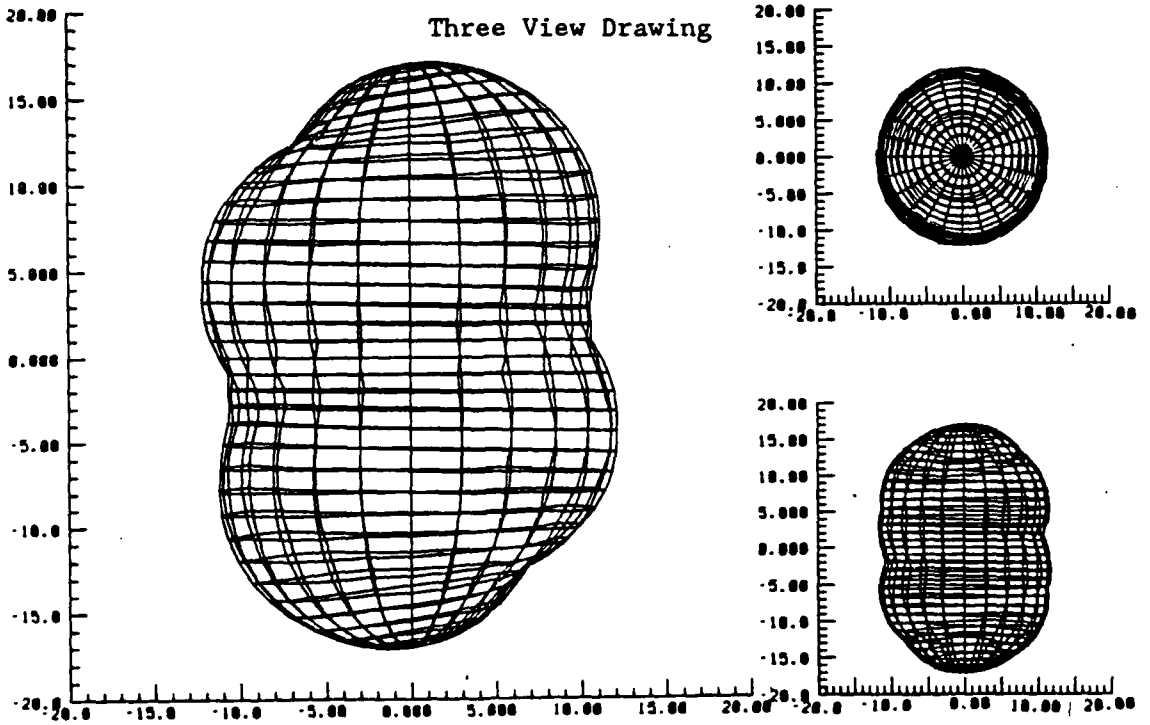

Figure 18 Rotated Circle Transient Spatial Gain

Figure 18 is comparable to Figure 12 showing the steady state for the same test and conditions. The lumpiness of the surface is the result of the precise timing of the waveform and mode. The gain is largest in the direction that the rotating circle is moving just as the mode's frequency is reached. This depends on the choice of frequency at T=0.0 of the start of the test and the exact mechanics for generating the swept sinusoid. It turns out that there is a problem with using Equation 2 ($\omega(t)$ below) for the test frequency. For short periods of time it produces very adequate results, however when the time, t, gets long the effects of sweep rate and time get mixed up. Consider the derivative of the argument with time:

$$\frac{d}{dt}\omega(t)t = \frac{d}{dt}\,\omega_o\, e^{(\ln 2/60)nt}\, t$$

$$= \omega_o(\ln 2/60)n\, e^{(\ln 2/60)nt}\, t \;+\; \omega_o\, e^{(\ln 2/60)nt} \qquad (28)$$

The first term in the expansion is an error term that grows with time. The second term is the swept frequency being sought. For the data shown here, the times and frequencies at the axes crossings were calculated and the frequency was linearly interpolated between axis crossings. The exact method of overcoming this problem will influence the shape of the gain in Figure 18.

To the extent that the gain in Figure 18 is different than the gain in Figure 12, the difference should be viewed as an error (that could occur any place spatially) caused by the sweep rate. As the frequency of the mode gets higher the size of the error gets smaller at given sweep rate. For test articles that exhibit modes in the 100 Hz region with sweep rates in the 1 to 2 oct/min range, this error is very small.

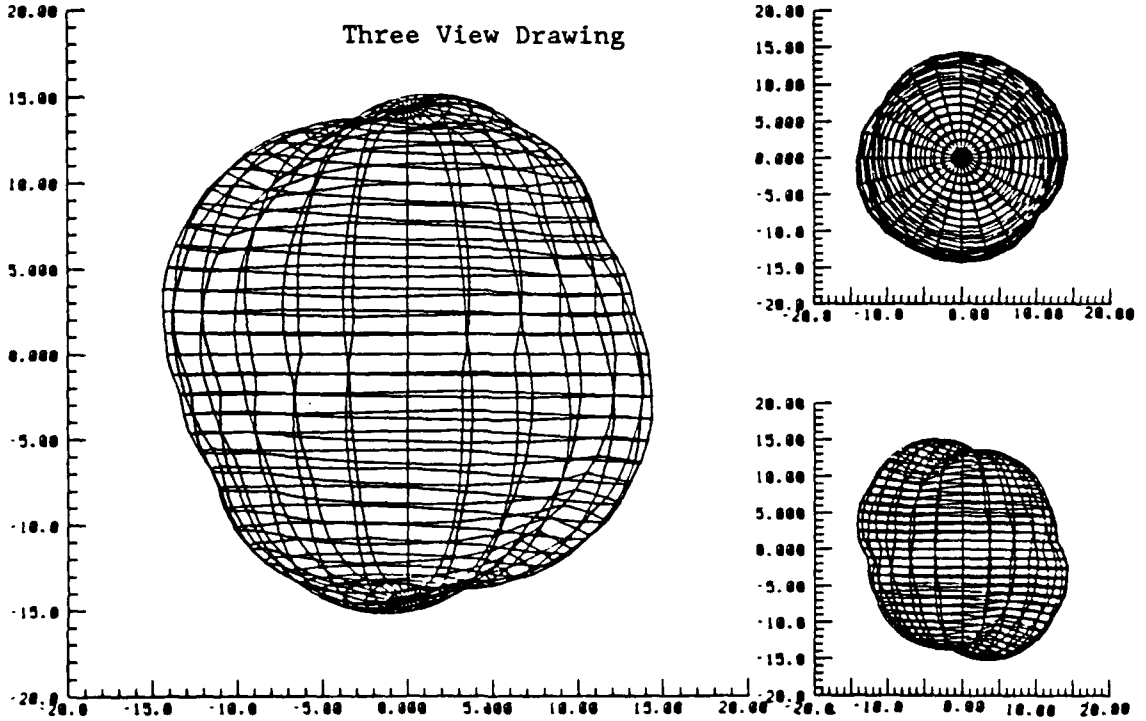

Figure 19 Tumbled Circle Test Transient Spatial Gain

The corresponding data for the tumbled circle test is shown in Figure 19. The same lumpiness is evident though it was also present in Figure 13 for the steady state data. Notice that the data is considerably more uniform for the tumbled circle case than for the rotated circle case.

3-D FATIGUE CYCLE COUNTING

Another use for a sine test besides enveloping the transient response of a shock spectra, is the application of a fixed number of cycles to test for potential fatigue failures. It is in this application that the 3-D test probably is most significant. The conventional three 1-D tests are very deficient in applying cycles to modes that are not oriented along the test axes.

Typically Miner's hypothesis is used to count cycles for estimating fatigue damage. Miner's hypothesis is that the damage caused by a cycle of oscillation accumulates linearly. If a test item can experience 1000 cycles at a level, then the damage caused by just one cycle will by 1/1000 of the total fatigue life of the item. Usually this is applied as a log-log SN curve, showing the stress (S) level versus the cycles (N) required to fail the specimen at that stress level. In the case of sine testing, it is necessary to use acceleration instead of stress to stay within the framework already presented. Equation 29 was adopted to represent the attenuation ratio of the fatigue cycle counts between the 1-D and the 3-D tests.[4]

$$\text{Fatigue Ratio} = \frac{\sum 0.5(\text{ABS}(\text{peak}))^{6.5}}{\text{1-D SUM}} \qquad 29)$$

The factor of 0.5 in the numerator reflects that peak values were estimated every half cycle.

It is possible to count either the input cycles or the shock spectra response cycles. For sine testing, it is far more meaningful to count the shock spectra response cycles since it indicates how a structural mode would really respond to this input. The normalizing factor used was the shock spectra for a conventional 1-D sine test *in the test direction*.

The analysis can be run on a conventional 1-D test by direction and this is shown in Figure 20. Along the Z axis in the test direction, the result is a ratio of 1 (by definition), however, away from the test direction the results are very poor. The conventional test has a major weakness in that it doesn't put very many cycles on a mode oriented at an angle to the test direction. The data shown is for ζ=2.5% and f=10 Hz with a 2 oct/min sweep rate, however, the situation does not completely correct itself at higher frequencies. The reason there is so much attenuation is the power the peak value is raised to (i.e., the equivalent of the slope of the SN curve) in Equation 29. It dramatically accentuates any irregularity in the peak amplitudes.

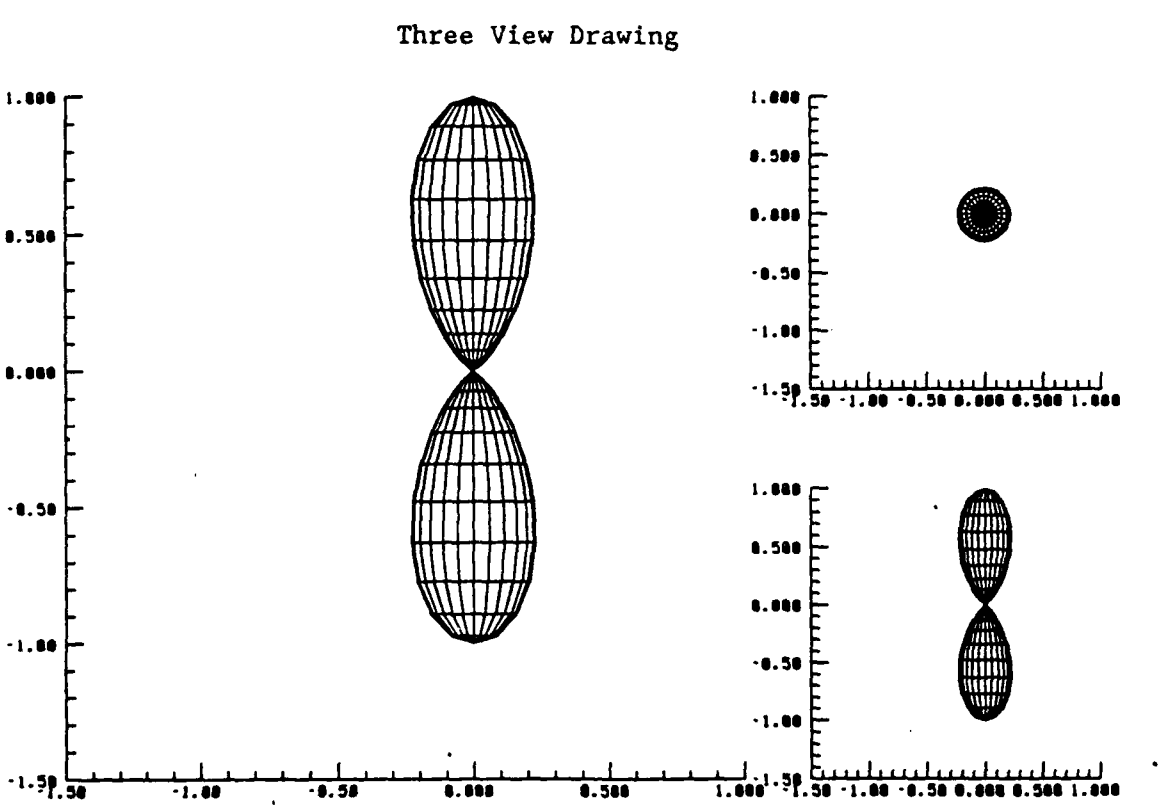

Figure 20 1-D Sine Test Fatigue Cycle Surface

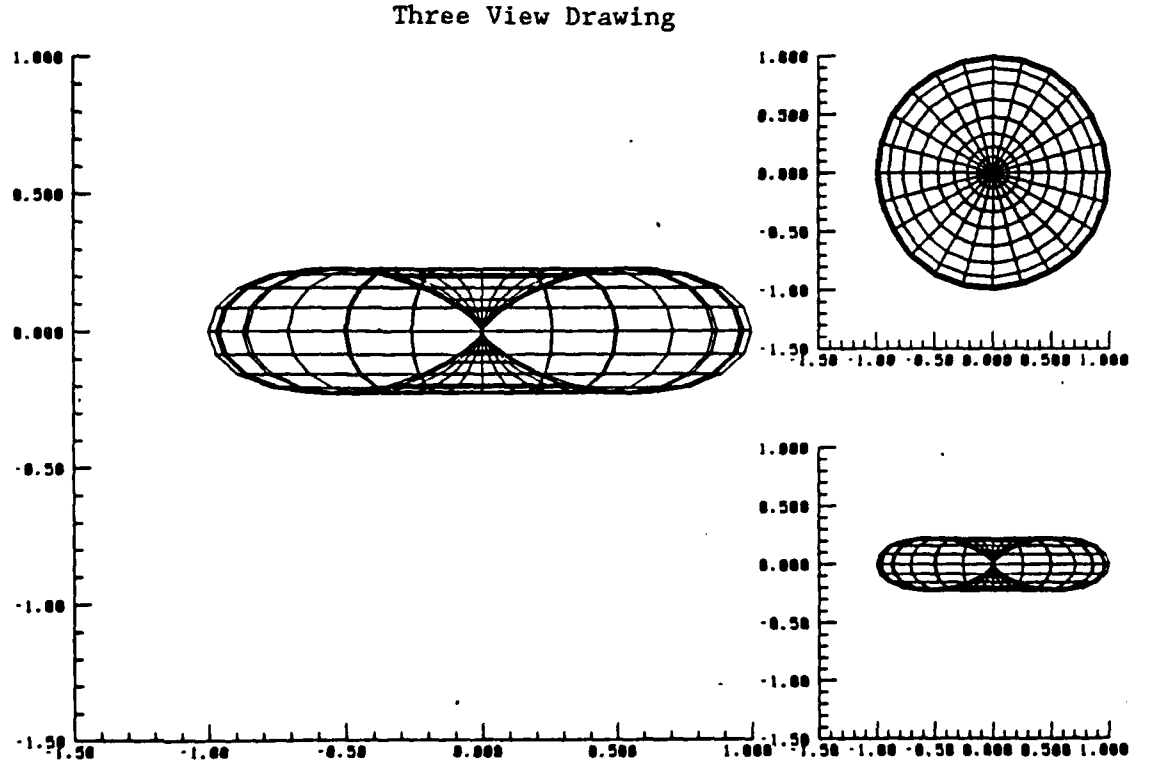

Figure 21 2-D Sine Test Fatigue Cycle Surface

The 2-D sine test shown in Figure 21 dramatically improves the situation. It should be kept in mind that both of these tests are run in three separate axes, thus there are two other pairs of figures just like the ones shown except oriented along the X and along the Y axes. The problem is the space left over between these figures. Any mode with an orientation such that it points along empty space, is essentially untested. There clearly are such directions in either the 1-D or even the 2-D case.

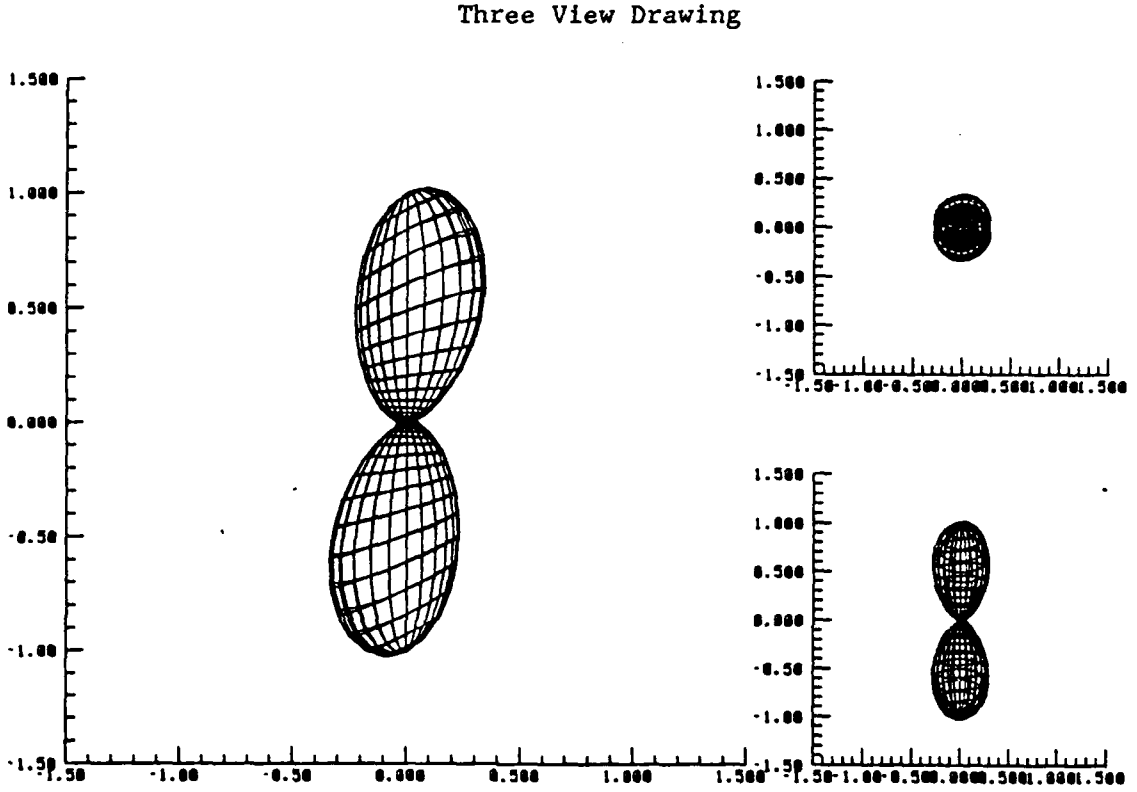

Figure 22 Rotated Circle Fatigue Cycle Surface

Because of the nature of the 3-D test, it seems reasonable that a 3-D waveform would correct these problems. Thus it is disappointing to see the result for the rotated circle test shown in Figure 22. The fact that the Z axis is a 1-D sine test dominates the picture. Figure 22 is almost exactly the same as Figure 20 for the 1-D sine test except that there is a slight fattening around the X-Y plane and the surface is tilted slightly on it's axis. The cycle count for the sine wave is so much higher than the cycle count for the modulated sinusoids that they are almost negligible. The slight off centered appearance of the data is caused by the lumpiness in the gain spikes due to the exact timing of the shock spectra response. This has been exaggerated because of being raised to the power 6.5 and has become a major feature of the curve.

There are fatigue cycles associated with the modulated sinusoids, they just don't add up to the same order magnitude of damage as in the sinusoid. Counting input cycles produces a more spherical shape. The results are consistent with the ratio of the polar to equatorial gains from Figure 8. The

polar gain was 20 while the equatorial gain was 12.6 thus $(12.6/20)^{6.5} = .05$, clearly the power 6.5 exaggerates any amplitude error.

Given this situation, it is not surprising that the tumbled circle test also is not very spherical. Figure 23 illustrates the same data for the tumbled circle test. While there is a factor of 2.5 between the two axes, it should be noted that this is an error of $1.15^{6.5}$. If the off axis irregularity were felt to be a problem the amplitude in the off axis directions could be raised by 1.15 times to compensate for the distortion. SN curve data is typically shown in log-log form hiding the extreme variability of the data. A factor of three is probably as close as we will be able to come.

Of more concern is the factor of 2 between the conventional sine test cycle count and the tumbled sine test cycle count. This suggests that the test duration would have to be increased by a factor of 2 to achieve the same cycle count. Alternatively the amplitude of all three axes could be raised by 1.11 to keep the cycle count the same.

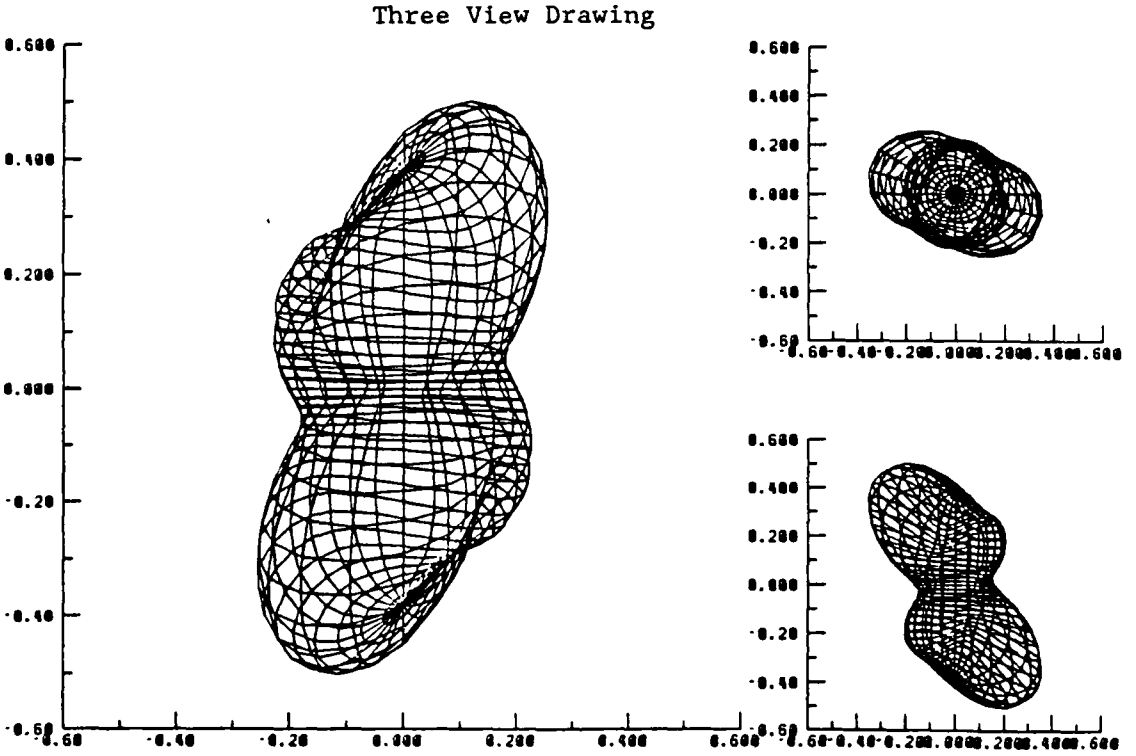

Figure 23 Tumbled Circle Fatigue Cycle Surface

As a practical matter, cycle counting is done using log cycle counts and these corrections are actually smaller than the uncertainty associated with the cycle count total that the test is designed to achieve. It probably accomplishes nothing to make the corrections other than take account the factor of two in duration between the two tests.

CONCLUSIONS

While the rotated circle and tumbled circle waveforms appear promising, on closer inspection using shock spectra and fatigue cycle counting, they still exhibit serious tendencies to have a preferred direction. There are a number of major obstacles to a 3-D sine test:

1. It is necessary to pick the modulation frequencies low enough that the bandwidth of the resulting test is small compared the half power points of the typical structural mode being excited. The test bandwidth is plus or minus the sum of the modulation frequencies and thus is proportional to the center frequency value. The half power points on the structural mode are at $\pm\zeta\omega$ and thus are also proportional to the center frequency value. There is loss of gain, fatigue cycles, etc. from this source at all frequencies. The error is not a function of the test frequency.

2. The separation of the test frequency into a set of frequencies above the nominal frequency and below the nominal frequency means that the gain spike can separate into two separate peaks. Since the half power points of the gain spike occur at $\pm\zeta\omega$, there is always a damping values, ζ, small enough that the gain spike will separate.

3. The smaller the modulation frequencies are, the longer the time to repeat becomes. The time for the waveform to repeat is equal to the smallest integer number of periods for all the modulation frequencies. Since the period is the inverse of the frequency, the smaller the frequencies are, the longer the period to repeat becomes. If the period to repeat gets long compared to the width of a mode, $\pm\zeta\omega$, complete spatial coverage will not be available. Again this error source does not depend on the test frequency. Both the period and width of the mode change equally with the test frequency.

4. Sweep rate effects limit the test performance at low frequencies. With an exponential sweep rate, each cycle is a fixed frequency width wide, i.e., $\Delta\omega$/cycle = n (ln 2/60), depending only on the sweep rate, n, independent of frequency. When the frequency gets high, $\pm\zeta\omega$ has more cycles of oscillation in it than when the frequency is low. Thus at low frequencies or high sweep rates there commonly are not enough cycles in the width of the mode to achieve steady state response.

5. The slope of the acceleration versus cycle to failure curve distorts any irregularity in the spatial gain to cause preferred directions in 3-D tests. While it is easy to move the preferred direction between axes, it is not very easy to get rid of the preferred directions.

A procedure to improve the tumbled sine test spatial coverage would be to perform three axes of the tumbled circle sine test, interchanging the roles of the X, Y, and Z axes. By doing different sweeps with different orientations (just as we do now with the conventional test), it is possible improve the 3-D coverage dramatically.

Still, in our pursuit of a 3-D answer to sine testing we should not overlook the elegant 2-D answer provided by testing in circles. The 2-D test (in three orthogonal directions) offers substantial improvement over the conventional 1-D

test in shock spectra response, fatigue cycle count, frequency content, and sweep rate attenuation. There is no down side to this test - thus it should be fairly easy to adopt as a standard. Potentially, even the rather limited input at 45° to all the axes can be overcome by testing in eight coordinate directions instead of four coordinate directions. The 2-D test appears to be the test with a future.

References

1. R. C. Stroud and G. A. Hamma, "Three Dimensional Vibration Control System," Institute of Environmental Sciences, 1984 Proceedings, p. 474-477.

2. D. L. Cronin, "Response Spectra for Sweeping Sinusoidal Excitations," Shock and Vibration Bulletin, No. 29, Part 4, 197-217.

3. D. O. Smallwood, " An Improved Recursion Formula for Calculating Shock Response Spectra," Shock and Vibration Bulletin, No. 51, Part 2, May 1981.

4. Harris, C. M., and Crede, C. E., Shock and Vibration Handbook, Vol. 2 of 3, p. 24-11 through 24-18.

CHAPTER 2 DISTRIBUTION THEORY IN 3-D RANDOM TESTING

INTRODUCTION

Traditional 1-D random testing uses a normal distribution clipped at 3 sigma as the underlying distribution behind the test. The mean of the normal distribution must be zero because the shaker system has limited travel. The standard deviation (sigma) is the wideband RMS of the test power spectral density (PSD). This has evolved as a standard for testing in the aerospace industry and elsewhere. With the advent of 3-D random testing, the statistical assumptions this test is based on need to be reexamined in light of the new test regime.

3-D random testing is implemented by using a clipped normal distribution on each axis. As will be demonstrated, this produces a major difference from the 1-D test in that the resultant vector is distributed chi-squared with degrees of freedom 3 instead of being normally distributed. Compared to the 1-D test, clipping at 3 sigma on the *resultant* vector produces far to much clipping because of differences between the distribution functions. In the 3-D test, clipping at 3 sigma will produce 2.9% of the points being clipped as opposed to 0.27% of the points for a 1-D test. Clipping at 3.76 sigma is called for if the resultant vector is to be clipped the same percentage of the time as in 1-D testing.

Of more concern, clipping can not currently be implemented on the resultant vector. All three shaker inputs are clipped individually, without regard to the value of the other inputs. This produces a box shaped region in which the shake table moves. Because the vector components are clipped normal distributions, finite probabilities occur of reaching the extreme corners of the box. Even when clipped the corners of the box are fairly far out at 5.2 sigma, and the probability of reaching them is fairly low (6.9 hours between events). This raises the spector of experiencing hard tests and easy tests within the same test specification depending on how high the peak amplitude gets during the course of the test.

This document will demonstrate these statistical results starting from the basics and working through the results quoted above. The conventional distributional theory is entirely drawn from Chapter 26, "Probability Functions" from Handbook of Mathematical Functions edited by Milton Abramowitz and Irene A. Stegun, first published in 1965 by Dover Publications, Inc., New York.[1] Of course words and interpretation have been added to the mathematical formulas in the Handbook. The work with clipped chi-squared distributions is believed to be original. All tables were calculated using an HP28C programmable pocket calculator which has both normal and chi-squared functions built into the calculator.

THE GAUSSIAN OR NORMAL DISTRIBUTION

The general form of the normal distribution is given by Equation 1 below. It is characterized by two parameters: the mean, μ, and the standard deviation, σ. Additionally, there is the value of the variable, x, often called the random deviate, whose probability is to be estimated. In the form shown in Equation 1, the probability is the ratio of the time that a

sample drawn at random from a normal distribution with mean, μ, and standard deviation, σ, will have a value less than or equal to x.

$$P(x|\mu,\sigma) = \frac{1}{\sigma\sqrt{2\pi}} \int_{-\infty}^{x} e^{-(t-\mu)^2/(2\sigma^2)} dt \qquad 1)$$

Since the normal distribution is a distribution, the expression approaches one as the value of x approaches ∞. Actually that is how the normalizing factor $\sigma\sqrt{2\pi}$ is arrived at. The integral part of the expression with $x=\infty$ approaches $\sigma\sqrt{2\pi}$ so dividing by that amount causes the overall expression to approach one. As with virtually all distributions, evaluation of the actual integral as a function of x is impossible, so tabulations are all that can be achieved.

Aside from integrating to one, the integral of a distribution must monotonically increase from zero at the lower limit of the range to a value of one at the upper limit of the range. This is because probabilities can only be positive. If the value of the integrand ever became negative, there would be a region where the probability would be negative and this doesn't make physical sense. There is, of course, no requirement that the range of a distribution be infinite.

Equation 2 gives the normalized integrand of Equation 1. This is illustrated in Figure 1 as the familiar bell shaped curve associated with the normal distribution. The probability calculated in Equation 1 is illustrated in Figure 1 as the cross hatched area of the curve. Equation 1 is sometimes referred to a the cumulative normal distribution.

$$Z(x|\mu,\sigma) = \frac{1}{\sigma\sqrt{2\pi}} e^{-(x-\mu)^2/(2\sigma^2)} \qquad 2)$$

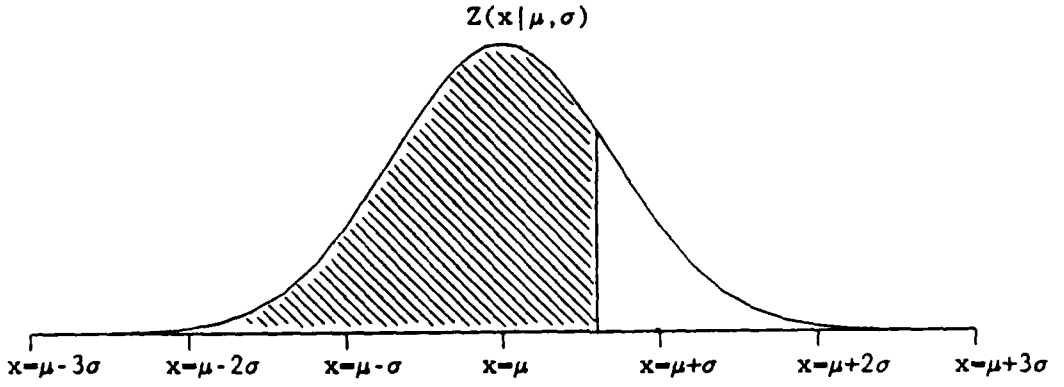

Figure 1 Integrand of the Normal Distribution

Different probabilities can be calculated by changing the limits of integration. In particular, the probability that a sample drawn at random

from a normal distribution with mean, μ, and standard deviation, σ, will have a value greater than or equal to x is given by Equation 3:

$$Q(x|\mu,\sigma) = \frac{1}{\sigma\sqrt{2\pi}} \int_x^{\infty} e^{-(t-\mu)^2/(2\sigma^2)} dt = 1 - P(x|\mu,\sigma) \qquad 3)$$

Notice that there is no problem with using equality in both directions in Equation 3 (i.e., $P(X \leq x|\mu,\sigma)$ while $Q(X \geq x|\mu,\sigma)$), since there is no probability associated with the occurrence that X=x. In general, the probability of observing a value between any two numbers x_1 and x_2 is given by Equation 4 ($x_1 \leq x_2$):

$$A(x_1,x_2|\mu,\sigma) = \frac{1}{\sigma\sqrt{2\pi}} \int_{x_1}^{x_2} e^{-(t-\mu)^2/(2\sigma^2)} dt \qquad 4)$$

This form of the normal equation is very difficult to tabulate since it involves so many variables: x_1, x_2, μ, and σ. Some simplification is achieved by tabulating either Equation 1 or Equation 3 since all three equations can be expressed in terms of any of the tabulations as shown below:

$$A(x_1,x_2|\mu,\sigma) = P(x_2|\mu,\sigma) - P(x_1|\mu,\sigma) \qquad 5)$$

$$A(x_1,x_2|\mu,\sigma) = Q(x_1|\mu,\sigma) - Q(x_2|\mu,\sigma)$$

$$Q(x|\mu,\sigma) = 1 - P(x|\mu,\sigma)$$

$$Q(x|\mu,\sigma) = A(x,\infty|\mu,\sigma)$$

$$P(x|\mu,\sigma) = 1 - Q(x|\mu,\sigma)$$

$$P(x|\mu,\sigma) = A(\infty,x|\mu,\sigma)$$

Even in the simplest of these forms, there are three variables: x, μ, and σ. It is prohibitively difficult to tabulate the normal distribution in this way. Luckily, there is a way to simplify the expression through a change of variables to produce the standard normal distribution.

THE STANDARD NORMAL DISTRIBUTION

If the variable of integration in Equation 1 is changed from t to $r = (t-\mu)/\sigma$, the three parameter normal distribution becomes a one parameter standard normal distribution in terms of X where $X=(x-\mu)/\sigma$.

$$P(X) = \frac{1}{\sqrt{2\pi}} \int_{-\infty}^{X} e^{-r^2/2} dr \qquad 6)$$

This is the distribution that is universally tabulated as the normal distribution in terms of the parameter, $X=(x-\mu)/\sigma$. Some tables give the lower tail of the distribution as shown in Equation 6, and some tables give

the upper tail of the distribution, Q(X), as shown below.

$$Q(X) = \frac{1}{\sqrt{2\pi}} \int_X^{\infty} e^{-r^2/2} dr \qquad 7)$$

Another possibility that is sometimes tabulated is the center part of the distribution with the tails excluded. This commonly is the probability that is desired. For example to determine the probability of observing an event less likely than 3σ, events with $-3 \leq X \leq 3$ have to be considered. To deal with these questions Equation 8 is often tabulated.

$$A(X) = \frac{1}{\sqrt{2\pi}} \int_{-X}^{X} e^{-r^2/2} dr \qquad 8)$$

Finally, tables sometimes tabulate R(X)=1-A(X) to estimate the probability of being in one of the tails of the distribution. The three main versions of the standard normal tables are interrelated as indicated below. The last three expressions are based on the fact that the normal distribution is symmetric.

$$P(X) + Q(X) = 1 \qquad 9)$$

$$P(-X) = Q(X)$$

$$A(X) = 2\,P(X) - 1$$

$$A(X) = 1 - 2\,Q(X)$$

Table 1 tabulates P(X), Q(X), A(X), R(X) and the normalized integrand of the standard normal distribution, Z(X), over a very wide range of X.

THE SPHERICAL NORMAL DISTRIBUTION

The standard normal distribution is expressed in only one dimension, X. Three axis testing requires a distribution that is multi-dimensional with each dimension being normal. This is a spherical normal distribution, and it is the simplest form of a trivariate normal distribution. Since the next step will be to transform the spherical normal distribution into a chi-squared distribution, it will be advantageous to write the symmetric form of the spherical normal distribution similar to distribution A(X) above.

$$S(X,Y,Z) = \frac{1}{2\pi\sqrt{2\pi}} \int_{-Z}^{Z} \int_{-Y}^{Y} \int_{-X}^{X} e^{-(x^2+y^2+z^2)/2} dx\, dy\, dz \qquad 10)$$

This can be transformed into the chi-squared distribution by simply converting into spherical coordinates and integrating out the two angles. First it is necessary to set X=Y=Z so the distribution is spherically symmetric. In practice this is not a serious limitation since one can stretch or contract one axis or another by changing its local value of RMS

Table 1 The Standard Normal Distribution

X	P(X) or Q(-X)	Q(X) or P(-X)	A(X)	R(X)	Z(X) or Z(-X)
0.0	0.500000000	0.500000000	0.000000000	1.000000000	0.398942280
0.1	0.539827837	0.460172163	0.079655675	0.920344325	0.396952547
0.2	0.579259709	0.420740291	0.158519419	0.841480581	0.391042694
0.3	0.617911422	0.382088578	0.235822844	0.764177156	0.381387815
0.4	0.655421742	0.344578258	0.310843483	0.689156517	0.368270140
0.5	0.691462461	0.308537539	0.382924923	0.617075077	0.352065327
0.6	0.725746882	0.274253118	0.451493765	0.548506236	0.333224603
0.7	0.758036348	0.241963652	0.516072696	0.483927304	0.312253933
0.8	0.788144601	0.211855399	0.576289203	0.423710797	0.289691553
0.9	0.815939875	0.184060125	0.631879749	0.368120251	0.266085250
1.0	0.841344746	0.158655254	0.682689492	0.317310508	0.241970725
1.1	0.864333939	0.135666061	0.728667878	0.271332122	0.217852177
1.2	0.884930330	0.115069670	0.769860660	0.230139340	0.194186055
1.3	0.903199515	0.096800485	0.806399031	0.193600969	0.171368592
1.4	0.919243341	0.080756659	0.838486682	0.161513318	0.149727466
1.5	0.933192799	0.066807201	0.866385597	0.133614403	0.129517596
1.6	0.945200708	0.054799292	0.890401417	0.109598583	0.110920835
1.7	0.955434537	0.044565463	0.910869074	0.089130926	0.094049077
1.8	0.964069681	0.035930319	0.928139362	0.071860638	0.078950158
1.9	0.971283440	0.028716560	0.942566880	0.057433120	0.065615815
2.0	0.977249868	0.022750132	0.954499736	0.045500264	0.053990967
2.1	0.982135579	0.017864421	0.964271159	0.035728841	0.043983596
2.2	0.986096552	0.013903448	0.972193105	0.027806895	0.035474593
2.3	0.989275890	0.010724110	0.978551780	0.021448220	0.028327038
2.4	0.991802464	0.008197536	0.983604928	0.016395072	0.022394530
2.5	0.993790335	0.006209665	0.987580669	0.012419331	0.017528300
2.6	0.995338812	0.004661188	0.990677624	0.009322376	0.013582969
2.7	0.996533026	0.003466974	0.993066052	0.006933948	0.010420935
2.8	0.997444870	0.002555130	0.994889739	0.005110261	0.007915452
2.9	0.998134187	0.001865813	0.996268373	0.003731627	0.005952532
3.0	0.998650102	0.001349898	0.997300204	0.002699796	0.004431848
3.1	0.999032397	0.000967603	0.998064794	0.001935206	0.003266819
3.2	0.999312862	0.000687138	0.998625724	0.001374276	0.002384088
3.3	0.999516576	0.000483424	0.999033152	0.000966848	0.001722569
3.4	0.999663071	0.000336929	0.999326141	0.000673859	0.001038281
3.5	0.999767371	0.000232629	0.999534742	0.000465258	0.000872683
3.6	0.999840891	0.000159109	0.999681783	0.000318217	0.000611902
3.7	0.999892200	0.000107800	0.999784401	0.000215599	0.000424780
3.8	0.999927652	0.000072348	0.999855304	0.000144696	0.000291947
3.9	0.999951904	0.000048096	0.999903807	0.000096193	0.000198655
4.0	0.999968329	0.000031671	0.999936658	0.000063342	0.000133830
4.1	0.999979342	0.000020658	0.999958685	0.000041315	0.000089262
4.2	0.999986654	0.000013346	0.999973309	0.000026691	0.000058943
4.3	0.999991460	0.000008540	0.999982920	0.000017080	0.000038535
4.4	0.999994587	0.000005413	0.999989175	0.000010825	0.000024942
4.5	0.999996602	0.000003398	0.999993205	0.000006795	0.000015984
4.6	0.999997888	0.000002112	0.999995775	0.000004225	0.000010141
4.7	0.999998699	0.000001301	0.999997398	0.000002602	0.000006370
4.8	0.999999207	0.000000793	0.999998413	0.000001587	0.000003961
4.9	0.999999521	0.000000479	0.999999042	0.000000958	0.000002439
5.0	0.999999713	0.000000287	0.999999427	0.000000573	0.000001487

Table 1 The Standard Normal Distribution, Continued

X	Q(X)	R(X)	Z(X)
0.0	5.000×10^{-1}	1.000×10^{0}	3.989×10^{-1}
1.0	1.587×10^{-1}	3.173×10^{-1}	2.420×10^{-1}
2.0	2.275×10^{-2}	4.550×10^{-2}	5.399×10^{-2}
3.0	1.350×10^{-3}	2.700×10^{-3}	4.432×10^{-3}
4.0	3.167×10^{-5}	6.334×10^{-5}	1.338×10^{-4}
5.0	2.867×10^{-7}	5.733×10^{-7}	1.487×10^{-6}
6.0	9.866×10^{-10}	1.973×10^{-9}	6.076×10^{-9}
7.0	1.280×10^{-12}	2.560×10^{-12}	9.135×10^{-12}
8.0	6.221×10^{-16}	1.244×10^{-15}	5.052×10^{-15}
9.0	1.129×10^{-19}	2.257×10^{-19}	1.028×10^{-18}
10.0	7.620×10^{-24}	1.524×10^{-23}	7.695×10^{-23}
15.0	3.671×10^{-51}	7.342×10^{-51}	5.531×10^{-50}
20.0	2.754×10^{-89}	5.507×10^{-89}	5.521×10^{-88}
25.0	3.057×10^{-138}	6.113×10^{-138}	7.654×10^{-137}
30.0	4.907×10^{-198}	9.813×10^{-198}	1.474×10^{-196}
35.0	1.125×10^{-268}	2.250×10^{-268}	3.940×10^{-267}
40.0	3.656×10^{-350}	7.312×10^{-350}	1.463×10^{-348}
45.0	1.676×10^{-442}	3.352×10^{-442}	7.547×10^{-441}
50.0	1.081×10^{-545}	2.161×10^{-545}	5.405×10^{-544}

Notes:

$X = (x-\mu)/\sigma$

$$Z(X) = \frac{1}{\sqrt{2\pi}} e^{-X^2/2}$$

$$P(X) = \int_{-\infty}^{X} Z(r)\, dr$$

$$Q(X) = \int_{X}^{\infty} Z(r)\, dr$$

$$A(X) = \int_{-X}^{X} Z(r)\, dr$$

$$R(X) = \int_{-\infty}^{-X} Z(r)\, dr + \int_{X}^{\infty} Z(r)\, dr$$

$P(X) = 1 - Q(X) = [A(X) + 1]/2 = 1 - R(X)/2$

$Q(X) = 1 - P(X) = [1 - A(X)]/2 = R(X)/2$

$A(X) = 1 - R(X) = 2\,P(X) - 1 = 1 - 2\,Q(X)$

$R(X) = 1 - A(X) = 2 - 2\,P(X) = 2\,Q(X)$

(i.e., sigma). Since X, Y, and Z are scaled by the value of σ, this doesn't create much of a limitation. Then, the area element for a sphere is ($r^2 \sin\theta\ dr\ d\theta\ d\phi$) replacing ($dx\ dy\ dz$) and $x^2+y^2+z^2 = r^2$. The two integrals with respect to angles simply cover the total solid angle of a sphere, thus the two outermost integrals give a value of 4π. At this point the result is the integral shown in Equation 11:

$$S(X) = \frac{2}{\sqrt{2\pi}} \int_{-X}^{X} r^2\ e^{-r^2/2} dr \qquad 11)$$

Making the further substitution that $r^2=t$, thus $2rdr = dt$, and also using $\chi^2=X^2$, gives the conventional form of the chi-squared distribution for degrees of freedom equal to three as shown in Equation 12:

$$S(\chi^2) = \frac{1}{\sqrt{2\pi}} \int_{0}^{\chi^2} t^{\frac{1}{2}}\ e^{-t/2} dt \qquad 12)$$

THE CHI-SQUARED DISTRIBUTION

If $X_1, X_2, \ldots, X_v$ are independent random variables distributed according to the standard normal distribution, then:

$$\chi^2 = \sum_{i=1}^{v} X_i^2 \qquad 13)$$

follows the chi-square distribution with v degrees of freedom and the probability that $X^2 \leq \chi^2$ is given by $P(\chi^2|v)$. Since the chi-square distribution is squared, it only runs from 0 to ∞.

In general, the chi-squared distribution is given as shown in Equation 14 below:

$$P(\chi^2|v) = [2^{v/2}\Gamma(v/2)]^{-1} \int_{0}^{\chi^2} x^{\frac{1}{2}v-1}\ e^{-x/2} dx \qquad 14)$$

For the case of a 1-D test where v=1, the chi-square distribution and the normal distribution are essentially the same. As long as the square of the standard deviation is used to look up the results and the region the probability is for is correctly handled (i.e., A(X) must be used), the numbers will be the same from either a chi-square with v=1 or normal distribution table.

However, if more than 1-D is involved, the distribution function associated with the magnitude of the displacement vector is the chi-squared (χ^2) distribution with the number of degrees of freedom equal to the number of test dimensions. This is for *uncorrelated cases* only (i.e., so the distribution functions are independent). Differences between the normal distribution and the chi-squared distribution are striking for test dimensions higher than 1-D as illustrated in Table 2.

Table 2 Chi-Squared Probabilities

	0 - 1 Sigma	1 - 2 Sigma	2 - 3 Sigma	3 - ∞ Sigma	Total	
	$\chi^2<1$	$1\leq\chi^2<4$	$4\leq\chi^2<9$	$9\leq\chi^2<\infty$	Total	Distribution
1-D	68.2	27.2	4.3	0.3	100.	$\left\{\begin{array}{c}\text{Normal or}\\ P(\chi^2\|v=1)\end{array}\right\}$
2-D	39.3	47.1	12.4	1.1	100.	$P(\chi^2\|v=2)$
3-D	19.9	54.0	23.2	2.9	100.	$P(\chi^2\|v=3)$

Typically tables of the chi-squared distribution are organized somewhat differently than tables of the normal distribution. Tables of the chi-squared distribution are usually used for significance testing and the issue is to determine what value of the random deviate, χ, is associated with the "confidence level," $P(\chi^2|v)$ for a two tailed test, given the number of observations in the table, v. The chi-square distribution is also capable of being tabulated in the same form as the standard normal distribution. This has been done in Table 3.

To calculate the results in Table 2 use Table 3. For example consider the case of the 2-D test between 1-2 sigma. From Table 3 look up $\chi^2 = 1^2 = 1$ for v=2 under $P(\chi^2|v=2)$. This number is 0.39347. Similarly, look up $\chi^2 = 2^2 = 4$ for v=2. This number is 0.86466. Then the integral from 0 to 1σ = .39347 while the integral from 0 to 2σ = .86466 and the integral from 1σ to 2σ = .86466 - .39347 = .47119 as shown in Table 2 above.

If there is correlation between the random variates it is necessary to switch to the statistics of a more general form of the bivariate normal (for 2-D) or trivariate normal (for 3-D). This is considerably more complicated.

CLIPPING THE RESULTANT VECTOR

Clipping is necessary to constrain the infinite domain of the chi-squared distribution to a region that the shaker can operate in. If the shaker travel is too extreme, the shaker will hit mechanical stops that limit the travel. This causes unacceptable, out of specification, high frequency input that potentially can destroy the test article. The mechanical stops are required to keep the shaker system together. The shaker would fall apart without them.

In a 1-D test system, the clipping is traditionally set to limit the maximum response level in the test to three sigma (3σ). Since the mean of the test input is zero, this is equivalent to clipping the signal at three times the wideband root mean squared (RMS) amplitude. This is clear from Equation 15 for the RMS amplitude and Equation 16 for the standard deviation of a signal.

Table 3 The Chi-squared Distribution

χ^2	$P(\chi^2 \mid v=1)$	$Q(\chi^2 \mid v=1)$	$P(\chi^2 \mid v=2)$	$Q(\chi^2 \mid v=2)$	$P(\chi^2 \mid v=3)$	$Q(\chi^2 \mid v=3)$
0.001	0.02522712	0.97477288	0.00049988	0.99950012	0.00000841	0.99999159
0.002	0.03567059	0.96432941	0.00099950	0.99900050	0.00002377	0.99997623
0.003	0.04368010	0.95631990	0.00149888	0.99850112	0.00004366	0.99995634
0.004	0.05042903	0.94957097	0.00199800	0.99800200	0.00006720	0.99993280
0.005	0.05637198	0.94362802	0.00249688	0.99750312	0.00009389	0.99990611
0.006	0.06174212	0.93825788	0.00299550	0.99700450	0.00012339	0.99987661
0.007	0.06667801	0.93332199	0.00349388	0.99650612	0.00015544	0.99984456
0.008	0.07126993	0.92873007	0.00399201	0.99600799	0.00018985	0.99981015
0.009	0.07558059	0.92441941	0.00448989	0.99551011	0.00022647	0.99977353
0.010	0.07965567	0.92034433	0.00498752	0.99501248	0.00026517	0.99973483
0.020	0.11246292	0.88753708	0.00995017	0.99004983	0.00074776	0.99925224
0.030	0.13750977	0.86249023	0.01488806	0.98511194	0.00136961	0.99863039
0.040	0.15851942	0.84148058	0.01980133	0.98019867	0.00210234	0.99789766
0.050	0.17693673	0.82306327	0.02469009	0.97530991	0.00292933	0.99707067
0.060	0.19350406	0.80649594	0.02955447	0.97044553	0.00383921	0.99616079
0.070	0.20866322	0.79133678	0.03439458	0.96560542	0.00482352	0.99517648
0.080	0.22270259	0.77729741	0.03921056	0.96078944	0.00587563	0.99412437
0.090	0.23582284	0.76417716	0.04400252	0.95599748	0.00699016	0.99300984
0.100	0.24817037	0.75182963	0.04877058	0.95122942	0.00816258	0.99183742
0.200	0.34527915	0.65472085	0.09516258	0.90483742	0.02241070	0.97758930
0.300	0.41611758	0.58388242	0.13929202	0.86070798	0.03997152	0.96002848
0.400	0.47291074	0.52708926	0.18126925	0.81873075	0.05975751	0.94024249
0.500	0.52049988	0.47950012	0.22119922	0.77880078	0.08110859	0.91889141
0.600	0.56142197	0.43857803	0.25918178	0.74081822	0.10356763	0.89643237
0.700	0.59721631	0.40278369	0.29531191	0.70468809	0.12679605	0.87320395
0.800	0.62890663	0.37109337	0.32967995	0.67032005	0.15053297	0.84946703
0.900	0.65721829	0.34278171	0.36237185	0.63762815	0.17457219	0.82542781
1.000	0.68268949	0.31731051	0.39346934	0.60653066	0.19874804	0.80125196
2.000	0.84270079	0.15729921	0.63212056	0.36787944	0.42759330	0.57240670
3.000	0.91673548	0.08326452	0.77686984	0.22313016	0.60837482	0.39162518
4.000	0.95449974	0.04550026	0.86466472	0.13533528	0.73853587	0.26146413
5.000	0.97465268	0.02534732	0.91791500	0.08208500	0.82820286	0.17179714
6.000	0.98569412	0.01430588	0.95021293	0.04978707	0.88838977	0.11161023
7.000	0.99184903	0.00815097	0.96980262	0.03019738	0.92810223	0.07189777
8.000	0.99532227	0.00467773	0.98168436	0.01831564	0.95398829	0.04601171
9.000	0.99730020	0.00269980	0.98889100	0.01110900	0.97070911	0.02929089
10.00	0.99843460	0.00156540	0.99326205	0.00673795	0.98143386	0.01856614
20.00	0.99999226	0.00000774	0.99995460	0.00004540	0.99983026	0.00016974
30.00	0.99999996	4.320×10^{-8}	0.99999969	3.059×10^{-7}	0.99999862	1.380×10^{-6}
40.00	1.00000000	2.54×10^{-10}	1.00000000	2.061×10^{-9}	0.99999999	1.066×10^{-8}
50.00	1.00000000	1.54×10^{-12}	1.00000000	1.39×10^{-11}	1.00000000	7.99×10^{-11}
60.00	1.00000000	9.49×10^{-15}	1.00000000	9.36×10^{-14}	1.00000000	5.88×10^{-13}
70.00	1.00000000	5.93×10^{-17}	1.00000000	6.31×10^{-16}	1.00000000	4.27×10^{-15}
80.00	1.00000000	3.74×10^{-19}	1.00000000	4.25×10^{-18}	1.00000000	3.07×10^{-17}
90.00	1.00000000	2.38×10^{-21}	1.00000000	2.86×10^{-20}	1.00000000	2.19×10^{-19}
100.0	1.00000000	1.52×10^{-23}	1.00000000	1.93×10^{-22}	1.00000000	1.55×10^{-21}

$$RMS = \sqrt{\frac{\sum_{i=1}^{n} x_i^2}{n}} \qquad 15)$$

$$\sigma = \sqrt{\frac{\sum_{i=1}^{n} (x_i - \bar{x})^2}{n-1}} \qquad 16)$$

Clearly there is very little difference between the two definitions if the mean is zero, $\bar{x}=0$. The factor used to normalize is slightly different, n instead of n-1. Other than that, the two equations are identical.

In the 3-D test the corresponding clipping would be ellipsoidal along the constant wideband RMS amplitude surfaces for the test. While this is not the way that 3-D test systems currently clip, this is the preferred clipping technique and hopefully will become available some day. This approach is preferred because of the spatial uniformity of the resulting peak amplitudes and more uniform test statistics. Even when clipping on the resultant vector, the chi-squared statistics of the resultant vector dictates a different clipping limit than the traditional 3σ. Consider for example the following table for the chi-squared distribution:

Table 4 Extrema of the Chi-Squared Distribution

σ	χ^2	Probability of Exceeding χ^2 1-D (v=1)	2-D (v=2)	3-D (v=3)
3.0	9.00	0.002700	0.011109	0.029291
3.1	9.61	0.001935	0.008189	0.022189
3.2	10.24	0.001374	0.005876	0.016632
3.3	10.89	0.000967	0.004318	0.012336
3.4	11.56	0.000674	0.003089	0.009059
3.5	12.25	0.000465	0.002187	0.006574
3.6	12.96	0.000318	0.001534	0.004724
3.7	13.69	0.000216	0.001065	0.003359
3.8	14.44	0.000145	0.000732	0.002363
3.9	15.21	0.000096	0.000498	0.001646
4.0	16.00	0.000063	0.000335	0.001134

From Table 4 above, clipping at 3σ for a 1-D test results in a probability of clipping of 0.00270 or .27% of the time. To put this into perspective, suppose the control system is operating to 800 Hz with a sampling rate of 2048 samples/second. This produces on average 2048×.00270 = 5.5296 clips per second. Every test has a great many clipped inputs.

In the case of the 2-D test, clipping at 3σ will result in a probability of clipping of 0.011109 or 1.1109% of the time. Using the same situation as above, this produces 2048×0.011109 = 22.7512 clips per second. To achieve the same rate of clipping as in the 1-D test, it is necessary to clip at 3.44σ.

Considering the 3-D test, clipping at 3σ produces a probability of clipping

of 0.029291 or 2.9291% of the time. This produces 2048×0.029291= 59.9880 clips per second - more than 10 times the 1-D clipping rate. In the 3-D test it is necessary to clip at 3.76σ in order to achieve the same clipping rate as in the 1-D test.

Too high a clipping rate will have a detrimental affect on the control loop since the signal will be reduced without any corresponding correction to the equalization. The system will increase the test amplitude to make up for this unexpected loss of signal. As long as the loss is very small, nothing significant happens; however, if clipping occurs too often the system can potentially become uncontrollable.

IMPLEMENTATION OF CLIPPING ON THE RESULTANT VECTOR

Typical current test control systems clip their output signal at an empirical value just before sending the signal to the power amplifier. Because of the central limit theorem, clipping tends to be somewhat empirical. In this context the central limit theorem says that any distribution will approach a normal distribution after a sufficiently large number of mathematical operations are performed on it. The clipped time history is operated upon by the physical amplifier and shakers, tending to return the distribution to a normal distribution, undoing the clipping. For this reason it is necessary to correlate the achieved level of clipping to the empirical level the signal was actually clipped at.

To clip based on the resultant vector, it would be necessary to calculate it - a step not currently taken. All three frames of data (X(t), Y(t), and Z(t)) would have to be available in one place to estimate the resultant: $R(t)^2 = X(t)^2 + Y(t)^2 + Z(t)^2$. Then the resultant would need to be compared to χ^2. If $R(t_o)^2 > \chi^2$ the ratio $\chi/R(t_o)$ would need to be multiplied individually times $X(t_o)$, $Y(t_o)$, and $Z(t_o)$ to produce the clipped signal in each axis respectively. All three inputs would need to be cut back proportionally to produce clipping that does not change the distribution of data spatially. In floating point this calculation is fairly slow and current systems do not clip this way. Instead, the individual components are clipped to a prescribed level without reference to the other component amplitudes. This is done by simply replacing values exceeding χ with the value χ and values less than $-\chi$ with the value $-\chi$.

While it is desirable to clip on the resultant vector, the advantages of 3-D testing are sufficient that it is <u>not</u> essential. Clipping on the individual components have an array of unfortunate side effects which will be discussed in detail in the following paragraphs. In the real world, inputs are also limited to some maximum upper bound, however, experience suggests that a factor of 3 between the RMS and the peak amplitude is far to small a number. In the transportation vibration environment, a factor of ten is more typical. Of course the distribution function is also <u>not normal</u> to observe values that high in practice. The probability of exceeding a 10σ value for a normal distribution is $1\text{-}A(10.) = 1.523971\times10^{-23}$. It is reassuring to realize that the clipping issue is of the same order of magnitude as the issue of the correct distribution function.

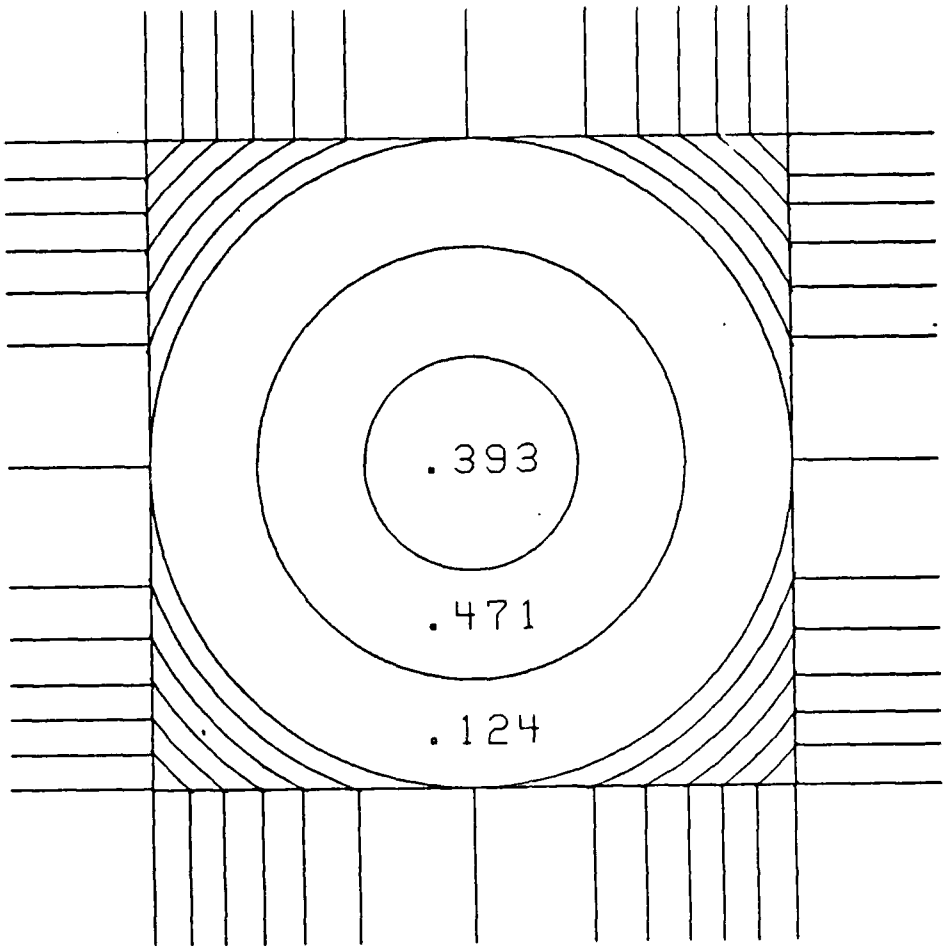

Figure 2 Regions of the Clipped 2-D Distribution

CLIPPING THE COMPONENT AMPLITUDES

Current control systems clip the individual shaker amplitudes instead of the composite resultant vector. Each shaker is limited to a range from -3σ to +3σ on a side. As has already been demonstrated, this is equivalent to -3×RMS to +3×RMS. Unfortunately this geometry results in the shaker being constrained to a region which is box shaped instead of the ellipsoidal shaped region which is desired. The probability space is distorted by the clipping to have 100% of the probability associated with the space inside the box. Detailed calculation of the clipped probability density function in three dimensions has proved difficult to date. However the calculation in 2-D has been done and is outlined below:

THE 2-D CLIPPED DISTRIBUTION FUNCTION

Calculating how the clipping will affect the distribution function is an exercise in plane geometry. Figure 2 illustrates the basic regions of the test and the icons in the margin indicate which region is currently being discussed.

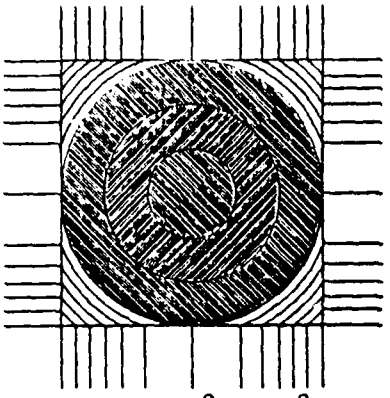

In the region where no clipping takes place (e.g., below 3σ), the distribution is chi-squared with degrees of freedom equal to two (because it is 2-D). The chi-squared distribution has already been discussed and the result is indicated below:

To get the probability between two values (e.g., 1σ to 2σ) for degrees of freedom equal to two, this is simply:

$$P(1^2 \le \chi^2 \le 2^2 | 2) = \frac{1}{2}\int_1^4 e^{-x/2}dx = e^{-1/2} - e^{-4/2} = .471195 \qquad 17)$$

This is a remarkably simple case for integrating a probability density function. It can be done in closed form! Notice that the multiplier on the exponential is -1/2. Thus the order of integration effectively changes and the 1/2 in front of the integral is cancelled.

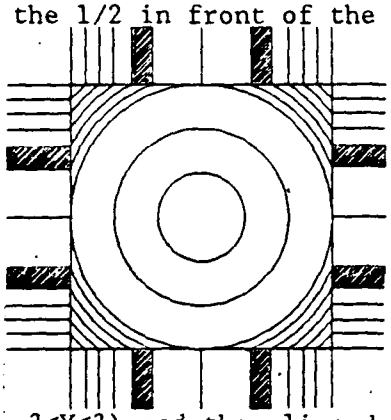

Referring to Figure 2, this is the appropriate calculation where no clipping is involved. In Figure 2, this is the region of concentric circles inside the box. The box represents the value at which the clipping takes place (3σ in Figure 2). The region outside the box is that part of the distribution where the signal would have exceeded the clipping limit. In these regions outside the box, all the probability to infinity will show up at a value defined by the unclipped shaker's signal. If the unclipped shaker is putting out $Y\sigma$ (where $-3 \le Y \le 3$) and the clipped shaker is putting out 3σ. Then the resultant will be as follows:

$$R = (3^2+Y^2)^{1/2}\,\sigma \qquad 18)$$

Since Y is 1-D and normally distributed, the resultant in this region will be normally distributed and the probability of both clipping and observing greater than or equal to $Y\sigma$ on the other axis is just:

$$P = N(X \ge 3\sigma) \times N(Y \ge Y\sigma) \qquad 19)$$

To calculate a category, e.g., 3.2σ to 3.4σ, first calculate how large a value of Y will produce a resultant in the correct range. Looking back at Equation 18 for the resultant, set R equal to 3.2 and calculate Y:

$$Y = (3.2^2 - 3^2)^{1/2}\,\sigma = 1.1\sigma \text{ to produce a clipped resultant of } 3.2\,\sigma \qquad 20)$$

$$Y = (3.4^2 - 3^2)^{1/2}\,\sigma = 1.6\sigma \text{ to produce a clipped resultant of } 3.4\,\sigma$$

Then the probability that the result is between 3.2σ and 3.4σ is given by the following:

$$N(X \geq 3\sigma) \times [N(Y \geq 1.11\sigma) - N(Y \geq 1.6\sigma)] \qquad 21)$$

$$0.001349898 \times [.1327355 - .05479929] = .0001052060$$

From Figure 2 there are eight of these regions. Thus the probability from all eight of these regions is .000841648 since they are all equal.

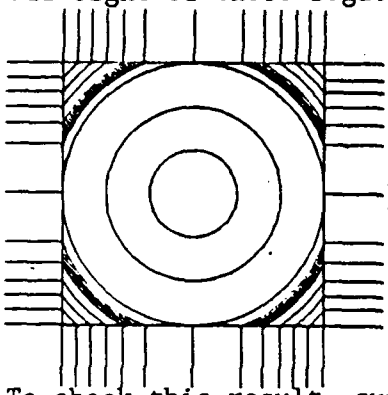

Next there is the circular arcs inside the box to be calculated. In this region the distribution is chi-squared with 2 degrees of freedom. Since the data is uniformly distributed with respect to the angular position, it is sufficient to calculate what part of the circle is included as a function of the radius. A little geometry produces the result that the arc length in radians is as shown below:

$$\text{Arc length} = 4(\pi/2 - 2\cos^{-1}(3/R)) \qquad 22)$$

To check this result, suppose $R=3\sqrt{2}$ so there is no arc left. Then the argument of the arc cosine goes to $\sqrt{2}/2$ and the arc cosine becomes $\pi/4$. This produces the correct result: zero.

Dividing by 2π to produce a ratio, the integral that needs to be evaluated is simply:

$$P(3.2^2 \leq \chi^2 \leq 3.4^2 | 2) = \frac{1}{2} \int_{3.2^2}^{3.4^2} [1 - \frac{4}{\pi} \cos^{-1}(\frac{3}{\sqrt{x}})] \, e^{-x/2} \, dx \qquad 23)$$

The square root of x is required in the argument of the arc cosine because the integrand is the square of the resultant amplitude instead of the resultant amplitude itself.

Evaluating this integral numerically, gives .001340544 for the probability associated with the curved areas from Figure 2. Adding this result to the one calculated earlier gives: .001340544 + .000841648 = .002182192 for the total probability associated with the region 3.2σ to 3.4σ.

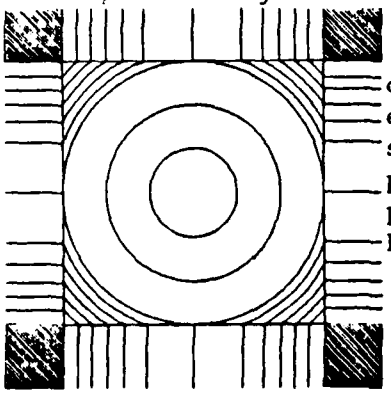

This leaves the square boxes on the outside corners of the box to be calculated. This is the easiest of the regions to calculate since both shakers are clipped in this region. Thus the probability of being in this region is simply the product of two normal distributions as shown in Equation 24.

$$P = N(X \geq 3) \times N(Y \geq 3) \qquad 24)$$

$$0.001349898^2 = .00000182222$$

There are four of these regions so the total probability associated with them is 0.00000728889, and since both signals are clipped they show up as a lump of probability at $3\sqrt{2}\sigma$.

Table 5 2-D Box Clipping

Clipping at	2.0 σ	2.2 σ	2.4 σ	2.6 σ	2.8 σ
0.0-0.2 σ	.019801327	.019801327	.019801327	.019801327	.019801327
0.2-0.4 σ	.057082327	.057082327	.057082327	.057082327	.057082327
0.4-0.6 σ	.087846135	.087846135	.087846135	.087846135	.087846135
0.6-0.8 σ	.109121174	.109121174	.109121174	.109121174	.109121174
0.8-1.0 σ	.119618377	.119618377	.119618377	.119618377	.119618377
1.0-1.2 σ	.119778404	.119778404	.119778404	.119778404	.119778404
1.2-1.4 σ	.111441157	.111441157	.111441157	.111441157	.111441157
1.4-1.6 σ	.097273798	.097273798	.097273798	.097273798	.097273798
1.6-1.8 σ	.080138601	.080138601	.080138601	.080138601	.080138601
1.8-2.0 σ	.062563416	.062563416	.062563416	.062563416	.062563416
2.0-2.2 σ	.088054994	.046413666	.046413666	.046413666	.046413666
2.2-2.4 σ	.027451718	.058447651	.032786855	.032786855	.032786855
2.4-2.6 σ	.012139578	.017937057	.037281284	.022087308	.022087308
2.6-2.8 σ	.005195305	.007710651	.011258562	.022852604	.014206360
2.8-3.0 σ	.000423414	.003218127	.004704815	.006786431	.013461444
3.0-3.2 σ		.000834908	.001914330	.002756253	.003927661
3.2-3.4 σ			.000706974	.001092659	.001549731
3.4-3.6 σ				.000402907	.000598102
3.6-3.8 σ				.000069694	.000216099
3.8-4.0 σ					.000061943
Maximum	2.82843 σ	3.11127 σ	3.39411 σ	3.67696 σ	3.95980 σ
Prob	.002070274	.000773223	.000268798	.000086907	.000026115
	1.000000000	1.000000000	1.000000000	1.000000000	1.000000000

Table 5 2-D Box Clipping, Continued

Clipping at	3.0 σ	3.2 σ	3.4 σ	3.6 σ	3.8 σ
0.0-0.2 σ	.019801327	.019801327	.019801327	.019801327	.019801327
0.2-0.4 σ	.057082327	.057082327	.057082327	.057082327	.057082327
0.4-0.6 σ	.087846135	.087846135	.087846135	.087846135	.087846135
0.6-0.8 σ	.109121174	.109121174	.109121174	.109121174	.109121174
0.8-1.0 σ	.119618377	.119618377	.119618377	.119618377	.119618377
1.0-1.2 σ	.119778404	.119778404	.119778404	.119778404	.119778404
1.2-1.4 σ	.111441157	.111441157	.111441157	.111441157	.111441157
1.4-1.6 σ	.097273798	.097273798	.097273798	.097273798	.097273798
1.6-1.8 σ	.080138601	.080138601	.080138601	.080138601	.080138601
1.8-2.0 σ	.062563416	.062563416	.062563416	.062563416	.062563416
2.0-2.2 σ	.046413666	.046413666	.046413666	.046413666	.046413666
2.2-2.4 σ	.032786855	.032786855	.032786855	.032786855	.032786855
2.4-2.6 σ	.022087308	.022087308	.022087308	.022087308	.022087308
2.6-2.8 σ	.014206360	.014206360	.014206360	.014206360	.014206360
2.8-3.0 σ	.008732098	.008732098	.008732098	.008732098	.008732098
3.0-3.2 σ	.007619716	.005132974	.005132974	.005132974	.005132974
3.2-3.4 σ	.002182192	.004144318	.002887307	.002887307	.002887307
3.4-3.6 σ	.000836076	.001163781	.002165758	.001554905	.001554905
3.6-3.8 σ	.000313871	.000432733	.000595715	.001087392	.000802008
3.8-4.0 σ	.000110912	.000157886	.000214853	.000292669	.000524518
4.0-4.2 σ	.000035600	.000054471	.000076124	.000102328	.000138000
4.2-4.4 σ	.000003341	.000017242	.000025602	.000035180	.000046750
4.4-4.6 σ		.000003702	.000007964	.000011517	.000015584
4.6-4.8 σ			.000002204	.000003511	.000004960
4.8-5.0 σ			.000000040	.000000966	.000001478
5.0-5.2 σ				.000000146	.000000402
5.2-5.4 σ					.000000090
Maximum	4.24264 σ	4.52548 σ	4.80833 σ	5.09117 σ	5.37401 σ
Prob	.000007289	.000001889	.000000454	.000000101	.000000021
	1.000000000	1.000000000	1.000000000	1.000000000	1.000000000

Table 5 summarize the results in 2-D. The table shows the theoretical probability of observing data in categories of 0.2σ increments. For example, if the clipping is set up at 3.0σ (across the top of the chart in the "Clipping at" row), the probability of observing data between 3.2σ and 3.4σ is .002182192 to nine decimal places. Of course, the reason data is observed above 3.0σ where the clipping was implemented is because the clipping is box shaped.

Notice that there is a line across the data at 3.0σ in the 3.0σ clipping column. This is the amplitude where the clipping starts to influence the table. Above the line, all the columns in the table have the same values. The constant data is determined from a chi-squared distribution of degrees of freedom 2 (since this is a 2-D test). Below the line, the data is partly determined from the chi-squared distribution of degrees of freedom 2 (in the diagonals of the box where the amplitude isn't clipped) and is partly determined from the normal distribution when the amplitude is clipped.

Finally, there is a fixed probability associated with the $3.0\times\sqrt{2}$ where both shakers are clipping the signal. The value of $3.0\times\sqrt{2}\sigma$ is given in the column labelled "Maximum" (i.e., 4.24264σ in this case) and the value of the probability associated with this value is given in the column labelled "Prob" (i.e., $.000007289\sigma$). Finally the sum of all the probabilities adds up to one (to nine decimal places) in the column below all the data.

The very last category in most cases will not be easily distinguished from the lump of data when both shakers are clipping. In the 3.0 σ clipping case, the category 4.2 σ up to 4.2426 σ is listed as a separate entity and has a probability of .000003341. It will be very difficult to distinguish these numbers from the data at 4.2426 σ, and it would be easiest to look for the data in the last two categories added together (i.e., .000003341 + .000007289 = .000010630 between 4.2σ and 4.4σ).

This "least likely" category gives an easy way to estimate how long the data will need to be averaged to verify the numbers in Table 5. For example, consider data limited to 800 Hz. There would be 2048 samples/second. This is calculated as the power of two above Nyquist folding at 2×800 Hz. The power of two is used because it is required for the fast Fourier transform algorithm used in the control system. For 1 minute, this would be 2048×60 = 122,880 samples/minute. If the "least likely" probability is .000010630 then this implies .000010630×122880 = 1.306 extreme data points per minute. To get a repeatable number it takes at least 20 data points, so 20/1.306 = 15.311 minutes of data need to be taken to demonstrate this probability.

Of course numerous numerical problems might occur if one took too much data. For typical floating point, single precision numbers, errors will result if more than 2^{23} = 8,388,608 samples (8388608/122880 = 68.2 minutes at 2048 samples/second) are used. If the person coding the computer was sensitive to this issue, the number of samples can be kept in integer form and be accurate to 2^{31} = 2,147,483,648 samples (12.1 days of data). Even better, if double precision is used, the number of samples would typically be accurate to $2^{47} = 1.407\times10^{14}$ samples (2179.0 years of data).

THE 3-D CLIPPED DISTRIBUTION FUNCTION

While the corresponding calculation for the 3-D clipped distribution function is difficult, some of the more important results are easy to calculate. The clipping constrains the shaker to a box shaped region around the center point of the shake table. The edges of the box are at $+3\sigma$ to -3σ or as shown earlier at +3×RMS to -3×RMS if the clipping is implemented at 3σ. The corners of the box are $3\sqrt{3}\sigma$ or 5.19615σ away. The probability of exceeding 5.19615σ in 1-D is 1.017277×10^{-7} so it is reasonable that a location this far off nominal will cause problems with obtaining a repeatable peak response amplitude for a random test implemented with this kind of clipping.

Since this value is observed whenever the unclipped drive signals to all three shakers individually exceed 3σ, the probability is simply given by $[1-N(-3\leq X\leq 3)]^3$ or 1.96785×10^{-8}. This calculation assumes that the response of the shakers is uncorrelated. If the shaker signals were correlated (as opposed to having individual frequencies that are coherent), then a much more difficult calculation would need to be performed using the trivariate normal distribution.

A probability this low causes repeatability problems with the peak amplitude of the test specification. Suppose the system were set up to control to 800 Hz. The sampling rate would be the first power of two to exceed the frequency required by Nyquist folding at 2×800 samples/second. This gives a sampling rate of 2024 samples/second. The expected time between peak responses is given by $2024\times3600\times1.96785\times10^{-8} = .1433857$ extreme data points per hour. This is 1/.1433857 = 6.974195 hours between extreme data points. For typical test times in minutes (not hours) the observed peak value will vary significantly from test to test.

If the peak amplitude must be more repeatable, the only parameter available to reduce the probability of hitting the corner is the level at which the clipping is implemented. Table 6 illustrates the same results derived above for a variety of levels of clipping.

In Table 6 the left most column (labelled "Clipping Sigma") indicates the level that the shakers are set to clip at. The next column is the probability that a 3-D point (composed of three random numbers) will be clipped. This column is labelled "Prob of Clipping" and is calculated as one minus the probability that all three shakers will not be clipped (i.e., $1 - N(-c\leq X\leq c)^3$ where c stands for the clipping level). For example, with clipping set at 2σ, $1 - .9544^3 = 13\%$ of the data points will be clipped. This is a very high rate that might reasonably be expected to cause problems with the test control system since the RMS amplitude and frequency distribution of the input will very likely be affected. To translate this result into more physical units, the clipping probability has been multiplied times the digitization rate (assumed to be 2048 samples/second) in the third column labelled "Clipping Times/Sec."

The column labelled "Sigma to Corner" is simply the square root of three times the clipping level. This indicates how many sigma away the corner of the clipping box is located at.

Table 6 3-D Clipping Rate Versus Frequency of Hitting the Corner

Clipping Sigma	Prob of Clipping	Clipping Times/Sec	Sigma to Corner	Prob of Hit Corner	Corner Times/Hour
2.00	.1303842	267.03	3.46	.000094198	694.50
2.10	.1034025	211.77	3.64	.000045610	336.27
2.20	.0811225	166.14	3.81	.000021501	158.52
2.30	.0629744	128.97	3.98	.000009867	72.746
2.40	.0483832	99.09	4.16	.000004407	32.492
2.50	.0367972	75.36	4.33	.000001916	14.123
2.60	.0277072	56.74	4.50	.000000810	5.9733
2.70	.0206579	42.31	4.68	.000000333	2.4580
2.80	.0152526	31.24	4.85	.000000133	.98392
2.90	.0111532	22.84	5.02	.000000052	.38311
3.00	.0080775	16.54	5.20	.000000020	.14509
3.10	.0057944	11.87	5.37	.000000007	.05343
3.20	.0041172	8.43	5.54	.000000003	.01914
3.30	.0028977	5.93	5.72	.000000001	.00666
3.40	.0020202	4.14	5.89	.000000000	.00226
3.50	.0013951	2.86	6.06	.000000000	.00074
3.60	.0009543	1.95	6.24	.000000000	.00024
3.70	.0006467	1.32	6.41	.000000000	.00007
3.80	.0004340	0.89	6.58	.000000000	.00002
3.90	.0002886	0.59	6.75	.000000000	.00001
4.00	.0001900	0.39	6.93	.000000000	.00000

Finally the probability of all three shakers being clipped at exactly the same time is calculated in the column labelled "Prob of Hit Corner." The way that the extreme corner of the box is reached is for all three shakers to be clipped at one time. This is just $[1 - N(-c \leq X \leq c)]^3$. In the case of clipping at 2σ this probability is $[1-.9544]^3 = .0094\%$. To put this into more physical units, this probability is multiplied by the sampling rate in samples/hour (2048×3600) to give 694.5 corner hits per hour as indicated in the column labelled "Corner Times/Hour."

The results in Table 6 indicate the degree of difficulty faced in trying to increase the probability of hitting the corner by decreasing the level clipping is implemented at. At 3σ 100×0.0080775 = 0.8% of the vectors are clipped and the corner is hit on average once every 1/.14509 = 6.9 hours. To get the average rate of hitting the corner down to 10 min (i.e., 60/5.9733) the clipping has to be increased to 2.6σ and 100×.0277072 = 2.7% of the vectors are clipped. This is a dangerously high clipping rate considering that the control system will be trying to undo the affects of the clipping. To decrease the average rate of hitting the corner down to 5 seconds (i.e., 3600/694.5) the clipping rate has to be increase to 100×.1303842 = 13% of the vectors. This much clipping may cause an out of specification condition on wideband RMS assuming the test is required to be ±10%.

By way of comparison, in a 1-D test clipping at 3σ the rate at which the most extreme number is reached is 0.0026997×2024 = 5.52918 hits/second or on average 1/5.52918 = .2 seconds between hits (compared to 6.9 hours for 3-D at 3σ). The rate at which numbers are clipped is 100×0.0026997 = 0.3% of

the numbers (compared to 0.8% for 3-D at 3σ). There is absolutely no way that the 1-D numbers can be matched using the existing 3-D clipping procedures.

RANDOM VIBRATION TEST SPECIFICATION FOR CLIPPING

One way out of the box shaped clipping problem is to write the specification in such a way that box shaped clipping is allowed. Current test specifications typically address the clipping as shown below:

> "The test input shall be Gaussian distributed noise, shaped in the frequency domain per the test specification from the previous section, and clipped at 3 sigma."

The simplest way of dealing with the box shaped clipping is to say something like the following:

> "The spatial components of the input shall be Gaussian distributed noise shaped in the frequency domain per the specification from the previous section, and clipped at 3 sigma. This produces a resultant vector which is distributed chi-squared and clipped at 3 sigma in the shaker directions and up to 5.2 sigma along the diagonals from the shaker directions."

In both cases there needs to be a tolerance statement stating that the peak amplitude for clipping is known ±10%.

If the customer objects to the high peak amplitude that may occur during the test it can be reduced by reducing the clipping level from 3σ to some other level such as 2.6σ based on Table 6. However this should not be a problem very often. In the real world, peak to RMS ratios as high as 10 are observed. There is nothing magic about the 3σ level that is in common practice for 1-D. It just produces a very good probability of clipping: low enough that it doesn't interfere with the test control system and high enough that clipping happens continuously thus creating a well defined maximum amplitude. Unfortunately there is no corresponding good level when the components (as opposed to the resultant vector) are clipped. If the resultant vector were clipped at 3.67σ it would result in the same probability of clipping as 3σ in the 1-D test.

MORE ADVANCED DISTRIBUTION FUNCTIONS

So far the normal distribution has been transformed into the standard normal distribution. The standard normal distribution was introduced in three Cartesian directions to get the spherical normal distribution. The spherical normal distribution was transformed into spherical coordinates to get the chi-squared distribution. Clipping was introduced into the chi-squared distribution to get the chi-squared distribution clipped on the resultant vector. Also clipping on the Cartesian components of the spherical distribution was introduced to get the 2-D and 3-D box clipped distributions.

Perhaps the ultimate distribution along these lines is the bivariate normal in 2-D or the trivariate normal in 3-D. These are distributions that allow correlation between the axes. For example, the bivariate normal is given by Equation 25:

$$L(X,Y|\rho) = \frac{1}{2\pi\sqrt{1-\rho^2}} \int_X^{\infty} \int_Y^{\infty} e^{-\frac{1}{2}(x^2-2\rho xy+y^2)/(1-\rho^2)} dy\, dx \qquad 25)$$

The correlation coefficient, ρ, allows the two axes to be interrelated in any way that can be specified through the use of a covariance matrix. More generally, the multivariate normal (including the trivariate normal) can be specified as shown in Equation 26 from Principles of Econometrics by H. Theil, page 67.[2]

$$\underset{1\times n}{P(\langle X\rangle|[V])} = \frac{1}{(2\pi)^{n/2}|V|^{\frac{1}{2}}} \int_{-\infty}^{X_n} \cdots \int_{-\infty}^{X_2} \int_{-\infty}^{X_1} e^{-\frac{1}{2}\underset{1\times n}{\langle x-\mu\rangle'} \underset{n\times n}{V^{-1}} \underset{n\times 1}{(x-\mu)}} dx_1 . dx_n \qquad 26)$$

Where: $-\frac{1}{2}\underset{1\times n}{\langle x-\mu\rangle'} \underset{n\times n}{V^{-1}} \underset{n\times 1}{(x-\mu)}$ is a rather long algebraic expression

$|V|$ stands for the determinant of the covariance matrix.

In practice, the standard methods for specifying random tests will almost always result in very nearly spherical normal distributions without any correlation between axes. This is partly a consequence of the central limit theorem, i.e., given a sufficient number of mathematical operations performed on the distribution any distribution will approximate a normal distribution. Using standard test methods there is no way to interrelate different frequencies in a deterministic way. Even if multiple axes are interrelated at a frequency through coherence, unless the same kinds of interrelationships are present in a lot of frequencies, the net effect is normal because of the central limit theorem.

As long as at least six spectral lines are at the maximum amplitude for a given test specification and the coherence is not uniformly high, the distribution is assured of being very nearly spherical normal. A procedure very much like root mean squaring together six spectral lines is in common practice for generating normally distributed random deviates. In the random number generator the numbers are uniformly distributed instead of being a sinusoid. Even when there is only one spectral line, this produces sinusoids that stop and restart at each frame boundary with a new random starting phase angle. A sinusoid all alone isn't too bad of an approximation for a normal distribution in the central part of the distribution. Of course anything beyond $\sqrt{2}\sigma$ simply isn't there for a single sinusoid, 100% of the probability happens between $-\sqrt{2}\sigma$ to $\sqrt{2}\sigma$.

High coherence can cause the observed test distribution to be trivariate normal instead of spherical normal. This is important because it helps explain why tests that reproduce measured data can sometimes produce failures when tests that envelope the environment don't. In the trivariate

normal distribution, a disproportionate amount of the test can be oriented in any arbitrary direction. The spatial distribution of the probability does not have to be uniform. As will be shown in the next Chapter, correlation between axes produce ellipsoidal RMS surfaces that can be arbitrarily oriented with respect to the test axes.

References

1. Abromowitz, M., and Stegun, I. A., Handbook of Mathematical Functions, 1965, Dover Publications, Chapter 26.

2. Theil, H., Principles of Econometrics, 1971, John Wiley & Sons, Inc.; page 67, equation 26.

CHAPTER 3 COVARIANCE THEORY IN 3-D

INTRODUCTION

In the previous chapter, distribution theory ended with the trivariate normal distribution expressed in terms of the covariance matrix. In this chapter the covariance matrix is discussed giving relationships governing the RMS and principal directions of the RMS surface. This is in preparation for considering the more complicated (but very similar) spectral matrix. With the exception of the section on physically realizable correlation coefficients which appears to be original, the material presented here is very standard and is the basis of factor analysis in statistics.

BASIC DATA

Suppose a set of n data points in three orthogonal directions were available as illustrated below, i.e., the control accelerometers:

$$\underset{1\times n}{\langle x\rangle} = \langle x_1, x_2, x_3, \ldots, x_n\rangle \quad \text{where: } \bar{x} = \sum_{i=1}^{n} x_i/n = 0$$

$$\underset{1\times n}{\langle y\rangle} = \langle y_1, y_2, y_3, \ldots, y_n\rangle \quad \text{where: } \bar{y} = \sum_{i=1}^{n} y_i/n = 0 \qquad 1)$$

$$\underset{1\times n}{\langle z\rangle} = \langle z_1, z_2, z_3, \ldots, z_n\rangle \quad \text{where: } \bar{z} = \sum_{i=1}^{n} z_i/n = 0$$

More concisely, represent the data as the matrix [X]:

$$\underset{n\times 3}{[X]} = \begin{bmatrix} x_1 & y_1 & z_1 \\ x_2 & y_2 & z_2 \\ x_3 & y_3 & z_3 \\ \vdots & \vdots & \vdots \\ x_n & y_n & z_n \end{bmatrix} \quad \text{where: } \underset{3\times n}{[X']}\underset{n\times 1}{(1)}/n = \underset{3\times 1}{(0)} \qquad 2)$$

(1) is a column vector of ones
(0) is a column vector of zero
[X'] indicates transpose of [X]

Note, there are no restrictions of any kind on the points comprising [X], except the constraint imposed physically by the shaker used to excite the motion - i.e., the data must not translate. The mathematics still holds without this constraint but the subsequent definitions must take into account the mean if it is not zero.

In particular, no assumption is required that the data is uniformly distributed random noise. It could just as well be sampled data from a sinusoid. Actually none of the results presented for the covariance matrix depend on any distributional assumption. At this point the data doesn't even have to come from a time series or be in any particular order. It is only necessary to keep <x,y,z> sets together. So x_1 must be associated with y_1 and z_1, but which data set comes first does not matter.

THE VECTOR METHOD OF DEMONSTRATING THE RMS SURFACE

The simplest method of measuring the RMS surface in any direction is to estimate the time history in the appropriate direction from the three control accelerometer signals. If one views the output of the control accelerometers as a continuous representation of the components of the instantaneous acceleration vector for the table, it is easy to estimate the rigid body acceleration in any direction by simply taking the vector components. For example, suppose the instantaneous acceleration time histories were represented by digital vectors sampled at some sampling interval as in Equation 1.

To estimate the time history along a vector through a point at (1,2,3) from (0,0,0) simply compute the direction cosines. The length of the vector is $R^2 = 1^2 + 2^2 + 3^2 = 14$. Thus the time history in that direction is just:

$$R(t) = (1/\sqrt{14})\ X(t) + (2/\sqrt{14})\ Y(t) + (3/\sqrt{14})\ Z(t) \qquad 3)$$

It is possible to compute the RMS of this time history and find the peak amplitudes.

To demonstrate that this works, it is necessary to measure a fourth accelerometer's time history and compare it to the computed value from the formula above. Errors will be introduced by this procedure primarily from three sources: 1) unless sample and hold techniques are used, the digitization will introduce slight time lags between the component time histories, 2) analog accelerometer scale factors are only accurate to one or two decimal places, and finally, 3) it is difficult to orient an accelerometer arbitrarily in space.

In doing this it is easiest to estimate the direction cosines after the fact to minimize the effects of these error sources. In general, the signal in any direction can be estimated by a least squares curvefit given the time history for the inputs from Equation 2 and the time history for the response, R, and n×1 vector of measured response values. The least squares curvefit for the direction cosines is:

$$\underset{3\times1}{\{\cos\}} = \underset{3\times n\ n\times3}{[[X]'[X]]^{-1}}\ \underset{3\times n\ n\times1}{[X]'\{R\}} \qquad 4)$$

Then these "cosine" values can be used to predict future signals very accurately by using the first value in place of $1/\sqrt{14}$ above, and so on. If this result doesn't produce numbers within about 10% of the theoretical direction cosines, there is probably a problem with the set up. If signs are wrong, there is a sign inversion in the accelerometer cabling or amplifiers. If the amplitude of the direction cosines is wrong, the gain of one of the amplifiers is wrong.

DEFINITION OF THE COVARIANCE MATRIX

The covariance matrix estimates the amount of variation in the x, y, and z components of matrix [X]. It is a generalization of the concept of the root mean squared (RMS) amplitude of a signal. Since it has been assumed that there is zero mean, the covariance matrix for the components of the signal is defined as shown in Equation 5:

$$[V]_{3\times3} = \begin{bmatrix} \sum_{i=1}^{n} x_i x_i/n & \sum_{i=1}^{n} x_i y_i/n & \sum_{i=1}^{n} x_i z_i/n \\ \sum_{i=1}^{n} y_i x_i/n & \sum_{i=1}^{n} y_i y_i/n & \sum_{i=1}^{n} y_i z_i/n \\ \sum_{i=1}^{n} z_i x_i/n & \sum_{i=1}^{n} z_i y_i/n & \sum_{i=1}^{n} z_i z_i/n \end{bmatrix} \quad 5)$$

Other equivalent notations representing the covariance matrix are as shown below:

$$[V]_{3\times3} = \begin{bmatrix} V_{xx} & V_{xy} & V_{xz} \\ V_{yx} & V_{yy} & V_{yz} \\ V_{zx} & V_{zy} & V_{zz} \end{bmatrix} = [X']_{3\times n}[X]_{n\times3}/n \quad 6)$$

From the definitions in Equation 5 above, the following relationship is obvious, proving that the covariance matrix is symmetric.

$$V_{xy} = \sum_{i=1}^{n} x_i y_i/n = \sum_{i=1}^{n} y_i x_i/n = V_{yx} \quad 7)$$

The covariance matrix is a corollary of the spectral matrix (used in a random test specification) without shifting into the frequency domain. The covariance matrix is simpler to understand than the spectral matrix and the results generally carry forward. Also, the covariance matrix comes up regularly in statistics so its properties are very well known. Both the covariance matrix and the spectral matrix are actually tensor quantities (since they rotate like tensors and have principal values) so there is no vector of values that multiply the matrix on the right. Instead the covariance and spectral matrices as defined here represent the state of vibration at a point in space. The matrices are to a tensor, like a single number is to a scalar, or component values are to a vector.

In other cases of the covariance matrix, the normalizing factor (i.e., 1/n) varies depending on what the covariance matrix represents. To keep things simple, a slightly biased estimate of the variance has been used here. Most commonly it is 1/(n-1).[1] For example, in the statistical procedure "regression" the unnormalized covariance matrix is inverted as part of the solution. Much of what follows is based on the statistical procedure

"factor analysis" which proceeds from the correlation matrix through an eigen vector transformation to principal components.

RMS VALUES AND THE CORRELATION MATRIX

From the definitions for the diagonal terms in Equation 5, it is clear that the RMS value of response in each direction is simply the square root of the corresponding diagonal "variance" term.

$$RMS_x = \sqrt{\sum_{i=1}^{n} x_i x_i / n} = \sqrt{V_{xx}} \qquad 8)$$

The correlation coefficient is a number between -1 and 1 indicating the degree of correlation between the data sets. It is generally defined as follows:

$$\rho_{xy} = \frac{\sum_{i=1}^{n} x_i y_i}{\sqrt{\left[\sum_{i=1}^{n} x_i x_i\right]\left[\sum_{i=1}^{n} y_i y_i\right]}} = \frac{V_{xy}}{\sqrt{V_{xx}}\sqrt{V_{yy}}} = \frac{V_{xy}}{RMS_x\ RMS_y} \qquad 9)$$

This may be viewed as a simple change of variables from the original data in Equation 1. If each data point in Equation 1 is divided by its corresponding RMS value, and the covariance matrix from Equation 5 is recomputed, the result is the correlation matrix:

$$[\rho]_{3\times3} = \begin{bmatrix} 1 & \rho_{xy} & \rho_{xz} \\ \rho_{yx} & 1 & \rho_{yz} \\ \rho_{zx} & \rho_{zy} & 1 \end{bmatrix} \qquad \text{where:} \quad \begin{aligned} X_{new} &= X/RMS_x \\ Y_{new} &= Y/RMS_y \\ Z_{new} &= Z/RMS_z \end{aligned} \qquad 10)$$

The result that the correlation coefficients are scaled between -1 and 1 is not very obvious. It is essentially identical to Cauchy's inequality stated as follows: $[\sum xy]^2 \le [\sum x^2][\sum y^2]$. Taking the square root of both sides and dividing through by RMS_x and RMS_y, gives: $\rho_{xy} \le \pm 1$.

To understand this result, consider the following three special cases: If $C\ x_i = y_i$ then $\rho_{xy} = 1$:

$$\rho_{xy} = \frac{\sum_{i=1}^{n} x_i y_i}{\sqrt{\left[\sum_{i=1}^{n} x_i x_i\right]\left[\sum_{i=1}^{n} y_i y_i\right]}} = \frac{C\sum_{i=1}^{n} x_i x_i}{\sqrt{\left[\sum_{i=1}^{n} x_i x_i\right] C^2 \left[\sum_{i=1}^{n} x_i x_i\right]}} = \frac{C}{C} = 1 \qquad 11)$$

If $-C\ x_i = y_i$ then $\rho_{xy} = -1$

$$\rho_{xy} = \frac{\sum_{i=1}^{n} x_i y_i}{\sqrt{\left[\sum_{i=1}^{n} x_i x_i\right]\left[\sum_{i=1}^{n} y_i y_i\right]}} = \frac{-C\sum_{i=1}^{n} x_i x_i}{\sqrt{\left[\sum_{i=1}^{n} x_i x_i\right] C^2 \left[\sum_{i=1}^{n} x_i x_i\right]}} = \frac{-C}{C} = -1 \qquad 12)$$

Clearly the magnitude of x_i and y_i are controlled by dividing by the RMS. The most extreme case occurs when there is only one non zero x defined as x_{big}.

$$\text{If } x_i = \left\{ \begin{array}{ll} x_{big} & \text{if } i = j \\ 0 & \text{if } i \neq j \end{array} \right\} \text{ then } \rho_{xy} = (y_j/\sqrt{n})/RMS_y$$

$$\rho_{xy} = \frac{\sum_{i=1}^{n} x_i y_i}{\sqrt{\left[\sum_{i=1}^{n} x_i x_i\right]\left[\sum_{i=1}^{n} y_i y_i\right]}} = \frac{x_{big}\, y_j}{x_{big}\sqrt{\sum_{i=1}^{n} y_i y_i}} = \frac{y_j/\sqrt{n}}{RMS_y} \qquad 13)$$

The correlation coefficient between two sets of numbers indicates the degree to which the two sets of numbers agree. When the correlation coefficient is zero the two sets of numbers are unrelated to each other, or in a sense, orthogonal to each other (i.e., if the sets of numbers are viewed as vectors, the dot product of the two vectors is zero: $\sum x_i y_i = 0$).

THREE DIMENSIONAL RMS

Because of the three dimensional nature of the motion, it makes sense to generalize the concept of the RMS value to define an RMS surface in space. Consider the direction cosines that define an arbitrary direction in space, i.e., $<\phi_x,\phi_y,\phi_z>$. The term ϕ_x is the component of the new direction oriented along the old x direction, and so on. In order to be direction cosines the sum of the squares of the components must equal one indicating unit length. Using the direction cosines it is possible to write the original vector's component in the new direction, as shown below:

$$<\hat{x}> = <\phi_x x_1+\phi_y y_1+\phi_z z_1, \phi_x x_2+\phi_y y_2+\phi_z z_2, \ \ldots\ , \phi_x x_n+\phi_y y_n+\phi_z z_n> \qquad 14)$$

The RMS of the response in this direction is simply the square root of the variance in this direction as shown below:

$$V_{\hat{x}\hat{x}} = \sum_{i=1}^{n} \hat{x}_i \hat{x}_i/n = \sum_{i=1}^{n} [\phi_x x_i+\phi_y y_i+\phi_z z_i][\phi_x x_i+\phi_y y_i+\phi_z z_i]/n \qquad 15)$$

Just expanding this out algebraically, starting with x_i for nine terms:

$$V_{\hat{x}\hat{x}} = \phi_x^2 \sum_{i=1}^{n} x_i x_i/n + \phi_x\phi_y \sum_{i=1}^{n} x_i y_i/n + \phi_x\phi_z \sum_{i=1}^{n} x_i y_i/n \quad (16)$$
$$+ \phi_y\phi_x \sum_{i=1}^{n} y_i x_i/n + \phi_y^2 \sum_{i=1}^{n} y_i y_i/n + \phi_y\phi_z \sum_{i=1}^{n} y_i z_i/n$$
$$+ \phi_z\phi_x \sum_{i=1}^{n} z_i x_i/n + \phi_z\phi_y \sum_{i=1}^{n} z_i y_i/n + \phi_z^2 \sum_{i=1}^{n} z_i z_i/n$$

Identifying the sums as the original variances from Equations 5 and 6, and rearranging:

$$V_{\hat{x}\hat{x}} = \phi_x V_{xx}\phi_x + \phi_x V_{xy}\phi_y + \phi_x V_{xz}\phi_z \quad (17)$$
$$+ \phi_y V_{yx}\phi_x + \phi_y V_{yy}\phi_y + \phi_y V_{yx}\phi_x$$
$$+ \phi_z V_{zx}\phi_x + \phi_z V_{zy}\phi_y + \phi_z V_{zz}\phi_z$$

Gathering up terms into matrix notation:

$$V_{\hat{x}\hat{x}} = \langle\phi_x,\phi_y,\phi_z\rangle \begin{bmatrix} V_{xx} & V_{xy} & V_{xz} \\ V_{yx} & V_{yy} & V_{yz} \\ V_{zx} & V_{zy} & V_{zz} \end{bmatrix} \begin{Bmatrix} \phi_x \\ \phi_y \\ \phi_z \end{Bmatrix} = \underset{1\times3}{\{\phi'\}} \underset{3\times3}{[V]} \underset{3\times1}{\{\phi\}} \quad (18)$$

The point is that variance (and RMS) rotate as vector quantities. The value in any arbitrary direction is a function of <u>all</u> the terms in the covariance matrix. The RMS in all directions can be swept out using the equations above. By plotting the value of the RMS as a point in the direction of the unit vector, $\langle\phi\rangle$, used to calculate the RMS, it is possible to sweep out a continuous surface showing the RMS value in all directions. This surface turns out to be surprisingly regular. It is simply an ellipsoid as illustrated in Figure 1.

PRINCIPAL COMPONENTS OF THE COVARIANCE MATRIX

The RMS displacements described by the covariance matrix are hard to interpret in terms of arbitrarily chosen coordinates. However any covariance matrix can be simplified to a diagonal covariance matrix through the application of a suitable change of coordinates. Suppose one took the eigen values and eigen vectors of the covariance matrix. The eigen vectors would give a unitary coordinate transformation which would diagonalize the covariance matrix (resulting in $\rho_{12} = \rho_{13} = \rho_{23} = 0$, where 1,2,3 indicate data associated with each of the three roots). The three eigen values would equal the squared RMS value of the response associated with each of the three eigen vector directions.

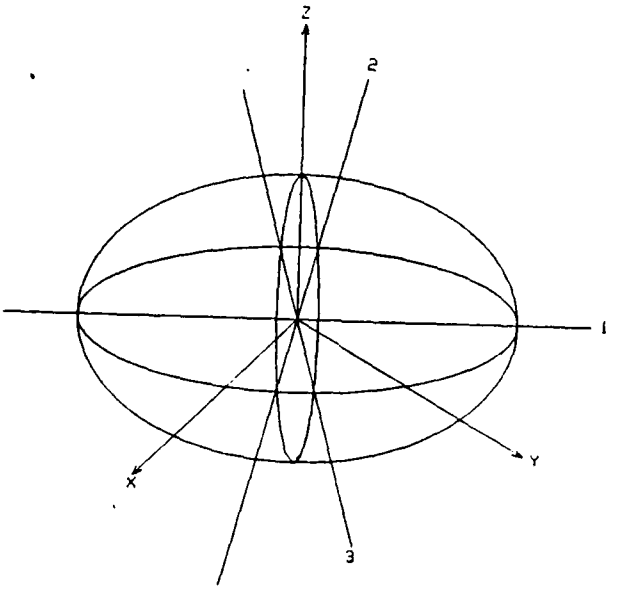

Figure 1 General Ellipsoidal RMS Surface

The shape of the RMS of any 3-D motion can always be reconciled into (at worst) an ellipsoid with arbitrary orientation. Other possibilities are a two dimensional ellipse (if one root is zero) or a straight line (if two roots are zero). In the case of the two dimensional ellipse, the total motion is 2-D, i.e., there is no motion out of the plane of the ellipse. In the case of the line, the total motion is 1-D, i.e., there is no motion out of the direction of the line. There are only four possible cases:

1) a 3-D ellipsoid
2) a 2-D ellipse
3) a 1-D straight line
4) a point at the origin

The limited number of outcomes is a consequence of the definition of the covariance matrix rather than a distributional result from assuming a normal distribution.

For example, if you were given a set of points that were supposed to be the path of a vehicle in 3-D, you could determine if the vehicle travelled in a straight line (in any direction), a plane (any plane), or in general in three dimensions. Just substitute the path into Equation 5 and calculate the roots as shown below. You would need to subtract the mean of each coordinate off the path in keeping with the assumptions build into these results (e.g., center the path at zero). Of course there may be easier ways of finding out the same information.

The roots of the variance matrix are found by setting the determinant of the perturbed variance matrix equal to zero:

$$\left|\begin{bmatrix} V_{xx}-\lambda & V_{xy} & V_{xz} \\ V_{xy} & V_{yy}-\lambda & V_{yz} \\ V_{xz} & V_{yz} & V_{zz}-\lambda \end{bmatrix}\right| = 0 \qquad 19)$$

Expanding out the characteristic equation:

$$\lambda^3 - (V_{xx} + V_{yy} + V_{zz})\lambda^2 + (V_{xx}V_{yy} + V_{xx}V_{zz} + V_{yy}V_{zz} \qquad 20)$$

$$- V_{xz}V_{xz} - V_{yz}V_{yz} - V_{xy}V_{xy})\lambda + (V_{xz}V_{xz}V_{yy}+V_{yz}V_{yz}V_{xx}+V_{xy}V_{xy}V_{zz}$$

$$-V_{xx}V_{yy}V_{zz}-V_{xy}V_{yz}V_{xz}-V_{xz}V_{xy}V_{yz}) = 0$$

Gathering up terms:

$$\lambda^3 + a_2\lambda^2 + a_1\lambda + a_0 = 0 \qquad 21)$$

where: $a_2 = -(V_{xx} + V_{yy} + V_{zz})$

$$a_1 = V_{xx}V_{yy} + V_{xx}V_{zz} + V_{yy}V_{zz} - V_{xz}V_{xz} - V_{yz}V_{yz} - V_{xy}V_{xy}$$

$$a_0 = V_{xz}V_{xz}V_{yy}+V_{yz}V_{yz}V_{xx}+V_{xy}V_{xy}V_{zz}-V_{xx}V_{yy}V_{zz}-V_{xy}V_{yz}V_{xz}-V_{xz}V_{xy}V_{yz}$$

One proceeds by defining:[2]

$$q = a_1/3 - a_2^2/9 \qquad 22)$$

$$r = (a_1a_2 - 3a_0)/6 - a_2^3/27$$

$$s_1 = [r + (q^3 + r^2)^{1/2}]^{1/3}$$

$$s_2 = [r - (q^3 + r^2)^{1/2}]^{1/3}$$

Then the roots are real if:

$$q^3 + r^2 \leq 0 \qquad 23)$$

And irrespective of whether the roots are real, the value of the roots are as follows:

$$V_1 = (s_1+s_2) - a_2/3$$

$$V_2 = -(s_1+s_2)/2 - a_2/3 + i\,(s_1-s_2)\,\sqrt{3}/2 \qquad 24)$$

$$V_3 = -(s_1+s_2)/2 - a_2/3 - i\,(s_1-s_2)\,\sqrt{3}/2$$

Also there are the following three identities based on the fact that the characteristic equation (Equation 21) must be the same for the diagonalized matrix as well as the original matrix.

$$V_1 + V_2 + V_3 = -a_2$$

$$V_1V_2 + V_1V_3 + V_2V_3 = a_1 \qquad 25)$$

$$V_1V_2V_3 = -a_0$$

PHYSICALLY REALIZABLE CORRELATION COEFFICIENTS

There is a further constraint imposed on the three correlation coefficients. Suppose $\rho_{xy}=\rho_{xz}=1$ but $\rho_{yz}=0$. The x array and the y array are completely correlated. The x array and the z array are completely correlated. But the y array and the z array are not correlated at all. This is clearly nonsense. To be physically realizable, the correlation coefficients must satisfy the following relationship:

$$\rho_{xy}^2 + \rho_{xz}^2 + \rho_{yz}^2 - 2\,\rho_{xy}\,\rho_{xz}\,\rho_{yz} \leq 1 \qquad 26)$$

Continuing with the example from above: $1+1+0-2\times0>1$, so the case described above is not physically realizable. Equality in Equation 26 implies no more than two dimensional motion and possibly only one dimensional motion.

Equation 26 follows from the third relationship in Equation 25. In Equation 25 it is obvious that it is both necessary and sufficient for a_0 to be equal to zero to insure that at least one of the roots is zero. Going back to Equation 21, the definition of a_0 was as shown below:

$$a_0 = V_{xz}V_{xz}V_{yy}+V_{yz}V_{yz}V_{xx}+V_{xy}V_{xy}V_{zz}-V_{xx}V_{yy}V_{zz}-V_{xy}V_{yz}V_{xz}-V_{xz}V_{xy}V_{yz} \qquad 27)$$

In order for the principal roots to all be positive, it is necessary for a_0 to be negative from Equation 25. Thus Equation 27 can be rearranged as shown below, by recognizing the required sign for a_0 is negative and dividing Equation 27 through by $V_{xx}V_{yy}V_{zz}$ (a positive quantity):

$$0 \geq \frac{a_0}{V_{xx}V_{yy}V_{zz}} = \frac{V_{xz}^2}{V_{xx}V_{zz}} + \frac{V_{yz}^2}{V_{yy}V_{zz}} + \frac{V_{xy}^2}{V_{xx}V_{yy}} - 1 - \frac{V_{xy}V_{yz}V_{xz}}{V_{xx}V_{yy}V_{zz}} - \frac{V_{xz}V_{xy}V_{yz}}{V_{xx}V_{yy}V_{zz}} \qquad 28)$$

Rearranging Equation 28 gives Equation 26. Empirically, this result is sufficient to cause the roots to be non negative and equality implies at least one zero root.

PRINCIPAL DIRECTIONS OF THE COVARIANCE MATRIX

Once the roots are known the vectors can be calculated by substituting the value of the root (e.g., V_1) for λ in Equation 19. Since the procedure used to calculate λ forced the matrix in Equation 19 to be singular (the determinant was set equal to zero), there are only (at most) two independent equations. The third equation is the normalizing equation declaring the vector to be unit length. For example, one might solve the following system, given numbers for the variance ("V") values.

$$(V_{xx}-V_1)\,\phi_{1x} + V_{xy}\,\phi_{1y} + V_{xz}\,\phi_{1z} = 0$$

$$V_{xy}\,\phi_{1x} + (V_{yy}-V_1)\,\phi_{1y} + V_{yz}\,\phi_{1z} = 0 \qquad 29)$$

$$\phi_{1z} = 1$$

Solving Equation 29 gives values for ϕ_{1x}, ϕ_{1y}, and ϕ_{1z} (usually). Then the roots are renormalized as shown in Equation 29.

$$\phi_{1x} = \phi_{1x} / \sqrt{\phi_{1x}^2+\phi_{1y}^2+\phi_{1z}^2}$$

$$\phi_{1y} = \phi_{1y} / \sqrt{\phi_{1x}^2+\phi_{1y}^2+\phi_{1z}^2} \quad \text{note: quantities on the right are unnormalized.} \qquad 30)$$

$$\phi_{1z} = \phi_{1z} / \sqrt{\phi_{1x}^2+\phi_{1y}^2+\phi_{1z}^2}$$

This works unless $\phi_{1z} = 0$ for the root being considered or the root is repeated. If $\phi_{1z} = 0$, the first two equations in Equation 29 will be singular. When this happens simply set another term equal to one (e.g., set $\phi_{1y} = 1$) and try again.

If the root being worked on is repeated, e.g., $V_2 = V_3$; then there is only one independent equation from Equation 19. Under these circumstances, first solve for the non repeated root and then use the orthogonality relations to solve for the other two roots. For example, suppose Equation 29 has already been solved for non repeated root V_1. Then the equations to solve to get the first repeated root V_2 would be as follows:

$$(V_{xx}-V_2)\,\phi_{2x} + V_{xy}\,\phi_{2y} + V_{xz}\,\phi_{2z} = 0$$

$$\phi_{1x}\,\phi_{2x} + \phi_{1y}\,\phi_{2y} + \phi_{1z}\,\phi_{2z} = 0 \qquad \text{orthogonality} \qquad 31)$$

$$\phi_{2z} = 1$$

Similarly the second repeated root, V3, would be found with two orthogonality equations, one for each mode that had already been extracted. Alternately, the vector cross product could be taken between the vector for V1 and the vector for V2 to get the orthogonal vector for V3.

There is one other possible problem, all three roots can be repeated. If that is the case, there are an infinite number of possible arrangements of the vectors (any orthogonal set). It is best to simply use unit vectors: $\phi_{1x}=1, \phi_{1y}=0, \phi_{1z}=0$; $\phi_{2x}=0, \phi_{2y}=1, \phi_{2z}=0$; $\phi_{3x}=0, \phi_{3y}=0, \phi_{3z}=1$.
The matrix of eigen vectors (ϕ) has the remarkable property that it diagonalizes the original covariance matrix, as shown below:

$$\begin{bmatrix}\phi_{1x} & \phi_{1y} & \phi_{1z}\\ \phi_{2x} & \phi_{2y} & \phi_{2z}\\ \phi_{3x} & \phi_{3y} & \phi_{3z}\end{bmatrix}\begin{bmatrix}V_{xx} & V_{xy} & V_{xz}\\ V_{yx} & V_{yy} & V_{yz}\\ V_{zx} & V_{zy} & V_{zz}\end{bmatrix}\begin{bmatrix}\phi_{1x} & \phi_{2x} & \phi_{3x}\\ \phi_{1y} & \phi_{2y} & \phi_{3y}\\ \phi_{1z} & \phi_{2z} & \phi_{3z}\end{bmatrix} = \begin{bmatrix}V_1 & 0 & 0\\ 0 & V_2 & 0\\ 0 & 0 & V_3\end{bmatrix} \qquad 32)$$

EULER ANGLE TRANSFORMATION AND THE PRINCIPAL RMS VALUES

The results above can be further refined by converting to RMS and a set of Euler angles indicating the principal directions. First the RMS is calculated in the usual way:

$$RMS_1 = \sqrt{V_1} \qquad RMS_2 = \sqrt{V_2} \qquad RMS_3 = \sqrt{V_3} \tag{33}$$

The Euler angles are a series of unitary (length preserving) rotations:

$$\begin{bmatrix} \cos\theta & -\sin\theta & 0 \\ \sin\theta & \cos\theta & 0 \\ 0 & 0 & 1 \end{bmatrix} \begin{bmatrix} \cos\phi & 0 & -\sin\phi \\ 0 & 1 & 0 \\ \sin\phi & 0 & \cos\phi \end{bmatrix} \begin{bmatrix} 1 & 0 & 0 \\ 0 & \cos\psi & -\sin\psi \\ 0 & \sin\psi & \cos\psi \end{bmatrix} = \tag{34}$$

$$\begin{bmatrix} \cos\theta\cos\phi & \sin\theta\cos\psi-\cos\theta\sin\phi\sin\psi & \sin\theta\sin\psi+\cos\theta\sin\phi\cos\psi \\ -\sin\theta\cos\phi & \cos\theta\cos\psi-\sin\theta\sin\phi\sin\psi & \cos\theta\sin\psi-\sin\theta\sin\phi\cos\psi \\ -\sin\phi & -\cos\phi\sin\psi & \cos\phi\cos\psi \end{bmatrix}$$

The eigen vectors can be equated to the matrix shown in Equation 34 above to physically interpret the transformation. Using the case shown, the first rotation (on the left) is about the original Z axis through an angle θ in the clockwise direction (clockwise because of the location of the -sin θ term). The next rotation is about the perturbed Y axis through an angle ϕ in the clockwise direction. Finally, the last rotation (on the right) is about the doubly perturbed X axis through an angle ψ in the clockwise direction.

In practice it is so hard to interpret the Euler angles that nothing is really gained by performing the transformation. It does make clear that there are only three independent variables in the eigen vectors (θ, ϕ, and ψ). There are nine terms for the eigen vectors, but there are 3 normalizing equations, and 3 orthogonality relations, leaving three independent variables. In addition to the eigen vectors there are the 3 RMS amplitudes - making a total of six variables. The original variance matrix in Equation 5 also had six independent variables since it was symmetric.

Unlike the Euler angles, the principal RMS values are easily interpreted. The largest RMS value in Equation 33 is the largest RMS value to be found in any direction. The next largest value is the largest RMS value to be found in any direction perpendicular to the first direction. Finally the third RMS value is the RMS perpendicular to the other two directions. This is the smallest RMS value in any direction.

CONCLUSIONS

At this point much of the previous material comes together. For example, consider Equation 18 illustrating how the covariance matrix rotates when multiplied by a set of direction cosines. The result in Equation 32 is

essentially identical to the result in Equation 18, except that there are three sets of direction cosines in Equation 32. Clearly V_1, V_2, and V_3 are rotated variances in the directions indicated by the phi matrix, $[\phi]$.

The principal directions are orthogonal - this is a property of the eigen transformation. The form of the rotated covariance matrix is diagonal. Looking back to the correlation matrix from Equation 10, it is clear that the principal directions are an orthogonal set in the sense that there is no correlation between the motions in these unique directions. This can be in the trivial sense, such as when the 3-D motion is entirely in a plane, or it can be in the sense of an average where $\sum xy = 0$ when there is no particular other relationship between x and y.

Suppose two of the roots are zero, e.g., $V_1 = V_2 = 0$. Clearly the motion would be 1-D with RMS amplitude equal to the square root of V_3. The motion would be directed along the line whose direction cosines was given by $<\phi_{3x},\phi_{3y},\phi_{3z}>$. This specification is general enough that the line can be pointed in any direction.

Suppose one of the roots is zero, e.g., $V_3 = 0$. The remaining two perpendicular eigen vectors define a 2-D plane in which the motion occurs with the variance (and RMS) in the shape of an ellipse. The variance in the direction of the major and minor axes of the ellipse is given by V_1 and V_2. Again, this specification is general enough to be able to orient the ellipse in any plane at all.

In the general case V_1, V_2, and V_3 are in no particular relationship to each other. Then the response is 3-D and in the shape of an ellipsoid, with the variance in each principal direction given by its root. Again, the ellipsoid can be oriented in any arbitrary way with respect to the axes the data was originally expressed in terms of.

In the special case where all three roots are equal, the variance (and RMS) is a sphere. Notice this is the case where repeated roots lead to an arbitrarily large number of possible eigen vectors. Similarly if two roots are the same (i.e., repeated), the variance in that plane is circular and the orientation of the eigen vectors in the plane is arbitrary.

Any physical variance matrix can be decomposed into principal components this way. Thus the only possible outcomes for any time history are the ones listed: an ellipsoid, an ellipse, a line, or trivially a point at the origin when all the values in Equation 1 are zero.

References

1. Beyer, W. H. (1981), CRC Standard Mathematical Tables, 26th Edition, CRC Press, p. 506.

2. Abramowitz, M. and Stegun, I.A. (1964), Handbook of Mathematical Functions, Dover Publications, p. 17.

CHAPTER 4 GENERIC 3-D RANDOM TESTING

INTRODUCTION

This chapter develops the interrelationships involved in writing test specifications for 3-D random tests. First the finite Fourier transform is very briefly introduced and the spectral matrix is developed from the Fourier transform. The power spectral density, the coherence function, and the transfer function are introduced. Roots and rotations of the spectral matrix are examined and a number of interrelationships of the data in the spectral matrix are uncovered. There is an interrelationship of the three phase angles involved such that a peculiar combination of phase angles (termed cyclic here) must sum to zero. There is an interrelationship of the coherences in that they have an inequality that must satisfied to be physically realizable just like the one for correlation coefficients. The roots of the complex spectral matrix are real, but the vectors are imaginary. This limits the use of *these* roots to procedures for generating an arbitrary spectral matrix. The vectors associated with the roots of the real part of the spectral matrix turn out to point in the direction of the largest values in space.

THE FOURIER TRANSFORM

Up to this point in the discussion of random data, the order that the data appears in does not effect the calculation as long as X, Y, Z sets are kept together. The equations depend on sums, so it doesn't matter what order the numbers are entered in. Which of the $\langle X_i, Y_i, Z_i \rangle$ is i=1 is irrelevant to the answer. However, typically the data represents a time series, and there is information about the signal contained in the order in which the data appears.

It is possible to perform a Fourier transformation of the data to express it in terms of sines and cosines. In this transformation each component (X,Y,Z) of the time history is represented by a series as follows for X(t):[1]

$$X(t) = \frac{C_0^x}{2} + \sum_{j=1}^{L}\left\{C_j^x \cos\frac{j\pi t}{LT} + S_j^x \sin\frac{j\pi t}{LT}\right\} = \frac{C_0^x}{2} + \sum_{j=1}^{L} A_j^x \sin\left(\frac{j\pi t}{LT} + \theta_j^x\right) \qquad 1)$$

Where:

C_0^x = 0 because the mean of the data is zero.

C_j^x = the j-th cosine coefficient in the expansion for X(t).

S_j^x = the j-th sine coefficient in the expansion for X(t).

A_j^x = the j-th amplitude in the expansion for X(t).

θ_j^x = the j-th phase angle in the expansion for X(t).

L = the number of terms in the series = (n-1)/2.

T = the time between samples = 1/sampling rate.

In this expansion the coefficients can be found from the following relationships:

$$C_j^x = \frac{1}{LT}\int_0^{2LT} X(t)\cos\frac{j\pi t}{LT}\,dt = A_j^x \sin\theta_j^x$$

$$S_j^x = \frac{1}{LT}\int_0^{2LT} X(t)\sin\frac{j\pi t}{LT}\,dt = A_j^x \cos\theta_j^x \qquad 2)$$

The vector amplitude and phase angle are found algebraically from the sine and cosine components using the second term in Equation 2. These follow from trigonometric identities using Equation 1.

$$A_j^x = \sqrt{C_j^{x2} + S_j^{x2}}$$

$$\theta_j^x = \tan^{-1}\frac{C_j^x}{S_j^x} \qquad 3)$$

If a full set of coefficients are included, the finite Fourier series expansion will go precisely through the data points, X(t), limited only by round off error. Since the series is limited to indices below j=L (where the frequency is equal to the Nyquist folding frequency at half the sampling rate), it can not also be time limited. Evaluation of the series in the negative time regime or above 2LT will show that the time history repeats itself endlessly.

More frequency points can be obtained by increasing the sampling rate while the total test time is held constant. However if the sampling rate is increased, the highest frequency in the series (the Nyquist folding frequency at 1/2T Hz) will increase proportionally. The spacing between frequencies will hold constant at π/LT radians/second or 1/2LT Hz (which is essentially equal to one over the total test time). By increasing the sampling rate, more frequencies are represented but the spectrum remains discontinuous. The frequency spectrum blossoms into a continuum when the total test time approaches infinity.

Expanding the Fourier series in terms of amplitudes and phase angles makes it clear that the Fourier coefficients are complex quantities. Both an amplitude and a phase angle are involved at each frequency of the summation. It takes two numbers at each frequency point to represent the data. Still the time history is not a complex quantity so Equation 1 is not written in a complex form. A complex number can not be equal to a scalar without some operator (e.g., $\Re$ = real or $\Im$ = imaginary). Instead, Equation 1 shows how the complex Fourier transform converts into a physically observable scalar time history.

The finite Fourier series can also be written in complex form as shown in Equation 4 below:

$$\bar{F}_x(\frac{j}{2LT}) \simeq S_j^x + i\, C_j^x = A_j^x\, [\cos\, \theta_j^x + i \sin\, \theta_j^x] = A_j^x\, e^{i\theta_j^x} \qquad 4)$$

Notice that the function of time has been suppressed in this notation. It is just convention how to reassemble the coefficients into time histories. Also notice that the transition between point estimates at frequency line j, and the underlying continuous function $\bar{F}_x(f)$ has been designated with the approximately equals ($\simeq$) operator instead of the full equality ($=$) operator. This has been used throughout to distinguish between theoretical and experimental variables.

SUMMATION VERSUS INTEGRATION

The integral signs in Equation 2 are somewhat deceptive because the actual evaluation is done with summations. Typically the trapezoid rule would be invoked to convert Equation 2 into the form shown below. To be rigorous, using the trapezoid rule the first and last term of the summations would have to be multiplied by factors of 1/2, however, this doesn't matter much because the first and last term of the time history, X(0) and X(n), need to be close to zero to avoid introducing step functions at the boundary where the time history repeats itself.

$$C_j^x = \frac{1}{LT}\int_0^{2LT} X(t)\, \cos\, \frac{j\pi t}{LT}\, dt \simeq \frac{1}{L} \sum_{k=0}^{n} X(k)\, \cos\, \frac{jk\pi}{L}$$

$$S_j^x = \frac{1}{LT}\int_0^{2LT} X(t)\, \sin\, \frac{j\pi t}{LT}\, dt \simeq \frac{1}{L} \sum_{k=0}^{n} X(k)\, \sin\, \frac{jk\pi}{L} \qquad 5)$$

Commonly some windowing procedure is used to enforce the requirement that the first and last terms of the time history need to be close to zero. The time history, X(t), is multiplied by a function which is numerically close to zero at the first and last time point. For example, consider the Hanning window:

$$X'(t) = X(t)\, \frac{1}{2}\, (1 - \cos\, \frac{\pi t}{LT}) \qquad 6)$$

The window forces the time history to have zero values at t=0 and t=nT. It also slightly perturbs the frequency coefficients producing changes, (possibly errors) of the order of 20%. The window smooths out the frequency response, tending to avoid sudden jumps unless they are associated with data from the center of the window. Whether this is an error or not depends on what you want to accomplish and what the data you are analyzing represents.

THE SPECTRAL MATRIX

The corollary of the covariance matrix in the frequency domain is the spectral matrix. Each term of the covariance matrix was of the form:

$$V_{xy} = \sum_{i=1}^{n} x_i y_i / n \qquad 7)$$

For the spectral matrix, the data is viewed as continuous so the summation is replaced by an integral from 0 to 2LT, the x_i and y_i terms are represented by their continuous series representation from equation 1, and the 1/n scaling is replaced by 1/2LT (notice n=2L+1 and T cancels the units of dt). The term is still the covariance so V_{xy} is still an appropriate symbol to represent it.

$$V_{xy} = \frac{1}{2LT} \int_0^{2LT} \sum_{j=1}^{L} \left\{ C_j^x \cos\frac{j\pi t}{LT} + S_j^x \sin\frac{j\pi t}{LT} \right\} \sum_{k=1}^{L} \left\{ C_k^y \cos\frac{k\pi t}{LT} + S_k^y \sin\frac{k\pi t}{LT} \right\} dt \qquad 8)$$

Several integrals related to the orthogonality of sines and cosines greatly simplify the expression in Equation 8. In particular:[2]

$$\int_0^{2LT} \cos\frac{j\pi t}{LT} \cos\frac{k\pi t}{LT}\, dt = \begin{cases} 0, & j \neq k \\ LT, & j-k \neq 0 \\ 2LT, & j-k=0 \end{cases}$$

$$\int_0^{2LT} \sin\frac{j\pi t}{LT} \sin\frac{k\pi t}{LT}\, dt = \begin{cases} 0, & j \neq k \\ LT, & j-k \neq 0 \\ 0, & j-k=0 \end{cases} \qquad 9)$$

$$\int_0^{2LT} \cos\frac{j\pi t}{LT} \sin\frac{k\pi t}{LT}\, dt = 0$$

Thus, Equation 8 can be simplified to give Equation 10:[3]

$$V_{xy} = \frac{1}{2} \sum_{j=1}^{L} (C_j^x C_j^y + S_j^x S_j^y) = \frac{1}{2} \sum_{j=1}^{L} A_j^x A_j^y \cos(\theta_j^y - \theta_j^x) \simeq \int_0^{1/2T} \Re\vec{G}_{xy}(f)\, df \qquad 10)$$

There are a number of ways of deriving the spectral matrix. Most commonly it is derived from the continuous theoretical definition of the Fourier transform (see reference 3 for both approaches). Here, the material is being developed in terms of the finite Fourier transform - which must be equivalent since the theoretical transform requires infinitely long time histories over all past and future time. The point of the integral part of Equation 10 is that the real part of the cospectral density function, $\Re\vec{G}_{xy}(f)$, is viewed as a continuous function of frequency, and the finite Fourier transform coefficient expression in the summation is the local estimate of the value of $\Re\vec{G}_{xy}$ at the coefficient's frequency, j/2LT Hertz. At this point, this is simply a definition.

The imaginary part of the complex, cospectral density function, $\Im\vec{G}_{xy}(f)$, can also be calculated from the finite Fourier transform coefficients by introducing a 90° phase lag into the expansion for Y(t) and calculating as shown in Equation 8. Again, the integral part of the relationship is simply a definition.

$$\int_0^{1/2T} \Im\vec{G}_{xy}(f)\, df \simeq \frac{1}{2}\sum_{j=1}^{L}\{S_j^x C_j^y - C_j^x S_j^y\} = \frac{1}{2}\sum_{j=1}^{L} A_j^x A_j^y \sin(\theta_j^y - \theta_j^x) \qquad 11)$$

Thus the covariance matrix is replaced in the frequency domain by the spectral matrix:

$$[G]_{3\times3} = \begin{bmatrix} G_{xx}(f) & \vec{G}_{xy}(f) & \vec{G}_{xz}(f) \\ \vec{G}_{yx}(f) & G_{yy}(f) & \vec{G}_{yz}(f) \\ \vec{G}_{zx}(f) & \vec{G}_{zy}(f) & G_{zz}(f) \end{bmatrix} \qquad 12)$$

From Equations 10 and 11 it is obvious that $\Re\vec{G}_{xy}(f) = \Re\vec{G}_{yx}(f)$ while $\Im\vec{G}_{xy}(f) = -\Im\vec{G}_{yx}(f)$ and so on. In Equation 10, the difference in sign of the phase angles for the real part doesn't matter because the cosine is an even function, i.e., the $\cos(-x)=\cos(x)$. In Equation 11 for the imaginary part, there is a sign change between $\Im\vec{G}_{xy}$ and $\Im\vec{G}_{yx}$, thus the complex conjugate, denoted by *, must be used to calculate one term from the other. The notation $*\vec{z}$ denotes the complex conjugate of the complex number $\vec{z}$. If $\vec{z}=x+yi$ then $*\vec{z}=x-yi$. The only use made here of * is to show that a complex conjugate pair is multiplied together to produce a real number.

Just as the covariance matrix could be rotated to give the variance and covariance oriented along arbitrary directions, the spectral matrix can be rotated to give autospectra and cospectra along an arbitrary direction. Just as before, given a set of direction cosines $\langle\phi_x, \phi_y, \phi_z\rangle$, the autospectra in the new direction can be calculated as follows:

$$G_{\hat{x}\hat{x}}(f) = \underset{1\times3}{\langle\phi_x,\phi_y,\phi_z\rangle}\underset{3\times3}{\begin{bmatrix} G_{xx}(f) & \vec{G}_{xy}(f) & \vec{G}_{xz}(f) \\ \vec{G}_{yx}(f) & G_{yy}(f) & \vec{G}_{yz}(f) \\ \vec{G}_{zx}(f) & \vec{G}_{zy}(f) & G_{zz}(f) \end{bmatrix}}\underset{3\times1}{\begin{Bmatrix}\phi_x\\ \phi_y\\ \phi_z\end{Bmatrix}} = \underset{1\times3}{\{\phi'\}}\underset{3\times3}{[G]}\underset{3\times1}{\{\phi\}} \qquad 13)$$

Expanding in Equation 14, terms like $\phi_x\vec{G}_{xy}\phi_y + \phi_y\vec{G}_{yx}\phi_x$ have their complex parts cancel since $\Im\vec{G}_{xy} = -\Im\vec{G}_{yx}$. The result is a real number indicating the value of the autospectrum in the new direction. The value of $G_{\hat{x}\hat{x}}$ is uneffected by the imaginary parts of the matrix.

$$\begin{aligned} G_{\hat{x}\hat{x}}(f) = {} & \phi_x G_{xx}\phi_x + \phi_x\vec{G}_{xy}\phi_y + \phi_x\vec{G}_{xz}\phi_z \\ & + \phi_y\vec{G}_{yx}\phi_x + \phi_y G_{yy}\phi_y + \phi_y\vec{G}_{yz}\phi_z \\ & + \phi_z\vec{G}_{zx}\phi_x + \phi_z\vec{G}_{zy}\phi_y + \phi_z G_{zz}\phi_z \end{aligned} \qquad 14)$$

Equation 13 motivates searching for the roots of the spectral matrix. The spectral matrix rotates according to the same type of matrix rotation as occurs with eigen vectors and eigen values. Further, the spectral matrix would be greatly simplified if it could be diagonalized. All the coherence and phase issues would drop out. The eigen vectors are a transformation that do this to a general matrix, thus it seems approriate to try rooting the spectral matrix.

Once again, it is possible to calculate principal directions as a function of frequency that produce uncoupled inputs. Once again, the roots of the spectral matrix can be found by setting the determinant of the perturbed spectral matrix equal to zero:

$$\left|\begin{bmatrix} G_{xx}(f)-\lambda & \vec{G}_{xy}(f) & \vec{G}_{xz}(f) \\ \vec{G}_{yx}(f) & G_{yy}(f)-\lambda & \vec{G}_{yz}(f) \\ \vec{G}_{zx}(f) & \vec{G}_{zy}(f) & G_{zz}(f)-\lambda \end{bmatrix}\right| = 0 \qquad (15)$$

Expanding Equation 15 gives as follows:

$$\begin{aligned} &\lambda^3 - (G_{xx} + G_{yy} + G_{zz})\lambda^2 + (G_{xx}G_{yy} + G_{xx}G_{zz} + G_{yy}G_{zz} \\ &- \vec{G}_{xz}{}^*\vec{G}_{zx} - \vec{G}_{yz}{}^*\vec{G}_{zy} - \vec{G}_{xy}{}^*\vec{G}_{yx})\lambda + (\vec{G}_{xz}{}^*\vec{G}_{zx})G_{yy} + (\vec{G}_{yz}{}^*\vec{G}_{zy})G_{xx} \\ &+ (\vec{G}_{xy}{}^*\vec{G}_{yx})G_{zz} - G_{xx}G_{yy}G_{zz} - \vec{G}_{xy}\vec{G}_{yz}\vec{G}_{zx} - \vec{G}_{xz}\vec{G}_{zy}\vec{G}_{yx} = 0 \end{aligned} \qquad (16)$$

Notice that all terms in Equation 16 are real (not complex). The last two terms are real because they have phase angles that go around in a circle and cancel out. The phase angles go through a complete cycle. For example, $\vec{G}_{xy}(f)$ has a phase angle which expresses the angle between the input X and the response Y at the frequency f. Thus $\angle\vec{G}_{xy}(f) = \theta_y(f) - \theta_x(f)$. Expanding out the other terms and adding up the angles gives zero. Notice that the choice of terms to add up is based on the terms that appear in the determinant of the spectral matrix in Equation 15.

$$\begin{aligned} \angle\vec{G}_{xy}\vec{G}_{yz}\vec{G}_{zx} &= \{\theta_y(f)-\theta_x(f)\} + \{\theta_z(f)-\theta_y(f)\} + \{\theta_x(f)-\theta_z(f)\} = 0 \\ \angle\vec{G}_{xz}\vec{G}_{zy}\vec{G}_{yx} &= \{\theta_z(f)-\theta_x(f)\} + \{\theta_y(f)-\theta_z(f)\} + \{\theta_x(f)-\theta_y(f)\} = 0 \end{aligned} \qquad (17)$$

Rooting Equation 16 gives the values of the three autospectra associated with the principal directions. The spectral matrix is a special form of a Hermitian matrix.[4] In general the roots of Hermitian matrices are real but the vectors are potentially complex. What has been found here is that this is the case with the spectral matrix: the roots are real and *positive* but the vectors are complex.

Complex vectors are a problem conceptually. As will be shown later, in the special case of the spectral matrix at a frequency, all three x components of the complex vectors have the same phase angle, all three y components have a second phase angle, and all three z components have a third phase angle. Further, the three phase angles in the vectors are predictable

based on the phase angles in the spectral matrix itself. This requires that the X, Y, and Z Fourier components must be shifted relative to each other by a fixed amount. While this might be useful in generating time histories with the desired characteristics, it does not indicate the principal directions under <u>real</u> rotation vectors.

The result found here and developed in the remaining sections of this writeup was that given Equation 17, the principal directions are indicated by rooting the real part of the spectral matrix. The imaginary part of the spectral matrix does not contribute to the value of the PSD. Thus to find the principal directions, it is sufficient to root the real part of the matrix. Then calculating eigen vectors for the roots of the real part of the matrix gives the rotation matrices indicating the principal directions. Empirically, this approach gives positive roots and real eigen vectors that indicate the maximum, minimum, and intermediate values of the rotated PSD.

POWER SPECTRAL DENSITIES AND THE RMS AMPLITUDE

The finite Fourier series for the time history can be converted to an estimate of the power spectral density (PSD) by taking the sum of the squares of the amplitudes. The integral of the PSD is the amount of the RMS associated with the frequency band the integral is taken over. The points in the PSD have units of G^2/Hz and represent a localized estimate of a continuum over frequency. Thus the PSD amplitude is defined as follows.

$$G_{xx}(j/2LT) \simeq (C_j^{x^2}+S_j^{x^2}) \text{ scale factor} = A_j^{x^2} \text{ scale factor} \qquad 18)$$

To calculate the scale factor, Equation 1 (which expresses the time history in terms of the Fourier coefficients) can be used to calculate the RMS. Referring to Equation 10 for V_{xy} and replacing the y with x:

$$RMS_x = \sqrt{\frac{1}{2}\sum_{j=1}^{L}\left\{C_j^{x^2} + S_j^{x^2}\right\}} \simeq \sqrt{\int_0^{1/2T} G_{xx}(f)\, df} \qquad 19)$$

The scale factor from Equation 18 is clear from Equation 19. The summation needs $(C_j^2+S_j^2)$ to be scaled by 1/2 to get the RMS. The integral must be multiplied by the frequency spacing in Hertz between the data points (1/2LT) to represent df. Thus it is necessary to multiply the coefficients C_j^2 and S_j^2 by LT to get the integrand to integrate to the RMS and have units G^2/Hz (C_j^2 and S_j^2 have units G^2 and LT has units of sec/cycle or 1/Hz). Thus the scale factor in Equation 18 is equal to LT.

THE COHERENCE FUNCTION

Just as the covariance matrix could be renormalized to give correlation coefficients, it is possible to renormalize the spectral matrix to give coherence functions. Since the on diagonal terms of the spectral matrix

are scalars, it is possible to divide the off diagonal terms through by the square root of the two diagonal terms.

$$\vec{\gamma}_{xy}(f) = \frac{\vec{G}_{xy}(f)}{\sqrt{G_{xx}(f)\ G_{yy}(f)}} \simeq \frac{A_j^x A_j^y [\cos(\theta_j^y - \theta_j^x) + i\ \sin(\theta_j^y - \theta_j^x)]}{A_j^x A_j^y} \qquad 20)$$

$$|\vec{\gamma}_{xy}(f)| \simeq \sqrt{\cos^2(\theta_j^y - \theta_j^x) + \sin^2(\theta_j^y - \theta_j^x)} = 1$$

A single finite Fourier transform of data from a time history always produces coherence equal to 1. However, if the constituent parts are averaged over a number of finite Fourier transforms, and then the coherence is calculated based on the averaged quantities, the magnitude of the coherence will vary between 0 and 1 and indicate the degree to which the data is responding in a repetitive fashion at that frequency. If the data isn't particularly repetitive, the cospectrum will vary widely and tend to average to zero. Coherence is a complex quantity with phase equal to the cospectrum's phase. When plotted as a real quantity, coherence is squared (by multiplying by the complex conjugate).

For example consider N estimates of the $\vec{G}_{xy}(f)$, $G_{xx}(f)$, and $G_{yy}(f)$. To estimate the coherence $\vec{\gamma}_{xy}(f)$, Equation 21 would be used:

$$\vec{\gamma}_{xy}(f) = \frac{\sum_{i=1}^{N} \vec{G}_{xy}^{\,i}(f)}{\sqrt{\sum_{i=1}^{N} G_{xx}^{\,i}(f) \sum_{i=1}^{N} G_{yy}^{\,i}(f)}} \qquad 21)$$

An example should help clarify how Equation 21 produces coherence values other than one. Suppose we had five estimates (N=5) of the spectral data at 10 Hertz, as follows (the numbers are arbitary and only exhibit the typical behavior):

Estimate	$\vec{G}_{xy}$	$\lvert\vec{G}_{xy}\rvert$	$\angle(\theta_y-\theta_x)$	G_{xx}	$\sqrt{G_{xx}}$	G_{yy}	$\sqrt{G_{yy}}$	$\lvert\vec{\gamma}_{xy}\rvert$
1	(.941,.588)	1.11	32°	.998	.999	1.234	1.111	1.0
2	(-.432,.812)	0.92	88°	.933	.966	.906	.952	1.0
3	(.756,-.840)	1.13	312°	1.302	1.141	.980	.990	1.0
4	(.865,.460)	0.98	28°	1.059	1.029	.906	.952	1.0
5	(.808,.294)	0.86	20°	.748	.865	.990	.995	1.0
	(2.938,1.214)			5.040		5.016		

$$\vec{\gamma}_{xy} = (0.584,.261) \text{ or } 0.64 \text{ at } \angle 24°$$

Each estimate individually has the amplitude of the coherence equal to 1.0 on a term by term basis. However, because the phase angle and PSD varies so much, the overall average is only 0.64. The issue now becomes, why would the phase angle and PSD vary?

It is easy to see physically how coherence can be less than one by considering a signal composed of electrical noise superimposed on structural data. Electrical noise typically is not the same in both the X(t) and Y(t) time histories - it is incoherent. Averaging the cospectrum between two signals with some noise on them will tend to eliminate the influence of the noise in the cospectrum because the relative phase angle between the two noise signals will vary between frames. On the other hand, the RMS amplitudes will always be <u>increased</u> by the noise. If the two signals are all electrical noise, the coherence will tend to be zero. The coherence indicates the degree to which the relationship (amplitude and phase) between two channels at a frequency is a constant.

A second less obvious way that coherence can be less than one (for a linear system) is to have multiple incoherent inputs. If there are three inputs X(t), Y(t), and Z(t) at the shake table and the three inputs are coherent at a frequency, that implies that the shake table is moving repetitively in either a straight line or an ellipse at that frequency. If the inputs are coherent, the motion is at most 2-D at that frequency and is sinusoidal. On the other hand, if the inputs are completely incoherent, the motion is random and 3-D. For an intermediate value of coherence, the motion can be decomposed into coherent and incoherent parts and summed.

In general, a coherence between 0 and 1 can only occur under one of the following conditions:[5]

1) Some form of noise is present in the signal.
2) There are multiple incoherent inputs to the system.
3) The system is not linear or is not at steady state.

Coherence follows the same equation as correlation coefficients to be physically realizable. Again the characteristic equation (Equation 16) gives the following result:

$$0 \geq a_0 = (\vec{G}_{xz}{}^*\vec{G}_{zx})G_{yy} + (\vec{G}_{yz}{}^*\vec{G}_{zy})G_{xx} + (\vec{G}_{xy}{}^*\vec{G}_{yx})G_{zz} \qquad 22)$$

$$- G_{xx}G_{yy}G_{zz} - \vec{G}_{xy}\vec{G}_{yz}\vec{G}_{zx} - \vec{G}_{xz}\vec{G}_{zy}\vec{G}_{yx}$$

By rearranging Equation 20 to solve for the cospectra in terms of the autospectra and the coherence, all references to cospectra in Equation 22 can be eliminated in terms of the complex coherence.

$$0 \geq \frac{a_0}{G_{xx}G_{yy}G_{zz}} = \vec{\gamma}_{xz}{}^*\vec{\gamma}_{zx} + \vec{\gamma}_{yz}{}^*\vec{\gamma}_{zy} + \vec{\gamma}_{xy}{}^*\vec{\gamma}_{yx} - 1 - \vec{\gamma}_{xy}\vec{\gamma}_{yz}\vec{\gamma}_{zx} - \vec{\gamma}_{xz}\vec{\gamma}_{zy}\vec{\gamma}_{yx} \qquad 23)$$

Rearranging Equation 23 gives the same final result as for correlation coefficients as follows:

$$1 \geq \vec{\gamma}_{xz}{}^*\vec{\gamma}_{zx} + \vec{\gamma}_{yz}{}^*\vec{\gamma}_{zy} + \vec{\gamma}_{xy}{}^*\vec{\gamma}_{yx} - 2\vec{\gamma}_{xy}\vec{\gamma}_{yz}\vec{\gamma}_{zx} \qquad 24)$$

Again, the last term in Equation 24 is not a vector because the phase angles go through a complete cycle.

THE TRANSFER FUNCTION

The transfer function between a single input and any output, e.g., X(t) and Y(t), can be estimated from their Fourier coefficients by simply taking the ratio of the two finite Fourier series.[6]

$$\vec{H}_{xy}(f) = \frac{\vec{F}_y(f)}{\vec{F}_x(f)} \simeq \frac{A_j^y}{A_j^x} e^{i(\theta_j^y - \theta_j^x)} = \frac{A_j^y[\cos(\theta_j^y-\theta_j^x)+i\ \sin(\theta_j^y-\theta_j^x)]}{A_j^x} \qquad 25)$$

However, this procedure has problems when more than one input is involved. According to Equation 25, the entire response at $\vec{F}_y(f)$ is from $\vec{F}_x(f)$. If there is some other input causing response at y, that response needs to be subtracted off of $\vec{F}_y(f)$ before taking the ratio! Instead, in general it is correct to estimate the terms of the spectral matrix and calculate the transfer function as follows:

$$\vec{H}_{xy}(f) = \frac{\vec{G}_{xy}(f)}{G_{xx}(f)} = \frac{\sqrt{G_{yy}(f)}\ \vec{\gamma}_{xy}(f)}{\sqrt{G_{xx}(f)}} \simeq \frac{A_j^y[\cos(\theta_j^y-\theta_j^x)+i\ \sin(\theta_j^y-\theta_j^x)]}{A_j^x} \qquad 26)$$

Notice that while $\vec{G}_{xy}(f)$ and $G_{xx}(f)$ are expressed in terms of amplitudes squared, one of the two A^x terms cancels leaving exactly the right ratio to be a transfer function. The sense in which this is a transfer function is made clear by multiplying by the Fourier transform for X(t) from Equation 4. In complex form, $\vec{F}_x(f)$ represents the Fourier transform of X(t) as shown below:

$$\vec{H}_{xy}(f)\vec{F}_x(f) \simeq \frac{A_j^y\ [\cos(\theta_j^y-\theta_j^x)+i\ \sin(\theta_j^y-\theta_j^x)]}{A_j^x} A_j^x\ [\cos\ \theta_j^x+i\ \sin\ \theta_j^x] \qquad 27)$$

$$= A_j^y\ [\cos\ \theta_j^y+i\ \sin\ \theta_j^y] \simeq \vec{F}_y(f)$$

From Equation 26 it is easy to see that the phase angle of the transfer function is equal to the phase angle of the off diagonal term of the spectral matrix. $G_{xx}(f)$ in Equation 26 is a scalar. Only the $\vec{G}_{xy}(f)$ term is a complex number and has a phase angle. From the third part of Equation 26 it is clear that the same phase angle applies to $\vec{\gamma}_{xy}(f)$. The fact that there is only one phase angle for the transfer function, coherence, and spectral matrix is the easiest way to see that the phase relationship of Equation 17 must hold. $\vec{H}_{xy}\vec{H}_{yz}\vec{H}_{zx}=\vec{H}_{xx}=1$. The cycle only guaranties that zero is the result of expanding the phase angle of the transfer function between X and Y, between Y and Z, and finally between Z and X. This produces the transfer function between X and X, i.e., 0° or some multiple of 2π radians phase angle.

SIGNIFICANCE OF AVERAGING

In discussing the spectral matrix, power spectral densities, coherence function, and the transfer function, the observation that multiple data

frames should be averaged to estimate these quantities has come up. Indeed, when more than one input is involved, it is not possible to correctly estimate the coherence or the transfer function without multiple frames of data. While the definitions will yield meaningful relationships that follow all the equations for a single set of time histories (with all coherences equal to one), there is absolutely no reason to expect the results to be predictive of future data if only one frame is used. By averaging, the coherence function establishes the degree to which the individual frames are repetitive and thus useful in predicting future behavior.

On the other hand, there are occasions when averaging data doesn't make sense. For example when working with time histories from staging transients for a rocket launch, the entire event fits in one frame. All one is doing with the Fourier transform is to convert a time history into the frequency domain so it is more easily processed. Since the data is transient in nature, it is not possible to produce meaningful averages. Under these circumstances, much attention must be given to overcoming the physical limitations of the Fourier transform, e.g., that the data at t=0 and t=nT be zero. Using the Laplace transform would be a better solution under these conditions.

3-D RESPONSE OF A MODE TO RANDOM EXCITATION

Consider the response of a structural mode to a random base input. Suppose the test article is cantilevered off a large mass at the base (e.g., the shaker table), so that the mode shape at the shaker table is small for all the modes in all three directions. Choosing some other point on the test article where the mode's response is large, the process through which the wide band random vibration becomes coherent through the filtering action of a structural mode can be examined.

The structural mode is represented by the following differential equation:

$$m_j \frac{d^2 q_j}{dt^2} + 2\zeta_j \omega_j m_j \frac{dq_j}{dt} + \omega_j^2 m_j q_j = \underset{1\times\ell}{\langle \phi_j^i \rangle} \underset{\ell\times 1}{(F^i)} \qquad 28)$$

The physical response all over the test article is given as follows:

$$\underset{\ell\times 1}{(x^i)} = \underset{\ell\times 1}{(\phi_j^i)}\ \underset{1\times 1}{q_j} \qquad 29)$$

The transfer function for a single mode between any two points on the test article can be calculated by solving for the steady state response in Equation 28 to sinusoidal forcing at the input location. This result is shown in Equation 30.

$$\vec{H}(\omega) = \frac{\vec{d}^{out}}{\vec{F}^{in}} = \frac{\phi_j^{in}\ \phi_j^{out}}{m_j} \left\{ \frac{1}{(\omega_j^2 - \omega^2) - i\ (2\zeta_j \omega_j \omega)} \right\} \qquad 30)$$

Equation 30 gives a displacement output for a force input to a single mode. To get more than one mode, simply sum Equation 30 over as many modes (j) as are desired. If an acceleration output is desired, it is necessary to multiply by $-\omega^2$. To get some other input besides a force, for a single input it is possible to ratio transfer functions to cancel the force required to produce a desired displacement or acceleration.

Manipulating the right hand side of Equation 28 it is clear that a structural mode responds to inputs in only one direction when the mode is excited at it's base. The excitation terms on the right of the equation call for a summation of the components of the force times the components of the modal response at the base. In terms of an equation this is as follows:

$$<\phi_j^i>\{F^i\} = \phi_j^x F^x + \phi_j^y F^y + \phi_j^z F^z = \vec{\phi}\cdot\vec{F} \qquad 31)$$

This is just the dot product of the instantaneous force vector with the local modal response vector. The dot product returns a scalar which is the projection of one vector on the other. Clearly the mode responds in only one direction (e.g., in the direction of the vector $<\phi_x,\phi_y,\phi_z>$). The input in this direction can be calculated from Equation 18 which showed how to rotate the spectral matrix around to calculate the spectra in any direction.

This also proves that the coherence at the modal frequencies will tend to be very high between responses in the mode's local direction. The mode only responds to one input, the one from Equation 18, irrespective of the fact that there may be three incoherent inputs at the base. One input is always coherent with itself. Thus the response in the modal direction between different points on the test specimen will always be very nearly completely coherent in the absence of noise.

MEANING OF REAL/IMAGINARY PARTS OF THE SPECTRAL MATRIX

It is apparent that the imaginary part of the spectral matrix does not influence the RMS amplitude or the spatial distribution of the PSDs. If you consider the last Equation in Chapter 2 reproduced for the 3-D case below:

$$P(\underset{1\times3}{<X>}\,|\,\underset{3\times3}{[V]}) = \frac{1}{(2\pi)^{3/2}|V|^{1/2}}\int_{-\infty}^{Z}\int_{-\infty}^{Y}\int_{-\infty}^{X} e^{-\frac{1}{2}\underset{1\times3}{<x>'}\underset{3\times3}{V^{-1}}\underset{3\times1}{\{x\}}}\,dx\,dy\,dz \qquad 33)$$

Where: $\underset{1\times3}{-\frac{1}{2}<x>'}\underset{3\times3}{V^{-1}}\underset{3\times1}{\{x\}}$ is a rather long algebraic expression

$|V|$ is the determinant of the covariance matrix.

The trivariate normal distribution function depends only on the covariance matrix. It determines all the spatial distribution issues of the RMS

signal. Depending on the covariance matrix, all possible spatial arrangements of the ellipsoidal RMS surface can be achieved.

Earlier in this section it was argued that the covariance matrix is the integral of the real part of the spectral matrix as shown below:

$$[V]_{3\times3} = \begin{bmatrix} \int G_{xx}(f)df & \int \Re\vec{G}_{xy}(f)df & \int \Re\vec{G}_{xz}(f)df \\ \int \Re\vec{G}_{yx}(f)df & \int G_{yy}(f)df & \int \Re\vec{G}_{yz}(f)df \\ \int \Re\vec{G}_{zx}(f)df & \int \Re\vec{G}_{zy}(f)df & \int G_{zz}(f)df \end{bmatrix} \quad 34)$$

Evidently only the real part of the spectral matrix influences the amplitude of the signal. The imaginary part of the signal must influence the relative timing of the X, Y, and Z components with respect to each other, since this is the only role left for it to play.

This issue is of *major* consequence. A structural mode filters the part of the signal it the mode's local direction and only responds to inputs in that direction. Detailed timing is of no consequence to a single structural mode. Thus a single mode will only be influenced by the real part of the spectral matrix. When there are repeated modes, it may be possible for there to be interactions between the repeated modes that cause the structure to react to the timing between the inputs. However, repeated modes don't occur very often. In the acoustic regime, the modal density gets high, and it seems likely that the detailed timing will become relevant. However this occurs at very high frequency and our excitation *is* base excitation not acoustic excitation there anyway. It appears that our order of preference for control should be:

1) the Diagonal
2) the Real Part of the Spectral Matrix
3) the Imaginary Part of the Spectral Matrix

Currently the control system at HDL is reportedly got the preference order below:

1) the diagonal
2) the amplitude (i.e., coherence) of the spectral matrix
3) the phase angles of the spectral matrix

While the choice of coherence as the second most significant parameter is intuitive and seemed reasonable, it is clear that this is the wrong choice since the imaginary part almost no structural consequence.

CONSTRAINTS ON SPECIFICATION WRITERS

There are numerous notational issues to be resolved. The spectral matrix can be defined any of the ways shown in Equations 35 through 39, as follows:

$$[G]_{3\times3} = \begin{bmatrix} G_{xx}(f) & \vec{G}_{xy}(f) & \vec{G}_{xz}(f) \\ \vec{G}_{yx}(f) & G_{yy}(f) & \vec{G}_{yz}(f) \\ \vec{G}_{zx}(f) & \vec{G}_{zy}(f) & G_{zz}(f) \end{bmatrix} \quad 35)$$

Equation 36 is Euler's Equation and helps explains the amplitude and phase notation for complex numbers (i.e., with the symbol "$\vec{}$").

$$|\vec{G}_{xy}(f)|\angle\vec{G}_{xy}(f) = |\vec{G}_{xy}(f)|e^{i\angle\vec{G}_{xy}(f)} = |\vec{G}_{xy}(f)|(\cos\angle\vec{G}_{xy}(f) + i\,\sin\angle\vec{G}_{xy}(f)) \quad 36)$$

Equation 35 can be written in terms of amplitudes and complex phase angles as shown in Equation 37.

$$[G]_{3\times3} = \begin{bmatrix} G_{xx}(f) & |\vec{G}_{xy}(f)|\angle\vec{G}_{xy}(f) & |\vec{G}_{xz}(f)|\angle\vec{G}_{xz}(f) \\ |\vec{G}_{yx}(f)|\angle\vec{G}_{yx}(f) & G_{yy}(f) & |\vec{G}_{yz}(f)|\angle\vec{G}_{yz}(f) \\ |\vec{G}_{zx}(f)|\angle\vec{G}_{zx}(f) & |\vec{G}_{zy}(f)|\angle\vec{G}_{zy}(f) & G_{zz}(f) \end{bmatrix} \quad 37)$$

This can also be written in terms of the PSD values on the diagonal and the complex coherence function (e.g. $\vec{\gamma}_{xy}(f)$) as follows:

$$[G]_{3\times3} = \begin{bmatrix} G_{xx}(f) & \sqrt{G_{xx}(f)\,G_{yy}(f)}\;\vec{\gamma}_{xy}(f) & \sqrt{G_{xx}(f)\,G_{zz}(f)}\;\vec{\gamma}_{xz}(f) \\ \sqrt{G_{yy}(f)\,G_{xx}(f)}\;\vec{\gamma}_{yx}(f) & G_{yy}(f) & \sqrt{G_{yy}(f)\,G_{zz}(f)}\;\vec{\gamma}_{yz}(f) \\ \sqrt{G_{zz}(f)\,G_{xx}(f)}\;\vec{\gamma}_{zx}(f) & \sqrt{G_{zz}(f)\,G_{yy}(f)}\;\vec{\gamma}_{zy}(f) & G_{zz}(f) \end{bmatrix} \quad 38)$$

Leaving out the functions of frequency so everything will fit (all terms are a function of frequency), this can be written in terms of the magnitude and phase of the coherence, as follows:

$$[G]_{3\times3} = \begin{bmatrix} G_{xx} & \sqrt{G_{xx}G_{yy}}\,|\vec{\gamma}_{xy}|\angle\vec{\gamma}_{xy} & \sqrt{G_{xx}G_{zz}}\,|\vec{\gamma}_{xz}|\angle\vec{\gamma}_{xz} \\ \sqrt{G_{yy}G_{xx}}\,|\vec{\gamma}_{yx}|\angle\vec{\gamma}_{yx} & G_{yy} & \sqrt{G_{yy}G_{zz}}\,|\vec{\gamma}_{yz}|\angle\vec{\gamma}_{yz} \\ \sqrt{G_{zz}G_{xx}}\,|\vec{\gamma}_{zx}|\angle\vec{\gamma}_{zx} & \sqrt{G_{zz}G_{yy}}\,|\vec{\gamma}_{zy}|\angle\vec{\gamma}_{zy} & G_{zz} \end{bmatrix} \quad 39)$$

Equations 35 through 39 indicate the notation and variables that the spectral matrix can be expressed in terms of. Equation 39 is written in terms of the variables that the HDL 3-D test specification is currently loaded into the system. For example, G_{xx} represents the PSD spectral line for an accelerometer oriented in the direction of the X axis. $|\vec{\gamma}_{xy}|$ represents the magnitude of the complex coherence function (or just the coherence when it is considered to be real) between an accelerometer

oriented along the X axis, and one oriented along the Y axis. $\angle\vec{\gamma}_{xy} = \angle\vec{G}_{xy}$ is the phase angle for the coherent part of the signal between an accelerometer oriented along the X axis relative to one oriented along the Y axis (the equality, $\angle\vec{\gamma}_{xy} = \angle\vec{G}_{xy}$, comes from comparing terms in Equations 37 and 39). Of course all three terms, G_{xx}, $|\vec{\gamma}_{xy}|$, and $\angle\vec{\gamma}_{xy}$, occur at a spectral line of frequency, f, and vary by frequency. In addition to the large number of relationships implied by Equations 35 through 39, there are also a number of other additional interrelationships.

The spectral matrix is Hermitian. Hermitian matrices are a complex version of a symmetric matrix. The real parts of the matrix are symmetric and the complex parts are symmetric in amplitude but opposite in sign. This structure allows the determinant and characteristic equation to be completely real. If the complex parts had the same sign, they would add instead of canceling each other. The spectral matrix is Hermitian because the variable being predicted is the PSD value at some point and orientation in space. The PSD is real, therefore the diagonal of the spectral matrix must be real.

$$\begin{aligned}
&\Re\vec{G}_{xy}(f) = \Re\vec{G}_{yx}(f) \text{ and } \Im\vec{G}_{xy}(f) = -\Im\vec{G}_{yx}(f) \\
&\Re\vec{G}_{xz}(f) = \Re\vec{G}_{zx}(f) \text{ and } \Im\vec{G}_{xz}(f) = -\Im\vec{G}_{zx}(f) \\
&\Re\vec{G}_{yz}(f) = \Re\vec{G}_{zy}(f) \text{ and } \Im\vec{G}_{yz}(f) = -\Im\vec{G}_{zy}(f)
\end{aligned} \tag{40}$$

Switching to complex coherence and PSD value variables, this is mathematically equivalent to the following:

$$\begin{aligned}
&\Re\vec{\gamma}_{xy}(f) = \Re\vec{\gamma}_{yx}(f) \text{ and } \Im\vec{\gamma}_{xy}(f) = -\Im\vec{\gamma}_{yx}(f) \\
&\Re\vec{\gamma}_{xz}(f) = \Re\vec{\gamma}_{zx}(f) \text{ and } \Im\vec{\gamma}_{xz}(f) = -\Im\vec{\gamma}_{zx}(f) \\
&\Re\vec{\gamma}_{yz}(f) = \Re\vec{\gamma}_{zy}(f) \text{ and } \Im\vec{\gamma}_{yz}(f) = -\Im\vec{\gamma}_{zy}(f)
\end{aligned} \tag{41}$$

The same relationship can be written in terms of the spectral matrix phase angles and amplitudes from Equation 37:

$$\begin{aligned}
&\angle\vec{G}_{xy}(f) = -\angle\vec{G}_{yx}(f) \text{ and } |\vec{G}_{xy}(f)| = |\vec{G}_{yx}(f)| \\
&\angle\vec{G}_{xz}(f) = -\angle\vec{G}_{zx}(f) \text{ and } |\vec{G}_{xz}(f)| = |\vec{G}_{zx}(f)| \\
&\angle\vec{G}_{yz}(f) = -\angle\vec{G}_{zy}(f) \text{ and } |\vec{G}_{yz}(f)| = |\vec{G}_{zy}(f)|
\end{aligned} \tag{42}$$

Again, this is equivalent to Equation 43 in terms of the amplitude and phase of the coherence from Equation 39:

$$\begin{aligned}
&\angle\vec{\gamma}_{xy}(f) = -\angle\vec{\gamma}_{yx}(f) \text{ and } |\vec{\gamma}_{xy}(f)| = |\vec{\gamma}_{yx}(f)| \\
&\angle\vec{\gamma}_{xz}(f) = -\angle\vec{\gamma}_{zx}(f) \text{ and } |\vec{\gamma}_{xz}(f)| = |\vec{\gamma}_{zx}(f)| \\
&\angle\vec{\gamma}_{yz}(f) = -\angle\vec{\gamma}_{zy}(f) \text{ and } |\vec{\gamma}_{yz}(f)| = |\vec{\gamma}_{zy}(f)|
\end{aligned} \tag{43}$$

Some of the phase angles must sum to zero because they are relative angles. The angles θ are the finite Fourier series phase angles, and they are angles relative to the start of the frame. The time of the start of the frame is totally arbitrary, thus only differences between θ values can have physical significance to the system:

$$\begin{aligned} \angle\vec{G}_{xy}\vec{G}_{yz}\vec{G}_{zx} &= \{\theta_y(f)-\theta_x(f)\} + \{\theta_z(f)-\theta_y(f)\} + \{\theta_x(f)-\theta_z(f)\} = 0 \\ \angle\vec{G}_{xz}\vec{G}_{zy}\vec{G}_{yx} &= \{\theta_z(f)-\theta_x(f)\} + \{\theta_y(f)-\theta_z(f)\} + \{\theta_x(f)-\theta_y(f)\} = 0 \end{aligned} \qquad 44)$$

Notice that terms from both above and below the diagonal (from Equation 35) are involved in both expressions in Equation 44. This is why all three terms can be positive. The indices of the variables cycle, e.g. x,y → y,z → z,x. Of course the product can be written in any order: $\angle\vec{G}_{xy}\vec{G}_{yz}\vec{G}_{zx} = \angle\vec{G}_{yz}\vec{G}_{xy}\vec{G}_{zx} = \angle\vec{G}_{zx}\vec{G}_{xy}\vec{G}_{yz}$; however, $\angle\vec{G}_{xy}\vec{G}_{yz}\vec{G}_{zx} \neq \angle\vec{G}_{xz}\vec{G}_{zy}\vec{G}_{yx}$, since they involve different variables. Any set of angles that can be algebraically rearranged to go around in a cycle will sum to zero, since this is the expression for estimating the transfer function phase angle between a variable and itself.

Again switching to the complex coherence as the variable, this is exactly equivalent to:

$$\begin{aligned} \angle\vec{\gamma}_{xy}\vec{\gamma}_{yz}\vec{\gamma}_{zx} &= \{\theta_y(f)-\theta_x(f)\} + \{\theta_z(f)-\theta_y(f)\} + \{\theta_x(f)-\theta_z(f)\} = 0 \\ \angle\vec{\gamma}_{xz}\vec{\gamma}_{zy}\vec{\gamma}_{yx} &= \{\theta_z(f)-\theta_x(f)\} + \{\theta_y(f)-\theta_z(f)\} + \{\theta_x(f)-\theta_y(f)\} = 0 \end{aligned} \qquad 45)$$

Physically there must be some constraint on the three coherence amplitudes. For example, if the X axis is completely coherent with respect to the Y axis, and the Y axis is completely coherent with respect to the Z axis, it is impossible for the X axis to be incoherent with respect to the Z axis. If $|\vec{\gamma}_{xy}(f)|=1$ and $|\vec{\gamma}_{yz}(f)|=1$ it is necessary that $|\vec{\gamma}_{xz}(f)|=1$. The general condition is found by requiring that the principal values of the rotated diagonals remain non negative. It is both necessary and sufficient for the following condition to be satisfied (* denotes multiplication of complex conjugates producing a real result) for the roots of the complex spectral to be non negative:

$$1 \geq \vec{\gamma}_{xz}^{*}\vec{\gamma}_{zx} + \vec{\gamma}_{yz}^{*}\vec{\gamma}_{zy} + \vec{\gamma}_{xy}^{*}\vec{\gamma}_{yx} - 2\vec{\gamma}_{xy}\vec{\gamma}_{yz}\vec{\gamma}_{zx} \qquad 46)$$

Equality in Equation 46 implies that at least one of the principal values of the complex spectral matrix is zero, thus the motion is at most 2-D. In terms of real variables, Equation 46 is as shown below:

$$1 \geq |\vec{\gamma}_{xz}|^2 + |\vec{\gamma}_{yz}|^2 + |\vec{\gamma}_{xy}|^2 - 2|\vec{\gamma}_{xy}||\vec{\gamma}_{yz}||\vec{\gamma}_{zx}| \qquad 47)$$

As far as we have found to date, these are the only restrictions that hold mathematically.

CONSTRAINING THE REAL PART OF THE SPECTRAL MATRIX

In developing Equation 47 it was obvious that the term on the right of Equation 47 was a statistic indicating the dimensionality of the data. When the expression is equal to one, one of the principal values must be equal to zero. If the expression is equal to zero, the coherences are all zero and the principal values are equal to the input diagonal. Clearly the potential is there to construct a statistic out of this expression. Since only the real part of the spectral matrix affects the amplitude, to calculate an amplitude estimator, it is necessary to form the equivalent of Equation 47 with only the real part of the spectral matrix. Since the condition involves only the real part of the spectral matrix, it can not be expressed in terms of coherence alone, independently of the phase angles. Instead, all three phase angles enter the expression. Proceeding just as before, consider obtaining the roots of the real part of the spectral matrix, as follows:

$$\left|\begin{bmatrix} G_{xx}(f)-\lambda & \Re\vec{G}_{xy}(f) & \Re\vec{G}_{xz}(f) \\ \Re\vec{G}_{yx}(f) & G_{yy}(f)-\lambda & \Re\vec{G}_{yz}(f) \\ \Re\vec{G}_{zx}(f) & \Re\vec{G}_{zy}(f) & G_{zz}(f)-\lambda \end{bmatrix}\right| = 0 \qquad 48)$$

Expanding Equation 48 gives as follows:

$$\lambda^3 - (G_{xx} + G_{yy} + G_{zz})\lambda^2 + (G_{xx}G_{yy} + G_{xx}G_{zz} + G_{yy}G_{zz} \qquad 49)$$
$$- \Re\vec{G}_{xz}\Re\vec{G}_{zx} - \Re\vec{G}_{yz}\Re\vec{G}_{zy} - \Re\vec{G}_{xy}\Re\vec{G}_{yx})\lambda + \Re\vec{G}_{xz}\Re\vec{G}_{zx}G_{yy} + \Re\vec{G}_{yz}\Re\vec{G}_{zy}G_{xx}$$
$$+ \Re\vec{G}_{xy}\Re\vec{G}_{yx}G_{zz} - G_{xx}G_{yy}G_{zz} - \Re\vec{G}_{xy}\Re\vec{G}_{yz}\Re\vec{G}_{zx} - \Re\vec{G}_{xz}\Re\vec{G}_{zy}\Re\vec{G}_{yx} = 0$$

The requirement guaranteeing non negative roots is:

$$0 \geq \Re\vec{G}_{xz}\Re\vec{G}_{zx}G_{yy} + \Re\vec{G}_{yz}\Re\vec{G}_{zy}G_{xx} + \Re\vec{G}_{xy}\Re\vec{G}_{yx}G_{zz} \qquad 50)$$
$$- G_{xx}G_{yy}G_{zz} - \Re\vec{G}_{xy}\Re\vec{G}_{yz}\Re\vec{G}_{zx} - \Re\vec{G}_{xz}\Re\vec{G}_{zy}\Re\vec{G}_{yx}$$

This can be expanded to give the following expression in terms of the coherence amplitude and cosine of the phase angles:

$$1 \geq |\vec{\gamma}_{xz}|^2\cos^2\angle\vec{\gamma}_{xz} + |\vec{\gamma}_{yz}|^2\cos^2\angle\vec{\gamma}_{yz} + |\vec{\gamma}_{xy}|^2\cos^2\angle\vec{\gamma}_{xy} \qquad 51)$$
$$- 2|\vec{\gamma}_{xy}||\vec{\gamma}_{yz}||\vec{\gamma}_{xz}|\cos\angle\vec{\gamma}_{xy}\cos\angle\vec{\gamma}_{yz}\cos\angle\vec{\gamma}_{xz}$$

or in terms of complex coherence variables:

$$1 \geq \Re\vec{\gamma}_{xz}^{\,2} + \Re\vec{\gamma}_{yz}^{\,2} + \Re\vec{\gamma}_{xy}^{\,2} - 2\,\Re\vec{\gamma}_{xz}\,\Re\vec{\gamma}_{yz}\,\Re\vec{\gamma}_{xy} \qquad 52)$$

The right hand side of Equation 51 or 52 indicates the dimensionality of the signal at that frequency. If the right hand side approaches one, then the signal is no more than 2-D. All spectral lines that have the same roots for the real part of the spectral matrix have the save value for the right side of Equation 51 and 52. For the shape of the ellipsoid to be the same between two spectral lines, it is necessary but not sufficient for the right side of Equation 51 and 52 to be equal.

References

1. Weast, R.C., et.al. (1970-1971), Handbook of Chemistry and Physics, 51st Edition, The Chemical Rubber Company, p. A219.

2. Hamming, R.W. (1983), Digital Filters, Second Edition, Prentice Hall Inc., p. 67.

3. Bendat, J.S., (1981) 'Definitions and frequency domain procedures for dynamic data analysis', Int. J. of Vehicle Design, vol. 2, no. 2, pp. 227-245.

4. Franklin, J.N. (1968), Matrix Theory, Prentice-Hall, p. 98.

5. Bendat & Piersol (1966), Measurement and Analysis of Random Data, Wiley, p. 104.

6. Harris & Crede (1961), Shock and Vibration Handbook, Vol. 2, Mc Graw-Hill, pp. 23-34.

CHAPTER 5 EMPIRICAL 3-D RANDOM TEST RESULTS

INTRODUCTION

To understand the limitations the constraints discussed in the last chapter impose, a number of specification examples have been developed depending on how the parts of the specification are determined. For example, the phase angles might be chosen at random while the coherence was fixed at a constant. Another way to select a test would be to adopt constant phase angles, but select the coherence as a random variable. By examining these two cases to determine what the principal components are in each case, it becomes obvious that these specifications produce unexpected, and unwanted responses in directions other than the input.

RANDOM PHASE, CONSTANT AMPLITUDE COHERENCE

In writing a test specification for a 3-D test machine, one must completely specify the spectral matrix at each frequency. Typically three PSD values in the X, Y, and Z directions are known from previous 1-D testing. These levels are usually determined by enveloping data in the relevant test directions. These three PSD values form the diagonal of the 3-D spectral matrix. For example suppose the PSD envelope is given as follows, and as illustrated in Figure 1a:

X & Y axes:

5 Hz to	10 Hz	0.05 g^2/Hz
10 Hz to	200 Hz	sloping at -4.6 db/oct to 0.0005 g^2/Hz
200 Hz to	500 Hz	0.005 g^2/Hz

wideband RMS = 1.9 g

Z axis:

5 Hz to	10 Hz	0.1 g^2/Hz
10 Hz to	200 Hz	sloping at -4.6 db/oct to 0.001 g^2/Hz
200 Hz to	500 Hz	0.005 g^2/Hz

wideband RMS = 1.6 g

The off diagonal terms are more difficult to specify. They are the cospectra or (after dividing by the square root of the PSD values) the complex coherence between the channels. There are two parts of each coherence number: a magnitude less than or equal to one and a phase angle. Because the terms below the diagonal are the complex conjugate of the terms above the diagonal there are only three coherence terms to be determined. Further, because the phase angles must go through a complete cycle, there are only two independent phase angles. Finally, because the coherence amplitudes are constrained, the third coherence is limited by the choice of the other two.

Suppose one observed that typical coherence data was around $\gamma^2 \sim 0.75$ and decided to set all the coherences at this value. Finally one might select two of the phase angles at random, and set the third angle to satisfy the angles constraint.

Figure 1 Random Phase, Constant Amplitude Coherence

Figure 1a The Test PSD Values

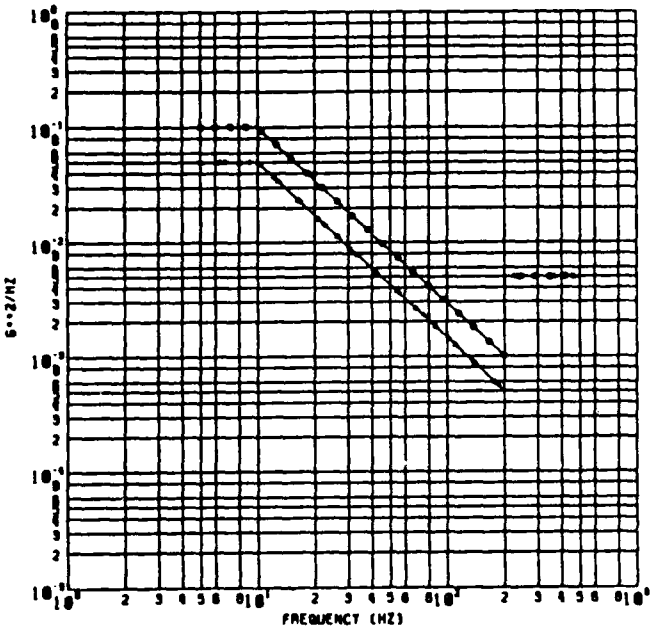

Figure 1b Roots of the Complex Matrix

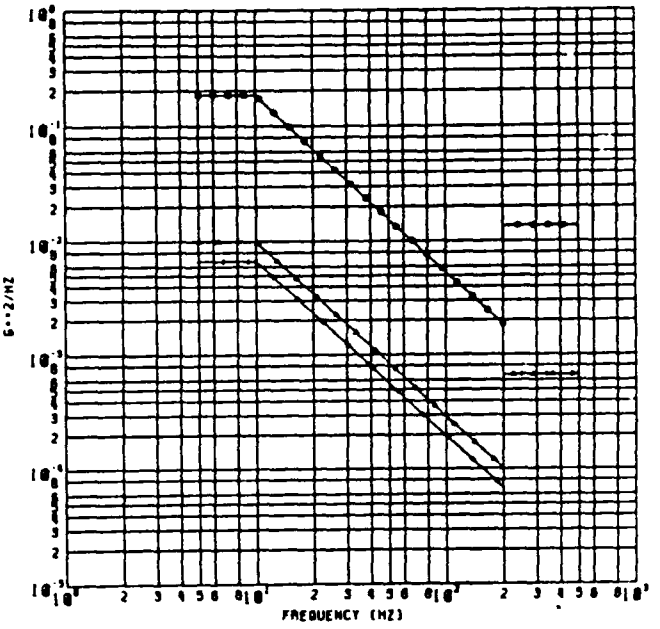

Figure 1c Roots of the Real Part

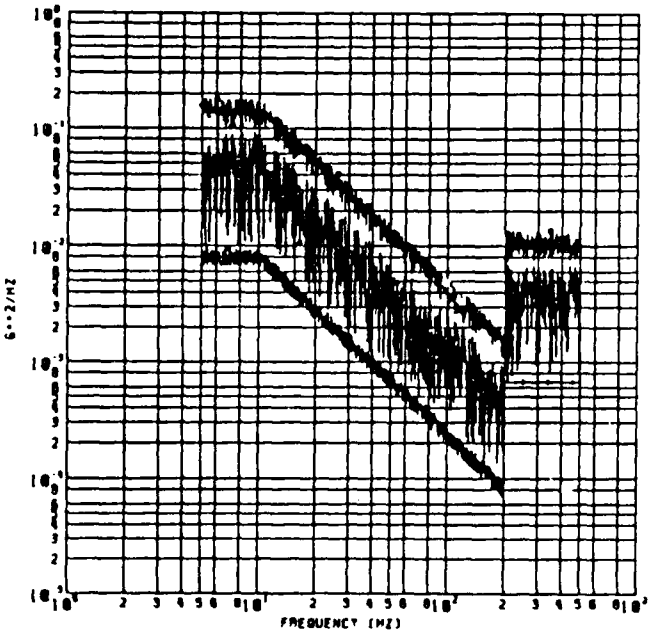

Figure 1d PSD at <.577,.577,.577>

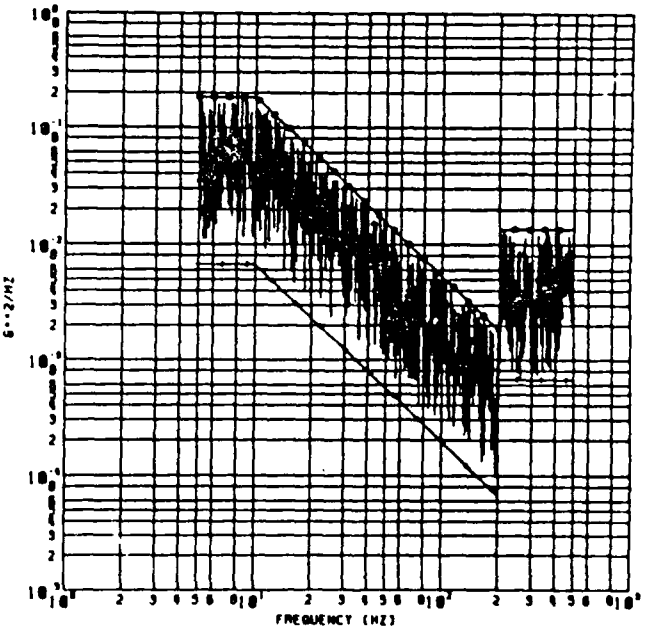

Generating data in this way, the complex spectral matrix was rooted producing the curves shown in Figure 1b. The significance of these roots is that they represent the largest and smallest values as a function of spatial orientation that might be observed in any direction at that frequency. For example, at 10 Hertz, while the largest input PSD was 0.1 g^2/Hz, this procedure for specifying the coherence and amplitude has resulted in a physical maximum spatially of 0.1833 g^2/Hz. Similarly the smallest input PSD was 0.05 g^2/Hz while the physical minimum spatially is 0.0067 g^2/Hz. Assuming the PSD data enveloped test data, this is seriously different than the test data that the PSD's were based on.

Evaluation of the vectors reveals a problem with this interpretation. The vectors are complex. The following complex results are typical:

Spectral Matrix:

(0.050000, 0.000000)	(0.043287, 0.001081)	(-0.036926, 0.048849)
(0.043287,-0.001081)	(0.050000, 0.000000)	(-0.035696, 0.049755)
(-0.036926,-0.048849)	(-0.035696,-0.049755)	(0.100000, 0.000000)

PSD_x = 0.05 g^2/Hz	$\lvert\vec{\gamma}_{xy}\rvert$ = 0.866	$\angle\theta_{xy}$ = 1.4°
PSD_y = 0.05 g^2/Hz	$\lvert\vec{\gamma}_{yz}\rvert$ = 0.866	$\angle\theta_{yz}$ = 125.7°
PSD_z = 0.10 g^2/Hz	$\lvert\vec{\gamma}_{xz}\rvert$ = 0.866	$\angle\theta_{zx}$ =-127.1°

Root:	Vector: Normalized so X component is real		
	X	Y	Z
0.183315 g^2/Hz =>	(0.490241,0.)	(0.490088,-0.012234)	(-0.434562,-0.574877)
0.009985 g^2/Hz =>	(0.509602,0.)	(0.509383,-0.012709)	(0.418073, 0.553071)
0.006700 g^2/Hz =>	(0.707116,0.)	(-0.706877, 0.017643)	(0.000009, 0.000009)

The phase angles of these roots are the same as the phase angles of the coherence vectors they came from. Since the vectors are normalized so the X component is all real, the relevant coherence angles are $\angle\theta_{yx}$ and $\angle\theta_{zx}$. All the phase angles are equal to the appropriate term or 180° (a minus sign) subtracted from it. This is illustrated below:

Angle of each vector:

0.183315 g^2/Hz =>	0.0°	-1.4°	-127.1°
0.009985 g^2/Hz =>	0.0°	-1.4°	52.9°
0.006700 g^2/Hz =>	0.0°	178.6°	52.9°

These vectors could be used to calculate Fourier series to be used in generating time histories, however, they are of no use in finding the direction of the maximum amplitude since they are complex.

As has already been demonstrated there is no interaction between the complex parts of the spectral matrix and the diagonal where the roots ultimately are found. For this reason it seemed reasonable to root the real part of the spectral matrix and numerically see if the maximum response was in the direction of the vectors from the real part of the matrix. This turns out to be the case.

Figure 2 Constant Phase, Random Amplitude Coherence

Figure 2a The Test PSD Values

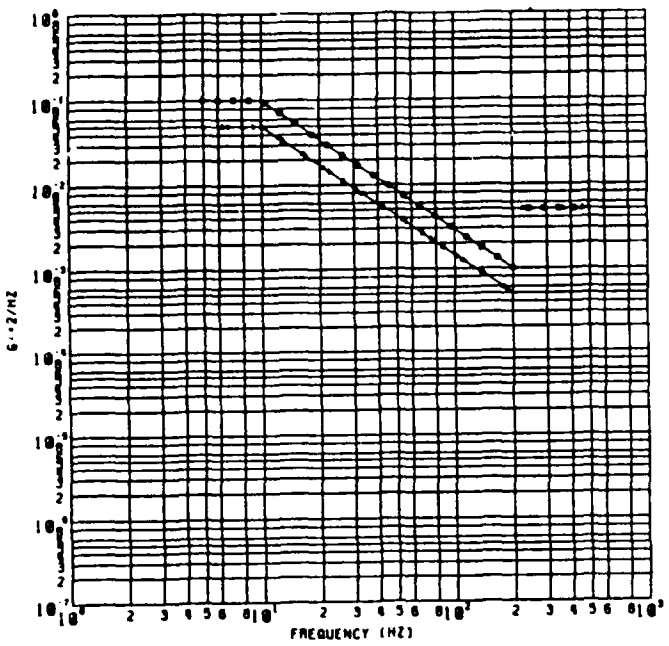

Figure 2b Roots of the Complex Matrix

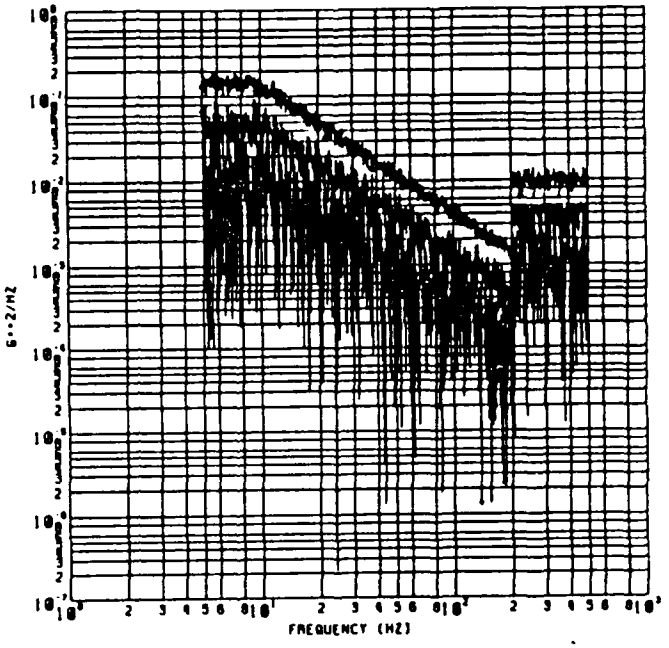

Figure 2c Roots of the Real Part

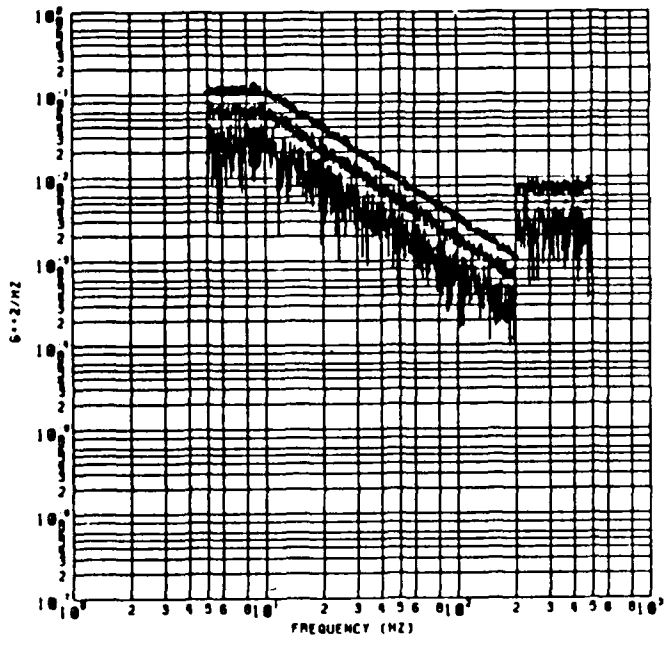

Figure 2d PSD at <.577,.577,.577>

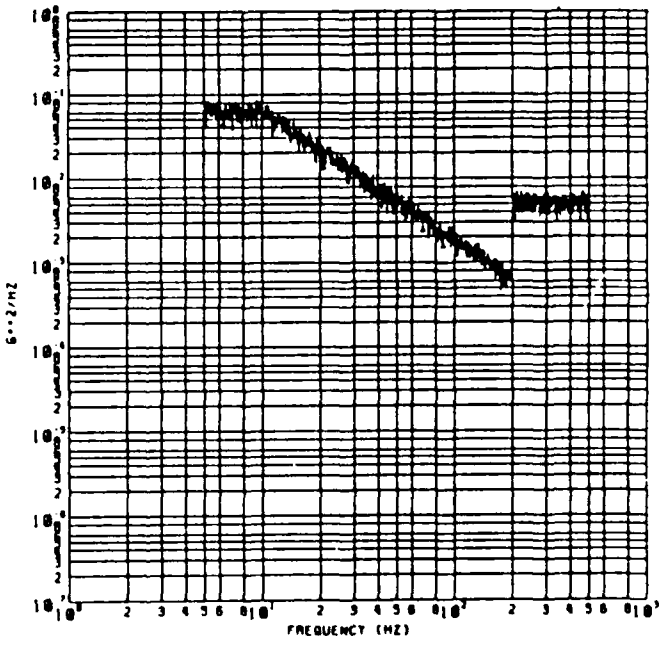

Proceeding with the same numbers as before and rooting the real part of the matrix, the real matrix roots are shown in Figure 1c. They are irregular and bounded by the complex matrix roots. The vectors are real and indicate the rotation vector required to point in the direction of each root. For the numerical example above the results are as follows:

Roots of the Real Part:		Vectors:	
	X	Y	Z
0.148107 g^2/Hz =>	0.486575	0.480224	-0.729815
0.045192 g^2/Hz =>	0.505105	0.526963	0.683505
0.006701 g^2/Hz =>	0.712821	-0.701210	0.013844

Pre and post multiplying these vectors times the spectral matrix produces an orthogonality matrix as follows:

Orthogonality Test:

(0.148107, 0.000000)	(0.000000, 0.069735)	(0.000000,-0.000129)
(0.000000,-0.069735)	(0.045192, 0.000000)	(0.000000,-0.000037)
(0.000000, 0.000129)	(0.000000, 0.000037)	(0.006701, 0.000000)

Rotating in the directions indicated by the eigen vectors, the value of the root is obtained as the PSD level at that frequency in that direction. Further, investigating the vicinity of the largest and smallest root reveals that they are a maximum and a minimum respectively.

Figure 1d illustrates the results of rotating the test specification to an arbitrary direction (e.g., <.577,.577,.577>). The maximum and minimum roots of the complex matrix have also been plotted for reference. Notice that the PSD in arbitrary directions is not smooth and ranges arbitrarily as a function of frequency between the maximum and minimum values.

The procedure of using constant coherence and randomly selecting phase for a test specification has serious deficiencies. The amplitude of the test is not limited to the range of numbers between the three input specifications. Further the test specification is irregular in any direction except the original X, Y, and Z axes. Finally, the maximum amplitude and minimum amplitude are irregular and depends on the randomly selected phase to determine both the direction and amplitude of the test. To much is being determined by a random number generator using this procedure.

CONSTANT ANGLE, RANDOM AMPLITUDE COHERENCE

A second procedure for writing a 3-D test specification would be to select the coherence amplitude with a random number generator ranged between 0 and 1 for two of the coherences and limited by the coherence constraint for the third coherence. The three phase angles would be set to constant angles (e.g., 45°, 90°, and -135°). The results of this procedure are shown in Figure 2.

Figure 3 90° Phase, Constant Amplitude Coherence

Figure 3a The Test PSD Values

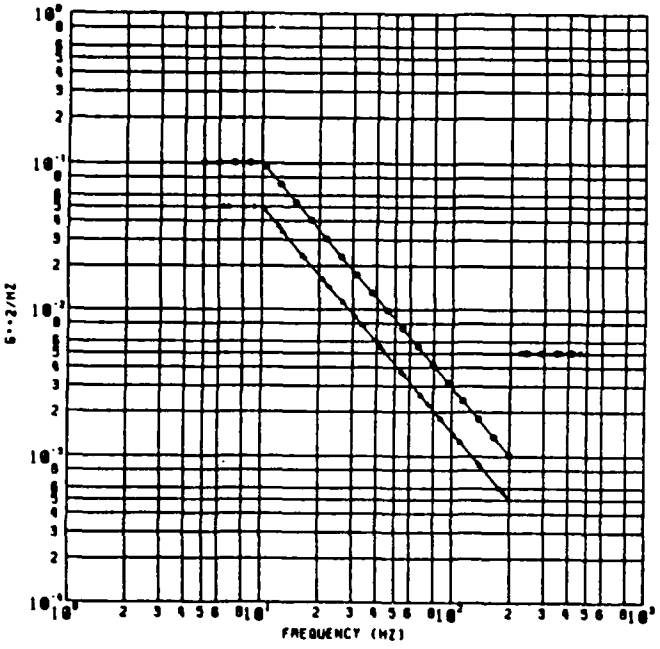

Figure 3b Roots of the Complex Matrix

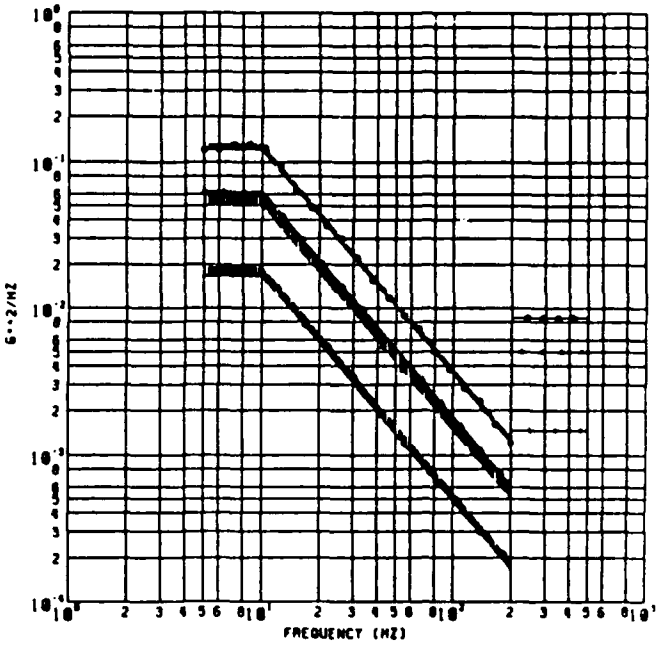

Figure 3c Roots of the Real Part

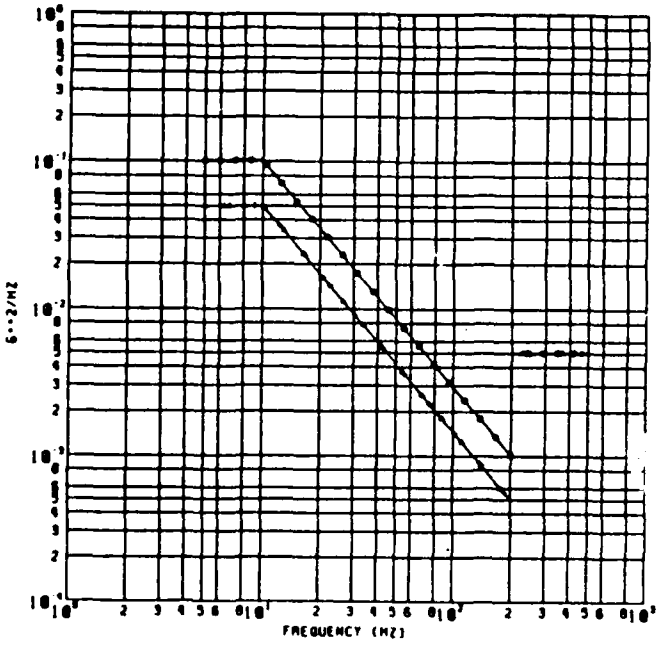

Figure 3d PSD at <.577,.577,.577>

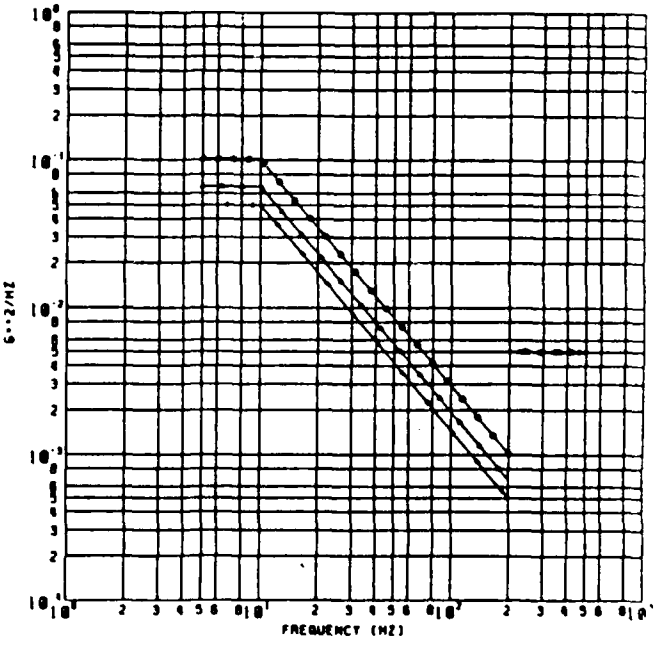

The roots of the complex spectral matrix are irregular with a tremendous variation in the smallest root as shown in Figure 2b. This reflects the fact that the smallest root will be equal to zero if the three coherent values form equality in the coherence constraint. Picking the coherence values with a random number generator produces values that come quite close to equality, thus the lower root comes very close to being zero.

Just as before, the roots of the real part of the spectral matrix are between the roots of the complex part as shown in Figure 2c. In particular, the smallest root is considerably better behaved when rooting the real part of the spectral matrix. Again the roots of the real part of the spectral matrix are the largest and smallest value of PSD that can be observed in any direction in 3-D space.

Finally, rotating to an arbitrary direction <.577,.577,.577> produces the PSD shown in Figure 2D. This result is considerably better behaved than the corresponding PSD from the previous example, however, it is still irregular.

This procedure suffers from much the same problem as before: PSDs larger than the input PSDs are observed spatially. Very low amplitudes occur in some directions, and the PSDs observed in directions other than the input directions are irregular.

90° PHASE, CONSTANT AMPLITUDE COHERENCE

The features desired in a test specification are as follows:

1. PSD values should not exceed the largest input specification or be smaller than the smallest input specification.

2. The roots of the real part of the spectral matrix should correspond to the input PSDs so the directions of the responses are fixed.

3. Rotated PSDs should be straight lines interpolating smoothly between the input PSDs.

The most complicated matrix that can achieve the second objective is one with no off diagonal real parts. In this way, illustrated in Figure 3, the input specification already diagonalizes the real part of the spectral matrix, and therefore are the roots of the matrix. The imaginary parts of the matrix still have to satisfy the requirements of the coherence and phase angle constraints. For the three phase angles to be at 90° and still add up to 0° (or 360°, etc.), it is necessary for one angle to be zero, and the other two to be +90° and -90°. This means one of the three coherence values has to be zero, to let the term with phase angle zero have no real part.

Selecting a constant coherence under these conditions is some what limiting. One coherence amplitude must be zero, so the coherence constraint reduces to Equation 1 below:

$$1 \geq \vec{\gamma}_{xz}{}^{*}\vec{\gamma}_{zx} + \vec{\gamma}_{yz}{}^{*}\vec{\gamma}_{zy} \qquad \text{where: } \vec{\gamma}_{xy} = (0.,0.) \qquad 1)$$

Figure 4 90° Phase, Random Amplitude Coherence

Figure 4a The Test PSD Values

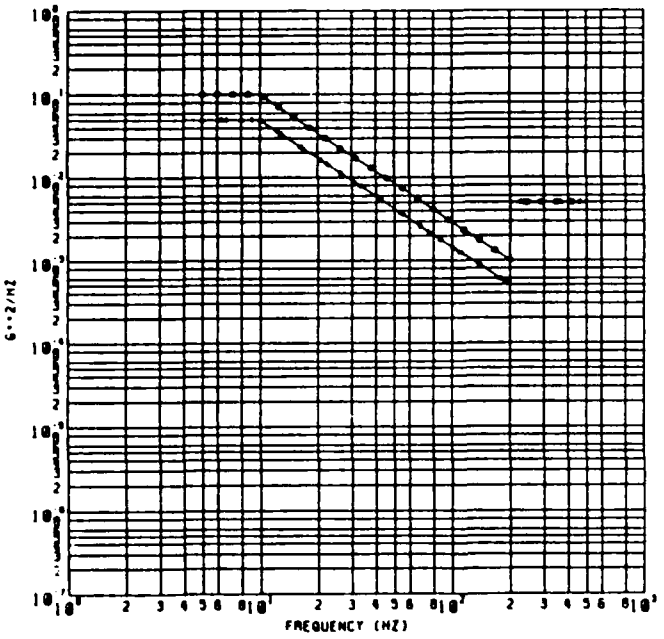

Figure 4b Roots of the Complex Matrix

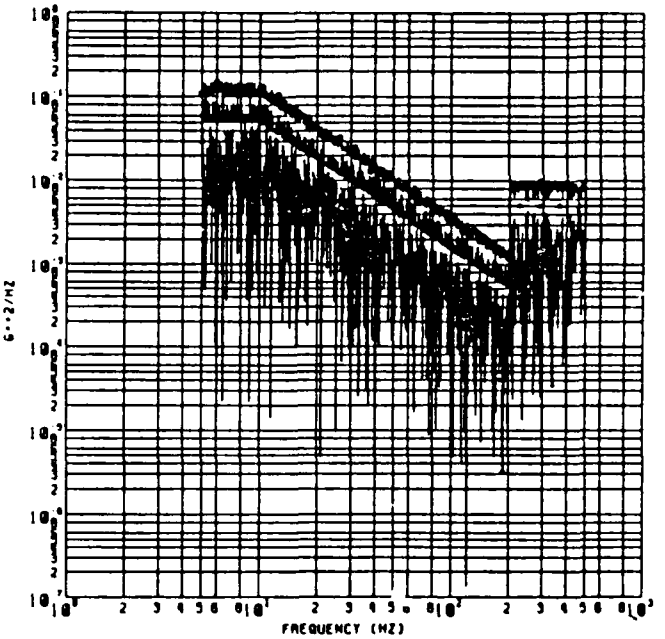

Figure 4c Roots of the Real Part

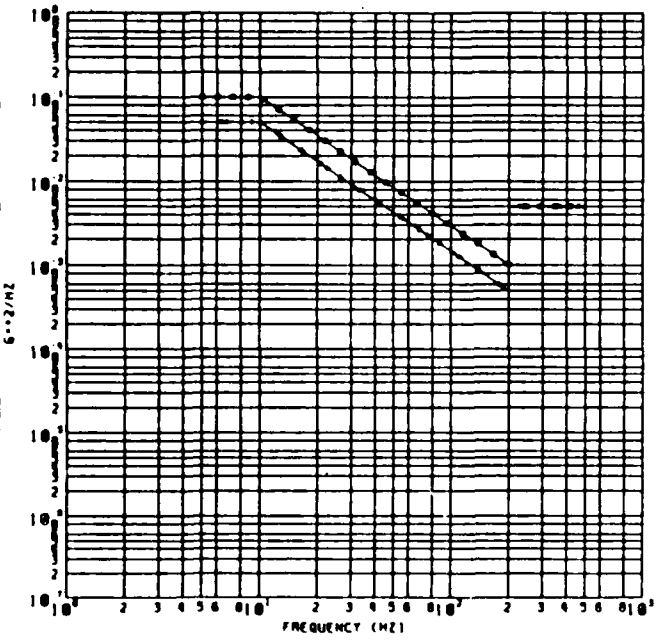

Figure 4d PSD at <.577,.577,.577>

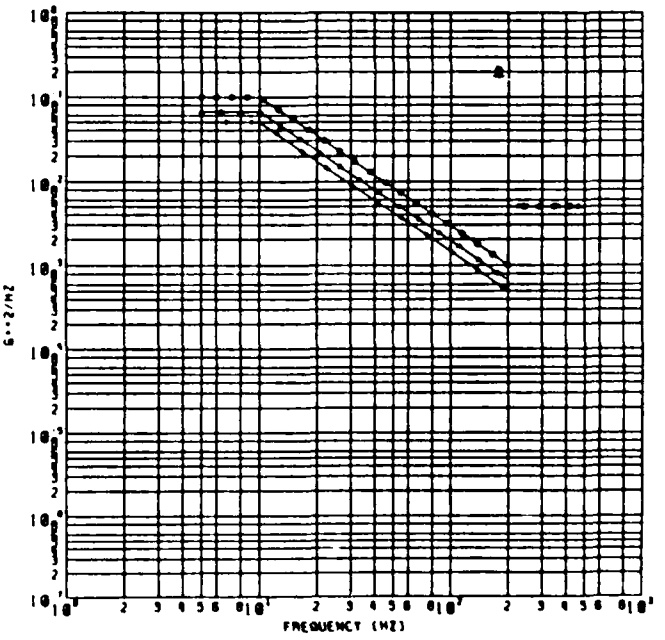

The largest constant value of coherence that can satisfy Equation 1 is 0.707 compared to the largest value that can satisfy the general coherence constraint which is 1.

Figure 3 illustrates the same set of curves as before for a coherence amplitude of 0.5 and randomly selected phase angles of 90°. The thickening of the lines in Figure 3b is because there are two sets of roots reflecting whether the zero coherence value aligns with the larger Z amplitude. This procedure satisfies all the requirements of a good 3-D test specification, but the value of the coherence is limited to a lower value than observed in the real world.

90° PHASE, RANDOM AMPLITUDE COHERENCE

Another possibility is to select one of the two arbitrary coherence amplitudes with a random number generator ranged between zero and one. Then Equation 1 can be used to select the range for a random number generator to select the other value. This procedure produces the results show in Figure 4. Just as before, the complex roots vary over a wide range depending on where the zero amplitude coherence is located in the matrix, and also depending on how close Equation 1 comes to equality.

The roots of the real part of the spectral matrix are well behaved and produce rotations that are reasonable using this procedure. Notice that when the amplitudes all become equal (from 200 to 500 Hz), the rotated PSD shown in Figure 4d also takes on the constant value. For three equal inputs the result is a sphere of constant amplitude.

A typical spectral matrix using this procedure is shown below:

Spectral Matrix:

```
( 0.050000, 0.000000) ( 0.000000, 0.036843) ( 0.000000, 0.000000)
( 0.000000,-0.036843) ( 0.050000, 0.000000) ( 0.000000,-0.035197)
( 0.000000, 0.000000) ( 0.000000, 0.035197) ( 0.100000, 0.000000)
```

PSD_x = 0.05 g^2/Hz $|\tilde{\gamma}_{xy}|$ = 0.736868 $\angle\theta_{xy}$ = 90°
PSD_y = 0.05 g^2/Hz $|\tilde{\gamma}_{yz}|$ = 0.497767 $\angle\theta_{yz}$ = -90°
PSD_z = 0.10 g^2/Hz $|\tilde{\gamma}_{xz}|$ = 0.000000 $\angle\theta_{zx}$ = 0°

```
Root:              Vector: Normalized so X component is real
                             X                 Y                      Z
0.122850 g²/Hz => (0.265500,0.) ( 0.000000,-0.524973) ( 0.808649, 0.000000)
0.071166 g²/Hz => (0.740874,0.) ( 0.000000,-0.425627) (-0.519565, 0.000000)
0.005984 g²/Hz => (0.616940,0.) ( 0.000000, 0.737052) ( 0.275934, 0.000000)
```

Roots of the Real Part:

	Vectors: X	Y	Z
0.100000 g^2/Hz =>	0.000000	0.000000	1.000000
0.050000 g^2/Hz =>	1.000000	0.000000	0.000000
0.050000 g^2/Hz =>	0.000000	1.000000	0.000000

CONCLUSIONS

Controlling the coherence of the three shaker inputs doesn't control the coherence away from the shaker. The coherence away from the shaker is controlled by the modal response. The mode only responds to an input in one direction, i.e., the direction of the modal response at the shaker. Any input perpendicular to the mode's direction is ignored regardless of coherence with other inputs. Since the whole mode responds to only one input, the response over the whole test article at that frequency is highly coherent when the local direction of the mode is compared to the local direction of the input.

The amplitude of the coherence determines the amount of the variation between principal axes of the ellipsoid at the frequency it applies to. The roots of the complex spectral matrix do not depend on the phase angle, only the amplitude of the coherence and the PSD values. Zero coherence produces uniform principal axes and consequently a sphere. The PSD values scale the ellipsoid up or down along the coordinates they apply to. The phase angles of the coherence orient the principal axes of the ellipsoid in space and time.

Controlling the narrow band amplitude in the direction of the local modal response at the shaker controls the amplitude of the response all along the test article. The 3-D shape of the random input at each frequency could be an arbitrarily oriented ellipsoid. Avoiding having the ellipsoid oriented along the three shaker directions requires coherence between the three shaker inputs. Coherence is the only way to get the response at an angle to the shakers to exceed the response in the direction of the shakers. The real part of the coherence reorients the principal axes of the 3-D random input so the ellipsoidal surface does not align with the shaker axes. This makes some other direction than one of the shaker directions have the largest amplitude.

Sufficient data to build a test specification with arbitrary axis orientation will rarely be available. Luckily, it is not really necessary. Since a mode will only respond to an input in one direction, the test input can be spherical at the correct amplitude and the mode will filter out the input in it's direction. The test specification can be obtained by enveloping 3-D data reduced to give principal responses, or simply by enveloping a large amount of data in all different directions. If distinctions between X, Y, and Z are desired, it is possible to specify different PSD levels in the different directions just as has always been done. Then taking zero coherence between the shakers, the input will be egg shaped with the principal directions aligned with the shaker directions. For more generality one of the 90° phase angle specifications can be used to enter non zero coherence values and still obtain the desired amplitudes.

For still more generalized coherence, the physical orientation of the test specimen must be controlled both in use and on the shaker. For example, if the test specimen is being tested for the transportation vibration environment, the test specimen must always be physically oriented in the same direction during transportation. A package can be set down in almost

any direction so spatial distinctions in the input accelerations (e.g., along path, cross path, and vertical) can not be correlated to the package orientation. Under these circumstances, the coherence should be zero and the amplitude should envelope the response in all three axes.

In the rare instances where the physical configuration is repeatable and there is sufficient experimental data to actually specify a complete spectral matrix; there is still the problem of averaging complex numbers to envelope a large amount of data. The phase angle fixes the relative signs of the inputs, and thus, the quadrant that the data falls in. It is necessary to use a procedure that keeps track of the phase angle in order to produce meaningful envelopes of the data. If one sets the amplitudes correctly and sets the phase angle wrong, the input will be large in some other direction than the data. It is like specifying a large X input because the data indicated that Z was high. Unless the data is to reproduce a single set of physical measurements at an input point, it does not seem advantageous to use a more general test specification.

On the other hand, there is tremendous advantage to using the PSD's in the three shaker directions and <u>zero</u> coherence. This specification requires no more data than currently is called out when three individual test axes are specified. It will excite the test article to the same levels achieved in the conventional test along the shaker axes. At angles to the shaker axes, the input would be ellipsoidal, faring a smooth curve between shaker inputs with maximum amplitude at the shaker. The ellipsoid will produce slightly higher inputs at directions other than the shaker direction, however, the total duration of exposure will be reduced by 1/3 to a single test rather than three individual tests.

CHAPTER 6 3-D COLOR GRAPHICS

INTRODUCTION

The 3-D shaker has unique display considerations arising from the three dimensional nature of the excitation. Also, a very capable multicolor display system (Evan and Sutherland, model PS 390) is available to calculate and output displays as required. Thus the issue is how the new display system can best be utilized to address 3-D testing.

The displays to be considered include the test control display used by the test operator to monitor the test's progress and also more general displays to demonstrate what is happening in real time or in the post test environment operating from data files. The objectives of these two types of displays are quit different. The operator needs to be shown the parameters that are under specification control to observe any out of specification conditions and to manually shutdown if they occur. Data that is not under specification control should not be shown as it potentially can distract the operator. To the extent possible, the operator's display should be very simple and independent from the test control system. Data entry should be kept to an absolute minimum to keep setup time short and to minimize the possibility of error. At the same time, the display should recalculate the data to provide an independent check on the test control system.

The data reduction class of display is quit different. Potentially it should cover all the relevant characteristics of each form of test. The tests under discussion are sine, random, and transient. Data reduction techniques can be classified as control, waveform, or response. Actually, either control or response measurements can be examined for waveform. However, the techniques are the same so it is simpler to call waveform a category rather than another dimension. Finally each of these data reduction techniques can be considered in the time or frequency domain. This produces the following buzz word generator to be examined for forms of data display:

Sine	Control	Frequency Domain
Random	Waveform	
Transient	Response	Time Domain

Sine Test Analysis of Control Channels in the Frequency Domain.
Wideband RMS and Tracking Filter

Sine Test Analysis of Control Channels in the Time Domain.
Oscillographs

Sine Test Analysis of Waveform in the Frequency Domain.
Zoom Fourier Transform

Sine Test Analysis of Waveform in the Time Domain.
3-D Oscilloscope

Sine Test Analysis of Response in the Frequency Domain.
Wideband RMS and Tracking Filter
Transfer Function

Sine Test Analysis of Response in the Time Domain.
- Oscillographs
- 3-D Oscilloscope

Random Test Analysis of Control Channels in the Frequency Domain.
- Principal Components
- Spectral Matrix

Random Test Analysis of Control Channels in the Time Domain.
- Distribution Function
- Autocorrelation and Cross Correlation

Random Test Analysis of Waveform in the Frequency Domain.
- Harmonic Analysis

Random Test Analysis of Waveform in the Time Domain.
- Distribution Function
- Autocorrelation and Cross Correlation

Random Test Analysis of Response in the Frequency Domain.
- Principal Components
- Spectral Matrix
- Transfer Function

Random Test Analysis of Response in the Time Domain.
- Distribution Function
- Autocorrelation and Cross Correlation

Transient Analysis of Control Channels in the Frequency Domain.
- Finite Fourier Transform
- Shock Spectra

Transient Analysis of Control Channels in the Time Domain.
- Oscillographs
- 3-D Oscilloscope

Transient Analysis of Waveform in the Frequency Domain.
- Finite Fourier Transform

Transient Analysis of Waveform in the Time Domain.
- Oscillographs
- 3-D Oscilloscope

Transient Analysis of Response in the Frequency Domain.
- Finite Fourier Transform
- Shock Spectra

Transient Analysis of Response in the Time Domain.
- Oscillographs
- 3-D Oscilloscope

Thus the following analysis types need to be discussed with respect to 3-D data.

a. Autocorrelation and Cross Correlation
b. Distribution Function
c. Finite Fourier Transform
d. Harmonic Analysis
e. Oscillographs
f. Principal Components
g. Spectral Matrix
h. Transfer Function
i. Wideband RMS and Tracking Filter
j. Zoom Fourier Transform
k. 3-D Oscilloscope

OPERATIONS PRIOR TO DATA DISPLAYS

A great deal of flexibility can be gained by allowing major operations before the data is to be displayed. When data first enters the system it is advisable to have a data descriptor file containing ids, labels, physical units, cable routing, default display order, etc. that identify the data. Given the color display system it might be a good idea to identify each channel with a default display color, for example three numbers indicating the intensity of red, green, and blue, to be used when displaying the data from the channel unless other considerations over ride this color scheme. The color scheme could be used to identify components of a test article, or instrumentation directions, or test configurations, or instrumentation types (accelerometers versus strain gages).

Given the 3-D nature of the system it would be very useful to have a set of direction cosines in the instrumentation file for each accelerometer. Data for this file could be easily generated by sinusoidal excitation at a very low frequency and level in X, followed by Y, followed by Z. Software could be set up to calculate the direction cosines from this series of tests. This procedure would also allow testing the calibrations to some extent because the overall amplitude should be very predictable. In spite of the fact that the data is taken from three different runs, the square root of the sum of the squares of the components should equal the test amplitude assuming all three tests are run at the same amplitude. If the measured amplitude was displayed in tabular form, any calibration errors would be very obvious. The system should also pay attention to sign, since accelerometers can be mounted upside down. Also, the system identification needs to identify triaxial measurements in some way. This allows rotations and coordinate transformations to be calculated for each triaxial measurement.

Similarly, there should be a calibration file organized by run id, containing the data needed to convert to physical units by specifying a scale factor and bias to be removed from each channel. Calibrations potentially need to be available by run id because the data changes occasionally between runs. Also, signal calibration data should be stored in the same file in time sequence, so the software can look backwards to calculate the calibrations. It is useful to have a description of the

calibration type (e.g. full scale sine calibration at 200 Hz, or 1.0 volt step calibration) and a value for the full scale in volts so that it can be converted to physical units and compared to the data (at the 95% level) to detect over ranging. Again, an automatic procedure should be available to produce calibration data. It should include full scale calibration data in both the plus and minus directions, and a zero calibration point allowing automatic removal of any bias in the data. If possible the calibration procedure should be simple enough to be run before each run.

Some systems include a polynomial that potentially can remove non linearities in the data (e.g., $OUT=C_0 + C_1\times(IN-BIAS) + C_2\times(IN-BIAS)^2 + C_3\times(IN-BIAS)^3 + C_4\times(IN-BIAS)^4) + \ldots + C_N\times(IN-BIAS)^N$. I don't recommend using this form because it slows conversion down slightly (you have to put the conversion process into a loop over a value of N loaded with the data) and isn't used very often except with N=1. On the other hand if you ever need it, it is very convenient to have a power series conversion built into the system.

Along the same lines, it is often handy to allow for digital filtering of the data before it is displayed. Recursive filtering for high pass, low pass, and bandpass operations are extremely cheap in terms of computational effort and can clean up a lot of problems. Perhaps VAMP provides enough capability in this area. Still, providing filtering capability on the front end of the data reduction system can cure a lot of problems.

Another predisplay function might be to provide for coordinate transformations of the triaxial data. Any three orthogonal measurements can be transformed to cylindrical or spherical coordinates. Again, coordinate transformations can be done after the fact in VAMP but it might be useful in interpreting control data for the sine test where the test is specified as angular velocities (i.e., rates of change of the angles) or in the zero coherence random test to investigate the test amplitude as a spherical normal distribution.

Another predisplay function that often is very useful is numerical integration or differentiation. Integration using the trapezoid rule is very effective as long as an adequate sampling rate is being used. Differentiation is most effective if the second order form of the differential is used, i.e., $dX(t)/dt \approx (X(t+\Delta t) - X(t-\Delta t)) / (2\times\Delta t)$. Neither of these forms extrapolate to unreasonable values because they only interpolate between two data points.

Some systems have a generalized calculation function available before the displays are output. It is easiest to implement this procedure in inverse polish notation. The most important functions are as follows: 1) scaler multiply a channel by a constant, 2) add or subtract two channels, 3) one dimensional and two dimensional table lookup, 4) take the log or exponent of a channel, 5) multiply and divide one channel by another, and so on. Again, this is a function that VAMP can fill.

The most important of the predisplay functions for a 3-D system is the ability to rotate the coordinates from a triaxial measurement through any orientation in space. Effectively all possible orientations of the measurement would be provided from a single triaxial measurement. A joy

stick could be used to load the rotation matrix into the system. Then there would be three inputs for each triaxial measurement which would be matrix multiplied by the rotation matrix to get three output signals in the new coordinate system. To the data reduction system it would appear that the measurements were coming from a triax with a different coordinate system orientation. All the displays in the system could be rotated using this procedure, not just the displays with spatial coordinates such as the 3-D oscilloscope. For example, the 3x3 spectral display could be viewed from any orientation not just the one that aligns with the shaker axes.

Any time a joy stick is used, it is essential that some simple method be provided for returning the joy stick to nominal. A home key is important to avoid being misled. Also, it is useful to be able to load precise coordinates from the keyboard, and to be able to read out precise coordinates from the display.

The result of this operation could be confusing without some system of providing for visual identification of the coordinate reference. An icon could be used for this purpose representing the shaker planes of the 3-D system. A perspective, hidden line, picture of a corner with one shaker plane colored red, one colored blue, and the last plane colored green might be cheap to calculate and easy to visualize. The backs of the planes might be darker than the fronts to indicate which side of the plane is being examined. Every effort should be made to keep the icon very simple and easy to calculate, it's display time will limit every display in the system.

DISPLAYS AUTOCORRELATION AND CROSS CORRELATION

The autocorrelation and cross correlation functions are a seldom used function displaying the correlation coefficient between one time history and another time history as a function of the time lag between them. In my experience, it has been most useful in looking for repeated events in transient test data. If wavelets come at regular intervals, autocorrelation is a good way of identifying the shape and timing of the wavelet. Because of its definition, it is difficult to calculate the correlation function continuously with time. It makes most sense when dealing with limited frames of data. Also, it is hard to see how autocorrelation and cross correlation extend into 3-D. There are six independent curves for a single triaxial set of measurements forming a 3x3 array with the off diagonal data being symmetric.

I'd put this at the bottom priority.

DISPLAYS DISTRIBUTION FUNCTION

The distribution function is fundamental to discussing the random test in the time domain. The integral of the distribution function over a region in space gives the probability of a data point being sampled in that region. Integrating over all of space gives a value of one. As a practical matter, it requires a huge amount of data to accurately represent the distribution function by direct measurement. Instead the moments of the distribution should be numerically calculated at least through the fifth moment and cross

moment for each axis, and an expansion in terms of the moments should be used. A theoretical value of the distribution function can be precalculated and the expansion could be done as a perturbation to the precalculated values.

The display itself resembles a puff ball in space. Possibly the nominal puff ball could be displayed using color shading and dot density to represent the local value with a plane or pie cut to see inside. Then the whole display could be rotated while holding the location of the plane or pie cut fixed to provide a spatially look at the data. Fixed contour levels such as 3σ could be shown as lines. Variations with time could be displayed as color changes and/or as contour changes. The averaging time for display variations could be adjustable so that the chaotic rapid displays could be slowed down to show the result averaging to the nominal distribution.

For zero coherence tests, the 1-D chi squared distribution of the resultant vector is equivalent to the much more complicated 3-D display.

DISPLAYS FINITE FOURIER TRANSFORM

The finite Fourier transform is useful for dealing with transient data in the frequency domain. Because the transient data isn't necessarily stationary, the only Fourier transformation into the frequency domain that is still defined is the finite Fourier transform, e.g., a two time point to one frequency point transformation that can't necessarily be averaged. For this application, the interesting question tends to be whether there is any regular frequency content to the signal and what frequency range the data is coming in. The amplitude at a frequency is hard to interpret and tends not to be a major consideration.

This situation lends itself to displaying the instantaneous finite Fourier transform data for the last five or six transforms (possibly decaying away with darker colors being earlier data) and the dynamic upper and lower envelopes of the previous data. This kind of a display needs a reset button to restart the process, and a hold button to make the display hold still.

Data would be available for three channels at a time in a 3-D test. It could be displayed as three 1-D transform amplitude and phase plots, or it could be displayed as instantaneous spectral data with three PSD diagonals, and three coherence functions, and three phase plots. This kind of a display is going to get extremely busy. The phase data is unlikely to be interpretable and might reasonably be held back most of the time.

For many transient waveforms it is possible to average the data. When this happens the conventional spectral display would probably be better.

DISPLAYS HARMONIC ANALYSIS

One of the ways of assessing waveform in the frequency domain is analysis of the higher harmonics of the signal. If a regular waveform exists which is not purely one sinusoid, it will show up in the frequency domain as a signal with regular harmonics of a (lowest, usually largest amplitude) fundamental

frequency. If the fundamental shows up at F, the harmonics show up at 2F, 3F, ... nF. Further, while the phase value at F may not be stable, the relative phase between F and the higher harmonics will be a fairly stable function. Each harmonic is characterized by a complex number whose amplitude is the ratio to the amplitude of the fundamental and whose phase is the phase angle relative to the fundamental. A linear regression between frequency lines in the frequency domain is one good way of identifying and quantifying harmonics.

For sine work, it is necessary to tell the system about the non stationary fundamental frequency moving through the system. Then the higher harmonics of the fundamental can be curvefit to give an average distortion for the waveform. If higher harmonics are curvefit continuously as the test progresses, it is possible to display a single cycle of the distorted signal to see what the waveform really looks like.

In 3-D this is much more complicated. The three axes of data potentially all hold harmonics of the signal. The biggest problem is to find something to call a fundamental in all the data available to be analyzed. For a sine test, other than a simple ellipse rotating in a fixed plane, the fundamental will be a collection of frequencies (typically 20 to 50 frequencies in the sine tests I have been proposing), and harmonics are potentially there for all the frequencies in all the directions. This is a gloriously complicated problem to figure out what to do with it all.

As a display, it is very effective to put bars up on the spectral type of display. One color could be used to represent a single fundamental and all it's harmonics over all 9 spectral curves. The extent to which each of the spectral plots (PSD, Coherence, Phase) is the result of the harmonic relation can be drawn in as the amplitude of the line for each spectral line.

Another form of plot that might be used is to reconstruct the waveform from the Fourier components, and plot it on the 3-D oscilloscope type of display. This could indicate the type of distortion that is present, e.g., square wave, triangular wave, clipping, something hitting, etc.

While harmonic analysis is important, it doesn't need to be implemented this formally to be available. An experienced test operator can look at a series of PSDs and see that something spectral is happening in the time history. Then the oscillograph type of display can reveal the waveform. For this reason I put formal harmonic analysis at the bottom priority.

DISPLAYS OSCILLOGRAPHS

The classical way of looking at raw data in the time domain is oscillograph plots. Typically these are done at slow speed with the envelope of the data as a function of time being displayed. To observe waveform, the plotting speed is increased. This kind of plot is most useful for sine testing, but it is also applicable to random data, and general transient data. The usefulness for random data is increase if a second color is used to superimpose the local RMS value over the top of the actual time history.

There are a number of extensions of this concept into the 3-D regime. The coordinate system that is being displayed can be changed to reflect a line of symmetry in the test article using cylindrical coordinates or spherical coordinates when the test is spherically symmetric as in a zero coherence random test or a 3-D sine test. The angular coordinates for the generic 3-D sine test will work out to be regular linear functions. Of course the angular coordinates will contain a discontinuity and it is best if the "pen" is lifted off the paper as the coordinate transitions between 0 and 2π. Data should be extrapolated to 2π and restarted at 0 without drawing anything between them. It is very useful to provide a variable discontinuity point under the operator's control. Any angle θ can be used for the discontinuity with θ-2π as the other side of the discontinuity. This issue is aggrandized with the name of Riemann surfaces.

Another 3-D extension is to plot the 3-D time history in space. This forms a puff ball display that can be opened up using a plane or wedge to see the hollow space inside in the case of a 3-D sine test or more puff ball in the case of the random test. By plotting only the end points of the vectors, a scatter plot results. Color coding can be used to show the third dimension of the data for a scatter plot.

If a coordinate transform can be used to drop the coordinate space to 2-D (e.g., using cylindrical coordinates and discarding the angular coordinate or just looking at two coordinates together), it is possible to draw the 2-D time history through time in the third dimension. The resulting shape is snake like in appearance and can be inspected for uniformity of spatial coverage and the extent of the envelope. Also clipping would show up this way. Of course you would want to use the joy stick to move around the 3-D display. This rotation would be nonstandard and would require additional coding because time (instead of space) is being used as a third dimension.

Another 3-D extension is to allow the user to identify a window from the three X, Y, and Z position plots in time. Then that 3-D geometry could be displayed in a 3-D oscilloscope type of display. Again, this path could be inspected in 3-D by changing the point it is viewed from, however, this rotation would be standard and would require no extra coding.

The oscillograph class of displays is probably the most fundamental of the possible displays. It should have the highest priority.

DISPLAYS PRINCIPAL COMPONENTS

In the random test, it is possible to find the principal amplitudes associated with the ellipsoidal surface at each test frequency. While these coordinates vary with frequency, they diagonalize the spectral matrix. Thus at any frequency point the coordinates can be changed to a set of three direction angles indicating the directions of the principle axes, three time phase angles indicating the timing of the peaks. and a set of three amplitudes indicating the largest, smallest, and orthogonal amplitude at that frequency. This is the same amount of data as is required in the spectral matrix at a frequency point. In the spectral matrix the nine numbers are the three PSD values, the three time phase angles between the channels, and the three coherence values.

Displaying the spectral matrix in principal component form has the advantage that the amplitudes are reported in physically understandable values. It is easier to interpret a value that is the largest or smallest RMS available over all of coordinate space. However, the spatial angles and time phase angles are not nearly so easily interpreted. Similarly, the coherence values for the conventional spectral matrix are easily understood physically and the PSD values, while misleading because they are not principal values in general, are at least easy to comprehend.

It might be good to present a mixed spectral display showing the largest principal value and the smallest principal value as envelopes around each of the three PSD values on the conventional display.

It would be easy to understand the spatial directions of the principal axes with frequency if a sea urchin type of display were used in 3-D to show all the principal directions in space. Then the length of the needle could be used to show frequency. Short needles should show higher frequencies, since they tend to be less important. It would be nice if the user could type in a frequency and the corresponding needle would turn red.

The time phase lag relationships don't mean much to me in the spectral type of display. The physical interpretation is the angle at that frequency which one channel makes with respect to the other in time. To make any sense of this, it is necessary to have the 3-D input available. For example, the relative phase angle between the input force vector and the response at a point will be 90° for a pure modal response. This kind of relationship probably exists between phase angles of principal directions in 3-D. As a display technique, one might highlight spectral lines that exhibit strong modal behavior on a conventional spectral display.

Some method of providing more interpretation of the information from the spectral display is highly desirable because the spectral data itself can hide so much physical behavior. Principal component analysis is a good start in that direction.

DISPLAYS SPECTRAL MATRIX

The spectral matrix is the most important display for 3-D random analysis because the random test is specified in terms of these variables. The only difference I have with what is currently being done is that I would not plot cospectra and phase for the off diagonal terms both above and below the diagonal. Instead, I would plot the phase alone below the diagonal, and the amplitude of the cospectra above the diagonal. This would allow more plot area to display the data in.

Another variation on the conventional display would be to show coherence and phase for the off diagonal terms. Again I would plot the coherence above the diagonal and the phase angle below the diagonal. This is more interpretable but not directly the coordinates being used to specify the test for the control system.

For the spectra, cospectra plot that is the test control plot, I would show the test tolerances around the measured test data. Color should be used to flag out of specification conditions with red flagging the problem. I would use a standard color scheme: red for out of specification data, black for test data within specification, green for the specification boundaries, and a hard to see color like yellow for the nominal test level. The nominal test level doesn't really mean anything, only the tolerance boundaries really matter.

To keep things comfortable to look at, the specification data should be averaged over a fixed time interval (e.g., 2 seconds). The averaging time should be under the test operator's control. Of course the nearest non zero integer number of frames would be the actual time average used in practice. If you want to show data from previous frames, the old curves should be redrawn in a lighter shade of gray (and red) before each new curve is drawn. By drawing all the curves over again in the inverse time order, the most important newer curves will lie on top of the older curves. Some maximum number of curves (e.g., 3; also under the operator's control) should be used to limit the data on the screen.

For looking at response data, I would tend to used a hybrid type of display. The principal components would be used as envelopes around all three PSD values. The coherence would be plotted above the axes. The background for the coherence might be illuminated with a different color depending on the how large the expression below turned out to be:

$$1 \geq |\vec{\gamma}_{xz}|^2 \cos^2 \angle\vec{\gamma}_{xz} + |\vec{\gamma}_{yz}|^2 \cos^2 \angle\vec{\gamma}_{yz} + |\vec{\gamma}_{xy}|^2 \cos^2 \angle\vec{\gamma}_{xy} \qquad 1)$$
$$- 2|\vec{\gamma}_{xy}||\vec{\gamma}_{yz}||\vec{\gamma}_{xz}| \cos\angle\vec{\gamma}_{xy} \cos\angle\vec{\gamma}_{yz} \cos\angle\vec{\gamma}_{xz}$$

By evaluating the expression and setting the background color on all three coherence plots accordingly, it would be easy to find structural modes or regions where the 3-D measurement was coherent for some reason. For example, the background could be colored light blue whenever the expression exceeded 0.95 total value. At these points the response would be virtually two dimensional and almost certainly would be the response of a structural mode.

Phase data is even harder to understand physically. The only phase relationship that can easily be understood is the relative phase between the control accelerometers and some other accelerometer. This is discussed under transfer functions.

I would consider the spectral display of test data to be among the highest priority displays in the system.

DISPLAYS TRANSFER FUNCTIONS

Transfer functions involve the identification of the input/output relationship between multiple channels. While the transfer functions between the control accelerometers could be calculated, they are not really interesting. The real application for transfer functions is between the control accelerometers (or base forces) and the response at other points in

the payload. Numerous physical relationships are known in this kind of transfer function and the modes of the payload.

The display for transfer functions between three control accelerometers and three response accelerometers would be a 3×3 matrix of frequency response curves similar to spectral data. However, each curve would have both amplitude and phase data associated with it. Unlike spectral data the transfer function between Xin and Yout is not the same as between Yin and Xout, so the off diagonal plots are all different! The information in the phase plot is mostly locating the 90° line (or 0° and 180° for accelerometer to accelerometer data). If any frequency band at which the phase was 90° were illuminated with a light color (e.g., a light green line across the entire plot at that frequency) on the corresponding amplitude curve, that would tend to convey most of the data in the phase angle curve without actually plotting it. It would be useful to plot another color for all bands on all the other plots where a 90° phase angle occurred. For example, a yellow line might indicate that some other curve had a phase angle of 90° on it. All nine plots would have the same yellow lines on them except for the one or more plots where that line was green.

DISPLAYS WIDEBAND RMS AND TRACKING FILTER

The traditional display for sine testing at JPL involves showing the RMS amplitude and the RMS amplitude of a tracking filter centered on the fundamental for the sine test. This allows a simple assessment of signal quality in that the two numbers are the same unless the signal is significantly distorted.

The tracking filter is extremely easy to implement for a sine test since there is typically a sine reference available to base the tracking filter on. Basically the tracking filter is just the integral of the sine reference times the raw signal for the "Co" part of the tracking filter, and the integral of the cosine reference times the raw signal for the "Quad" part of the signal. The cosine reference is computed from the sine reference by differentiating the sine reference to get the sign of the cosine reference and the amplitude can easily be done as a lookup table based on the current value of the sine reference. The lookup table simply expresses $\cos(\omega t)=\mathrm{SQRT}[1-\sin^2(\omega t)]$.

No FFT is involved in the processing as implemented at JPL. Frequency is calculated by counting axis crossings on the sine reference channel.

This procedure is immediately applicable to the 2-D sine test that seems to be preferred method for implementing sine testing. One simply calculates "Co" and "Quad" for all three response channels based on the cosine and sine values available from the input.

I would classify this as a high priority type of analysis. It potentially can double check the control system for the 2-D sine test, and it can be very effective as a response analysis.

DISPLAYS ZOOM FOURIER TRANSFORM

The zoom Fourier transform is accomplished by a combination of filtering and multiplying the signal times a sinusoid of known frequency at the bottom of the zoom range. $\text{Sin}(\omega_1 t)\times\text{Sin}(\omega t)=.5\times\cos(\omega_1-\omega) - .5\times\cos(\omega_1+\omega)$ If ω_1 is the bottom of the zoom range and $\text{Sin}(\omega t)$ is a Fourier coefficient of the data, you effectively drop the frequency that the data comes at to $\omega_1-\omega$ by multiplying be $\text{Sin}(\omega_1 t)$. If the data is band pass filtered between ω_1 (to eliminate lower frequencies) and ω_2 at the top of the frequency range to be zoomed, and then multiplied by a sinusoid at ω_1. The resulting time history can be converted to the frequency domain using an FFT. The FFT results can be rearranged to give the correct Fourier data for the zoomed frequency region.

This is useful for looking at signals that are slightly distorted in frequency such as the 3-D sine test data. Because the full range of the FFT is effectively used to expand a potentially small frequency region between ω_1 and ω_2, the frequency resolution can be very accurate. This is really the only way to look closely at the frequency content of the 3-D sine test. The signal harmonics are grouped in a band about 1/20 times the fundamental. For example at 100 Hz everything interesting happens between 95 Hz and 105 Hz.

As a display, the signals would look very much like Fourier data except that the frequency axis would be expanded. Potentially the display might be centered on the current test frequency so that the display holds still with time. In this mode, unlike Fourier data, the phase data should be stationary for the control channels, thus the display could usefully show the phase.

While this display is potentially very interesting it is also very technical. It would take a 5 minute discussion of why this is important to show it to someone unfamiliar with the 3-D system. I would classify this as being a bottom priority.

DISPLAYS 3-D OSCILLOSCOPE

Waveform has historically been analyzed using an oscilloscope. On an oscilloscope there are basically two controls: a trigger to decide how often the oscilloscope refreshes the image, and a "frequency" control that varies how long the display is put on the screen after the trigger. Actual the frequency control is really a period control, adjusting the time duration until it is just one cycle. Because the images usually come very fast (for electrical signals), the properly adjusted oscilloscope appears to freeze the waveform on the screen with time as the X axis. In vibration test control, oscilloscopes tend to be too slow at the low end of the frequency range.

For 3-D work, we need something equivalent to an oscilloscope that captures a short duration burst of 3-D data (i.e., three orthogonal channels instead of just one channel) over a short period of time. Then when the same point in the cycle is reached again, the signal might be "refreshed" just as it is

with an oscilloscope. An oscilloscope can be set up to free run or operate as a storage scope on a single frame. These same modes need to be available for the 3-D oscilloscope. The trigger needs to be able to detect data in a spatial area, e.g., X around 1.0 g, Y around -1.0 g, and Z around 0.0 g. Then some fixed amount of data would be acquired, such as 10240 points for each of the three channels. Once the data was acquired, the duration control would allow looking at some shorter segment of the data to find a repetitive pattern. Because three orthogonal channels were acquired together, 3-D images of the path could be drawn on the shaker. Using a joy stick it would be possible to move around the image spatially.

Anyone who has used a real oscilloscope knows that free running displays are too hard to adjust. Just varying the "frequency" control is theoretically enough to freeze a repetitive image, but in practice it is much easier to do if the trigger is set up to restart the signal at a regular interval. This same problem will be even more pronounced when trying to "stop" a 3-D waveform where the user has to visualize the waveform in 3-D from a 2-D display. A good control would be a time lag forcing some elapsed time before starting to look for the next trigger (i.e., a adjustable control offering something like 2.0 seconds minimum time between triggers). The user will need to examine an image fully before picking up another one.

This kind of waveform examination is very general, and potentially of use for any test type. It is also very arty, with good intuitive understanding from large segments of the engineering public. For this reason, I would consider this to be a high priority display.

CONCLUSIONS

Pre display functions seem very important at this juncture. A good job needs to be done of interfacing the measurement channels and the data displays. If this is done in an ad hoc way, the result will be extensive rewriting of the displays as the issues in passing the physical data to the displays become resolved. Standard subroutines need to be developed to address the issues of physical units, channel identification, calibration data, etc. on the front end of each display. This needs to be very carefully thought out or it will seriously limit the system.

Perhaps the most interesting idea in this write up is the concept of providing identification of all triaxial measurements and providing a standard per analysis method of rotating them. Potentially this allows all triaxial measurements to be viewed in 3-D with very little code. Effectively any orientation of measurement can be deduced from the triaxial data, so the orientation can of the measurements can be rotated without changing any of the display functions.

The highest priority displays seem to be the spectral data, the oscillograph data, the 3-D oscilloscope, and the tracking filter. There are a number of interesting things that can be done with all of these displays beyond simply implementing a single static type of display. The spectral display can have variable averaging time, envelopes and overlays for the test specification, cospectra and phase versus coherence and phase, decaying curves from previous averaging times, and so on. The oscillograph data can be converted

into different coordinates, the time scale can be varied, parts of the signal can be passed to the 3-D oscilloscope type of display for viewing in 3-D, if axes of symmetry exist, 3-D data can be transformed into 2-D data for viewing in 3-D as a function of time, and so on. The tracking filter can display wideband and filtered RMS, and phase information relative to the other axis (perhaps in the form of a circle that distorts if the signals get out of phase).

There are a large number of intermediate priority displays: the distribution function, the finite Fourier transform, principal components, and transfer functions. Some are clearly less important: autocorrelation and cross correlation, harmonic analysis, and the zoom Fourier transform.